Developed at the request of:

Research conducted by:

Climate: Observations, projections and impacts: China

Met Office
Simon N. Gosling, University of Nottingham
Robert Dunn, Met Office
Fiona Carrol, Met Office
Nikos Christidis, Met Office
John Fullwood, Met Office
Diogo de Gusmao, Met Office
Nicola Golding, Met Office
Lizzie Good, Met Office
Trish Hall, Met Office
Lizzie Kendon, Met Office
John Kennedy, Met Office
Kirsty Lewis, Met Office
Rachel McCarthy, Met Office
Carol McSweeney, Met Office
Colin Morice, Met Office
David Parker, Met Office
Matthew Perry, Met Office
Peter Stott, Met Office
Kate Willett, Met Office
Myles Allen, University of Oxford
Nigel Arnell, Walker Institute, University of Reading
Dan Bernie, Met Office
Richard Betts, Met Office
Niel Bowerman, Centre for Ecology and Hydrology
Bastiaan Brak, University of Leeds
John Caesar, Met Office
Andy Challinor, University of Leeds
Rutger Dankers, Met Office
Fiona Hewer, Fiona's Red Kite
Chris Huntingford, Centre for Ecology and Hydrology
Alan Jenkins, Centre for Ecology and Hydrology
Nick Klingaman, Walker Institute, University of Reading
Kirsty Lewis, Met Office
Ben Lloyd-Hughes, Walker Institute, University of Reading
Jason Lowe, Met Office
Rachel McCarthy, Met Office
James Miller, Centre for Ecology and Hydrology
Robert Nicholls, University of Southampton
Maria Noguer, Walker Institute, University of Reading
Friedreike Otto, Centre for Ecology and Hydrology
Paul van der Linden, Met Office
Rachel Warren, University of East Anglia

The country reports were written by a range of climate researchers, chosen for their subject expertise, who were drawn from institutes across the UK. Authors from the Met Office and the University of Nottingham collated the contributions in to a coherent narrative which was then reviewed. The authors and contributors of the reports are as above.

Developed at the request of:

Department of Energy & Climate Change

Research conducted by:

Met Office Hadley Centre

The University of Nottingham
UNITED KINGDOM · CHINA · MALAYSIA

Walker Institute

Centre for Ecology & Hydrology
Natural Environment Research Council

University of Leeds

Tyndall Centre for Climate Change Research

Climate: Observations, projections and impacts

China

We have reached a critical year in our response to climate change. The decisions that we made in Cancún put the UNFCCC process back on track, saw us agree to limit temperature rise to 2 °C and set us in the right direction for reaching a climate change deal to achieve this. However, we still have considerable work to do and I believe that key economies and major emitters have a leadership role in ensuring a successful outcome in Durban and beyond.

To help us articulate a meaningful response to climate change, I believe that it is important to have a robust scientific assessment of the likely impacts on individual countries across the globe. This report demonstrates that the risks of a changing climate are wide-ranging and that no country will be left untouched by climate change.

I thank the UK's Met Office Hadley Centre for their hard work in putting together such a comprehensive piece of work. I also thank the scientists and officials from the countries included in this project for their interest and valuable advice in putting it together. I hope this report will inform this key debate on one of the greatest threats to humanity.

The Rt Hon. Chris Huhne MP, Secretary of State for Energy and Climate Change

There is already strong scientific evidence that the climate has changed and will continue to change in future in response to human activities. Across the world, this is already being felt as changes to the local weather that people experience every day.

Our ability to provide useful information to help everyone understand how their environment has changed, and plan for future, is improving all the time. But there is still a long way to go. These reports – led by the Met Office Hadley Centre in collaboration with many institutes and scientists around the world – aim to provide useful, up to date and impartial information, based on the best climate science now available. This new scientific material will also contribute to the next assessment from the Intergovernmental Panel on Climate Change.

However, we must also remember that while we can provide a lot of useful information, a great many uncertainties remain. That's why I have put in place a long-term strategy at the Met Office to work ever more closely with scientists across the world. Together, we'll look for ways to combine more and better observations of the real world with improved computer models of the weather and climate; which, over time, will lead to even more detailed and confident advice being issued.

Julia Slingo, Met Office Chief Scientist

Introduction

Understanding the potential impacts of climate change is essential for informing both adaptation strategies and actions to avoid dangerous levels of climate change. A range of valuable national studies have been carried out and published, and the Intergovernmental Panel on Climate Change (IPCC) has collated and reported impacts at the global and regional scales. But assessing the impacts is scientifically challenging and has, until now, been fragmented. To date, only a limited amount of information about past climate change and its future impacts has been available at national level, while approaches to the science itself have varied between countries.

In April 2011, the Met Office Hadley Centre was asked by the United Kingdom's Secretary of State for Energy and Climate Change to compile scientifically robust and impartial information on the physical impacts of climate change for more than 20 countries. This was done using a consistent set of scenarios and as a pilot to a more comprehensive study of climate impacts. A report on the observations, projections and impacts of climate change has been prepared for each country. These provide up to date science on how the climate has already changed and the potential consequences of future changes. These reports complement those published by the IPCC as well as the more detailed climate change and impact studies published nationally.

Each report contains:

- A description of key features of national weather and climate, including an analysis of new data on extreme events.
- An assessment of the extent to which increases in greenhouse gases and aerosols in the atmosphere have altered the probability of particular seasonal temperatures compared to pre-industrial times, using a technique called 'fraction of attributable risk.'
- A prediction of future climate conditions, based on the climate model projections used in the Fourth Assessment Report from the IPCC.
- The potential impacts of climate change, based on results from the UK's Avoiding Dangerous Climate Change programme (AVOID) and supporting literature. For details visit: http://www.avoid.uk.net

The assessment of impacts at the national level, both for the AVOID programme results and the cited supporting literature, were mostly based on global studies. This was to ensure consistency, whilst recognising that this might not always provide enough focus on impacts of most relevance to a particular country. Although time available for the project was short, generally all the material available to the researchers in the project was used, unless there were good scientific reasons for not doing so. For example, some impacts areas were omitted, such as many of those associated with human health. In this case, these impacts are strongly dependant on local factors and do not easily lend themselves to the globally consistent framework used. No attempt was made to include the effect of future adaptation actions in the assessment of potential impacts. Typically, some, but not all, of the impacts are avoided by limiting global average warming to no more than 2 °C.

The Met Office Hadley Centre gratefully acknowledges the input that organisations and individuals from these countries have contributed to this study. Many nations contributed references to the literature analysis component of the project and helped to review earlier versions of these reports.

We welcome feedback and expect these reports to evolve over time. For the latest version of this report, details of how to reference it, and to provide feedback to the project team, please see the website at www.metoffice.gov.uk/climate-change/policy-relevant/obs-projections-impacts

In the longer term, we would welcome the opportunity to explore with other countries and organisations options for taking forward assessments of national level climate change impacts through international cooperation.

Summary

Climate observations

- Warming has been widespread over China over the period 1960 to 2010 with greater warming in winter then summer.
- There has been a strong decrease in the frequency of cool nights since 1960 and an increase in the frequency of warm nights.
- There has been a general increase in winter temperatures averaged over the country as a result of human influence on climate, making the occurrence of mild winter temperatures more frequent and cold winter temperatures less frequent.
- Recent studies have found some evidence to suggest that annual total precipitation over China is increasing, as are days with heavy precipitation.

Climate change projections

- For the A1B emissions scenario projected changes in temperature are higher over northern and western parts of the country, with changes of up to around 4.5°C. In the southeast, projected changes are typically around 3°C. There is good agreement between the models from the CMIP3 ensemble over most of China.
- Precipitation is projected to increase over almost the entire country. Increases of up to 20% are projected with high ensemble agreement between the CMIP3 models across the northeast of China. Lower increases of between zero and 10% are projected for the southeast of the country, but with less agreement amongst CMIP3 models.

Climate change impacts projections

Crop yields

- Although the picture is mixed, global- and regional-scale studies considered here generally project decreases in the yield of China's major crops: rice, wheat, and most markedly of maize, as a consequence of climate change.

- Some global-scale studies suggest that the magnitude of, and balance between, detrimental ozone effects and CO_2 fertilisation may determine whether crop yield losses or gains are realised under climate change.

Food security

- China currently has very low levels of undernourishment. Global-scale studies of food security vary in their conclusions for China, however they generally project that the country will become less food secure with climate change.

- National-scale studies confirm the uncertainty in food security estimates with some suggesting that China could experience large food shortages, while others suggest it may not face pressures on food security with climate change.

Water stress and drought

- Global-scale studies included here agree that south-eastern China currently suffers from a moderate to high level of water stress.

- Global- and regional-scale studies included here show no consensus as to the sign of change in drought or water stress in China with climate change.

- However some global- and national-scale studies included here project that water stress could increase in China for global-mean warming scenarios of around 2°C, but may decrease under higher warming or higher emission scenarios, due to a projected increase in precipitation and runoff.

- Recent simulations by the AVOID programme project a median increase of 6% of China's population to be exposed to water stress increases, and 20% to water stress decreases under the A1B emissions scenario by 2100. Under a mitigation scenario where global temperature increases are limited to 2°C these values are 2% and 9% respectively.

Pluvial flooding and rainfall

- The IPCC AR4 noted the potential for increased precipitation over East Asia, and also an increase in extreme precipitation in parts of China.

- Results from recent studies suggest that changes in precipitation extremes tend to be larger under higher emissions scenarios.

Fluvial flooding

- Observations show that heavy precipitation events have increased over recent decades in parts of China, and flooding events have become more frequent in a number of river basins.

- Climate change impact studies suggest that this trend could continue, although uncertainties are large, resulting in a wide spread in responses among different climate models.

- Simulations by the AVOID programme show a general tendency towards higher flood risk in China, particularly later in the century and under the A1B scenario.

Tropical cyclones

- There remains large uncertainty in the current understanding of how tropical cyclones might be affected by climate change.

- There is relatively less uncertainty regarding the intensity of cyclones in the western Pacific basin, compared to their frequency. A number of global- and regional-scale studies included here project that cyclone intensity could increase considerably in the future in this basin. These increases in intensity could be greatest for the most severe cyclones, which could lead to large increases in cyclone damages in China.

- China is particularly vulnerable to cyclone damages due to its high coastal population density and the valuable economic assets located in coastal regions.

Coastal regions

- Recent global-scale assessments of the impact of sea level rise (SLR) on coasts, which include national estimates for China, suggest that China is one of the countries across the globe that could experience the most severe impacts.

- One study showed that based upon an analysis of 136 port cities, China was the country simulated to have the largest increase in exposure to SLR by 2070 relative to the present day.

- Another study showed that around 17% of China's coastal land area and coastal population could be affected by a 10% intensification of the current 1-in-100-year storm surge combined with a 1m SLR.

Table of Contents

Chapter 1 – Climate Observations

Rationale

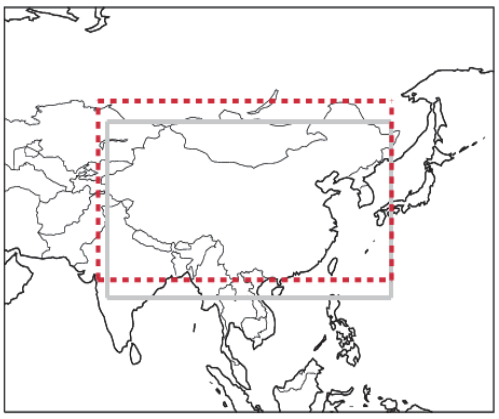

Figure 1. *Location of boxes for the regional average time series (red dashed box) in Figures 3 and 5 and the attribution region (grey box) in Figure 4.*

Present day weather and climate play a fundamental role in the day to day running of society. Seasonal phenomena may be advantageous and depended upon for sectors such as farming or tourism. Other events, especially extreme ones, can sometimes have serious negative impacts posing risks to life and infrastructure and significant cost to the economy. Understanding the frequency and magnitude of these phenomena, when they pose risks or when they can be advantageous and for which sectors of society, can significantly improve societal resilience. In a changing climate it is highly valuable to understand possible future changes in both potentially hazardous events and those reoccurring seasonal events that are depended upon by sectors such as agriculture and tourism. However, in order to put potential future changes in context, the present day must first be well understood both in terms of common seasonal phenomena and extremes.

The purpose of this chapter is to summarise the weather and climate from 1960 to present day. This begins with a general climate overview including an up to date analysis of changes in surface mean temperature. These changes may be the result of a number of factors including climate change, natural variability and changes in land use. There is then a focus on extremes of temperature, precipitation and storms selected from 2000 onwards, reported in the World Meteorological Organization (WMO) Annual Statement on the Status of the Global Climate and/or the Bulletin of the American Meteorological Society (BAMS) State of the Climate reports. This is followed by a discussion of changes in moderate extremes from 1960 onwards using an updated version of the HadEX extremes database (Alexander et al., 2006) which categorises extremes of temperature and precipitation. These are core climate variables which have received significant effort from the climate research community in terms of data acquisition and processing and for which it is possible to produce long high quality records for monitoring. No new analysis is included for storms (see the methodology section that follows for background). For seasonal temperature extremes, an attribution analysis then puts the seasons with highlighted extreme events into context of the recent climate versus a hypothetical climate in the absence of anthropogenic emissions (Christidis

et al., 2011). It is important to note that we carry out our attribution analyses on seasonal mean temperatures over the entire country. Therefore these analyses do not attempt to attribute the changed likelihood of individual extreme events. The relationship between extreme events and the large scale mean temperature is likely to be complex, potentially being influenced by *inter alia* circulation changes, a greater expression of natural internal variability at smaller scales, and local processes and feedbacks. Attribution of individual extreme events is an area of developing science. The work presented here is the foundation of future plans to systematically address the region's present and projected future weather and climate, and the associated impacts.

The methodology section that follows provides details of the data shown here and of the scientific analyses underlying the discussions of changes in the mean temperature and in temperature and precipitation extremes. It also explains the methods used to attribute the likelihood of occurrence of seasonal mean temperatures.

Climate overview

China is a vast country on the eastern seaboard of Asia, extending between latitudes 20-50°N and including both long stretches of coastline and regions that are huge distances from any sea. Topography ranges from coastal lowlands in the east to high plateaux and mountains in central and western regions. The climates of China are therefore complex and diverse. A phenomenon that steers the climate of much of China is the 'Asiatic Monsoon' in which, in summer, moist winds blow onshore from the Pacific (and Indian) Oceans towards low atmospheric pressure that develops over the hot Asian interior. These warm moist winds bring most of China's rainfall. Conversely, in winter, very cold and dry winds blow outwards from the huge high atmospheric pressure system that develops over Siberia and central Asia.

The climate of the relatively low-lying eastern side of China can be divided into three latitudinal bands, each containing a section of the Pacific coastline. Annual average temperatures range from 4°C at Harbin in the north-east to 22°C at Guangzhou (Canton) in the south-east. In north-eastern China winters are very cold with frequent light snow and typical January daily temperature maxima ranging from 2°C at Beijing (40°N) to -13°C at Harbin (46°N). Summers are warm and humid but with unreliable rainfall and some drought years. Annual average rainfall at Beijing is 521 mm. Further south in central-eastern China there is more precipitation (annual average rainfall 1112mm at Shanghai) and, although the main wet season is summer, winter is more changeable than further north with alternating mild and cold spells bringing some rain and some snow. South-eastern China is the warmest and wettest part of China in summer, with particularly heavy rainfall along the coast (annual average rainfall 1683mm at Guangzhou). Winters here are mild.

Inland southern China towards the borders with Vietnam and Laos is hilly or mountainous but still has mild or warm winters with very little precipitation. Only rarely does cold air penetrate here from the north, bringing occasional frost at higher levels. Summers are wet at higher levels (Kunming annual average rainfall 1007mm) but in sheltered valleys the rainfall is not excessive. Further northwest is Tibet, a region of high plateaux bordered by even higher mountains. Here winters are very cold (mean January temperature -2°C at Lhasa), but summers are warm in daytime (reaching ~22°C), albeit cool at night. The winters have frequent light snow but most of the precipitation falls in summer, when moist air is drawn into Tibet by the Asian monsoon winds. North of Tibet, the northern interior of China contains vast high plains that are desert or semi-arid. This area has a very continental type of climate with a large temperature range between summer and winter (Urumqi has mean temperature of -13°C in January but 25°C in July). According to latitude, summers are warm or hot and

winters are cold or very cold, sometimes made more hazardous by dust-laden strong winds. Annual precipitation is low (Urumqi 236 mm); nonetheless, towards the north of Inner Mongolia the ground is snow covered for up to 150 days per year.

Typhoons are frequent between July and October in south-east coast regions and can cause wind damage and very heavy rainfall for several consecutive days, which can lead to flooding. Occasionally, typhoons move further north to affect the central eastern coast. Other disruptive weather events in China include droughts, snow storms and extremes of cold (particularly away from the south) and extremes of heat (particularly over the western desert plains).

Analysis of long-term features in the mean temperature

CRUTEM3 data (Brohan et al., 2006) have been used to provide an analysis of mean temperatures from 1960 to 2010 over China using the median of pairwise slopes method to fit the trend (Sen, 1968; Lanzante, 1996). The methods are fully described in the methodology section. In agreement with increasing global average temperatures (Sánchez-Lugo et al., 2011), there is a widespread warming signal over China, consistent with previous studies (Cruz et al., 2007). This signal is more robust and spatially consistent over winter (December to February) than in summer (June to August) as shown in Figure 2. For the summer, while warming is predominant, there are mixed signals and low confidence in a high proportion of grid boxes. For winter there is a far more spatially coherent signal of warming and confidence is high for the vast majority of grid boxes. This is consistent with previous studies which find that temperature has increased more in winter than summer (Zhai and Pan, 2003) and that there are regional differences in the level of warming. Regionally averaged trends (over grid boxes included in the red dashed box in Figure 1) calculated by the median of pairwise slopes show warming with high confidence as the 5^{th} to 95^{th} percentiles of the slope are of the same sign. There is stronger warming during winter at 0.37 ^{o}C per decade (5^{th} to 95^{th} percentile of slopes: 0.21 to 0.54 ^{o}C per decade) than during summer at 0.17 ^{o}C per decade (5^{th} to 95^{th} percentile of slopes: 0.11 to 0.22 ^{o}C per decade).

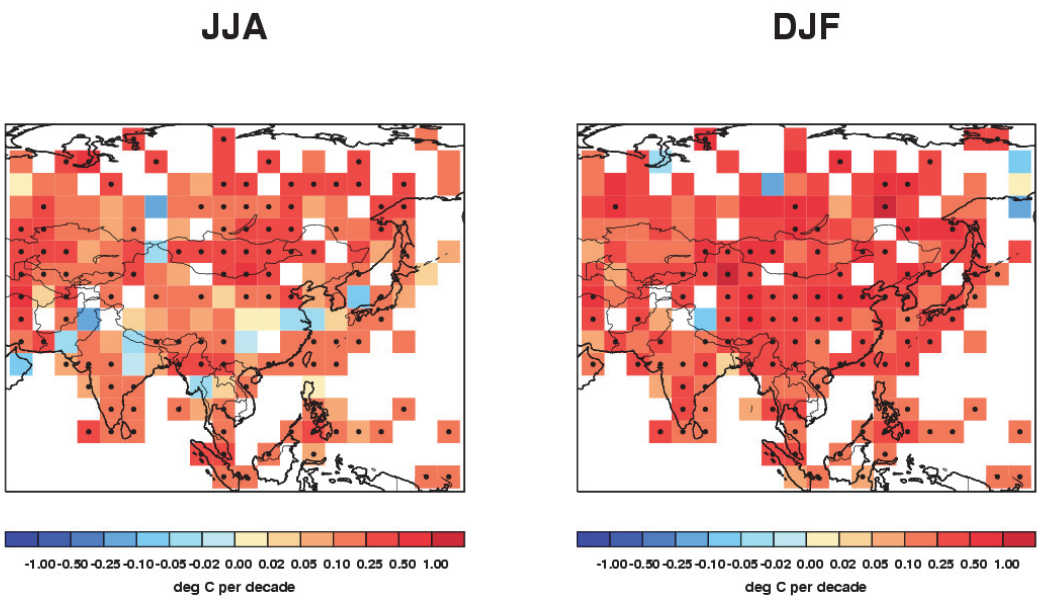

Figure 2. *Decadal trends in seasonally averaged temperatures for China and the surrounding regions over the period 1960 to 2010. Monthly mean anomalies from CRUTEM3 (Brohan et al., 2006) are averaged over each 3 month season (June-July-August – JJA and December-January-February – DJF). Trends are fitted using the median of pairwise slopes method (Sen, 1968; Lanzante, 1996). There is higher confidence in the trends shown if the 5th to 95th percentiles of the pairwise slopes do not encompass zero because here the trend is considered to be significantly different from a zero trend (no change). This is shown by a black dot in the centre of the respective grid box.*

Temperature extremes

Both hot and cold temperature extremes can place many demands on society. While seasonal changes in temperature are normal and indeed important for a number of societal sectors (e.g. tourism, farming etc.), extreme heat or cold can have serious negative impacts. Importantly, what is ‘normal’ for one region may be extreme for another region that is less well adapted to such temperatures.

Table 1 shows selected extreme events since 2000 that are reported in WMO Statements on Status of the Global Climate and/or BAMS State of the Climate reports. The severe winter of 2008 is highlighted below as an example of a recent extreme temperature event that affected China.

Year	Month	Event	Details	Source
2003	Jul	Heat wave	Affected provinces of Zhejiang, Jiangxi, and Hunan.	BAMS (Grover-Kopec, 2004)
2005	Summer	Heat waves	Frequent heat waves in central eastern China. Maximum temperatures above 35 °C. Extreme daily maximum temperatures of 38–42 °C in North China, western Huanghuai Region, and South China.	BAMS (Ren & Gao, 2006)
2006	Jun-Aug	Heat wave	Record-breaking heat wave affected Chongqing and eastern parts of Sichuan. Mid-July to late August, Chongqing had 21 days where the daily maximum temperature greater than 38°C.	BAMS (Wang & Ye, 2007)
2008	Jan	Cold	Most severe winter weather in 5 decades. Persistent low temperature and icing affected millions of people, causing damage to agriculture, and disruption to transport and energy supply.	WMO (2009)
2009	Jun	Heat wave	Northern China: daily maximum temperatures rose above 40°C; historical maximum temperature records were broken for the summer in some locations.	WMO (2010)

Table 1. *Selected extreme temperature events reported in WMO Statements on Status of the Global Climate and/or BAMS State of the Climate reports since 2000.*

Recent extreme temperature events

Severe cold, January 2008

The severe winter in China in January 2008 was the worst winter weather experienced for half a century, with over 78 million people affected by the freezing temperatures and heavy snow (WMO, 2009). The average temperature in China during the winter months was −4.4°C making it the coldest winter since 1986/87 (Guo et al., 2009). Record breaking conditions were experienced where, averaged across southern China, 19 successive days occurred with a daily mean temperature of below 1°C. In addition to this, an accumulated mean snowfall of 42.4 mm was recorded (Rogers et al., 2009).

Extreme low temperatures, freezing rain, and snow persisted over most of southern China from 10th January to 2nd February, leading to the deaths of 107 people, and over US$15 billion in damage (Guo et al., 2009). These conditions affected millions of people through damage to agriculture, and disruption to transport, energy supply and power transmission (WMO, 2009).

The severe winter weather across much of China and central Asia was attributed to Eurasia's largest January snow cover extent on record, where snow covered 1.3 million square kilometres across 15 provinces in southern China (WMO, 2009).

Analysis of long-term features in moderate temperature extremes

GHCND data (Durre et al., 2010) have been used to update the HadEX extremes analysis for China from 1960 to 2010 using daily maximum and minimum temperatures. Here we discuss changes in the frequency of cool days and nights and warm days and nights which are moderate extremes. Cool days/nights are defined as being below the 10th percentile of daily maximum/minimum temperature and warm days/nights are defined as being above the 90th percentile of the daily maximum/minimum temperature. The methods are fully described in the methodology section.

Over the analysed period (1960-2009), as shown in Figure 3, there is a strong decrease in cool night frequency and a corresponding increase in warm night frequency, consistent with other studies (Zhai and Pan, 2003), and there is high confidence that these trends are different from zero throughout the region. The trend is stronger in the north east of China

and also to the south west, around the Himalayas. South-eastern regions, where there are a larger number of stations for each grid box, show a smaller trend.

On average there is a decrease in the number of cool days, with higher confidence in the signal over most of the west and northeast compared to the south and east. These latter areas have a smaller signal, and the area around the Guizhou region shows a small increase. Similar to cool nights, there is a stronger signal towards the Himalayas although station density is low here. The increase in the number of warm days is much more uniform in magnitude and high confidence in the signal is widespread. These findings are consistent with previous studies (Zhai and Pan, 2003; You et al., 2010).

The small numbers of stations present in most grid boxes means that even if some of the signals have higher confidence than others, uncertainty in the signal over the wider grid box is large.

a)

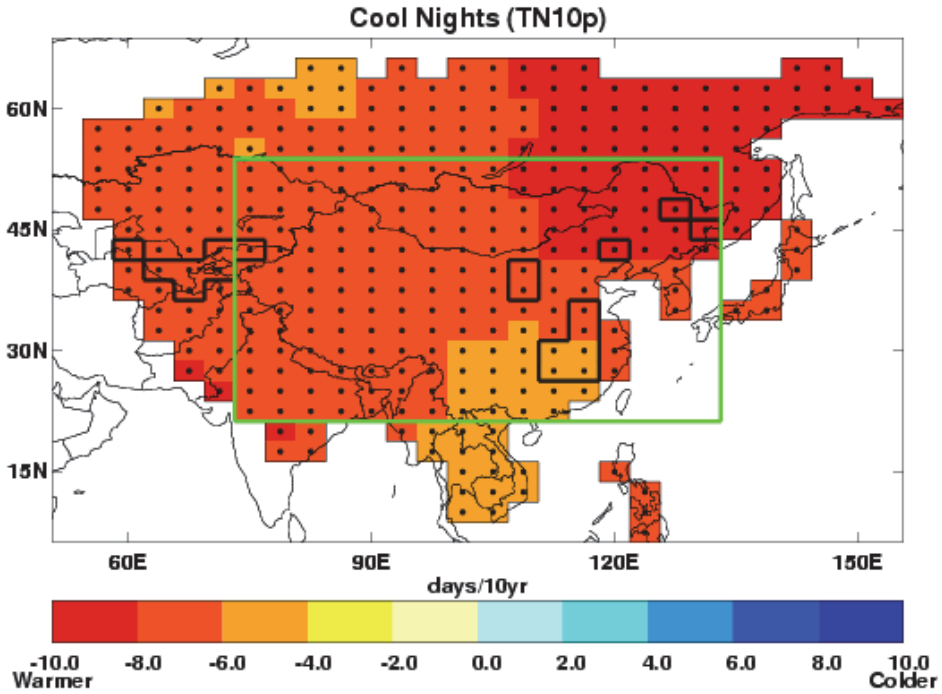

b)

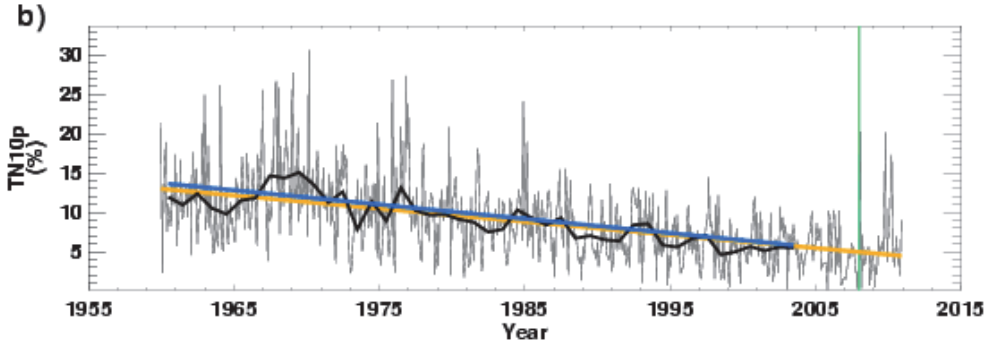

Monthly: -1.67% per decade (-1.90 to -1.45)
Total change of -8.37% from 1960 to 2010 (-9.50% to -7.25%)

Annual: -1.82% per decade (-2.33 to -1.51)
Total change of -7.28% from 1960 to 2003 (-9.32% to -6.03%)

c)

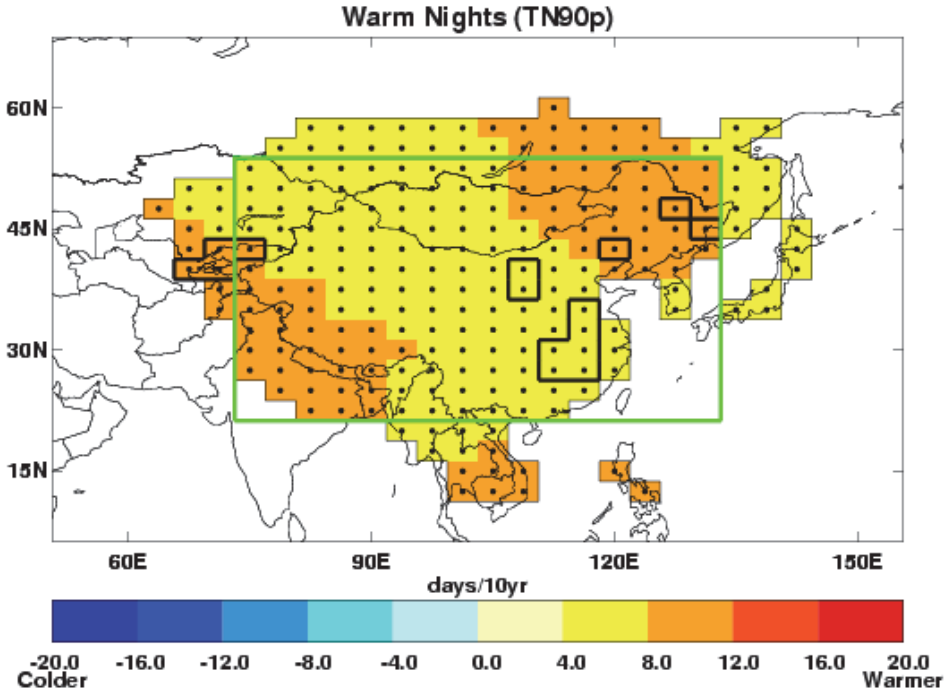

d)

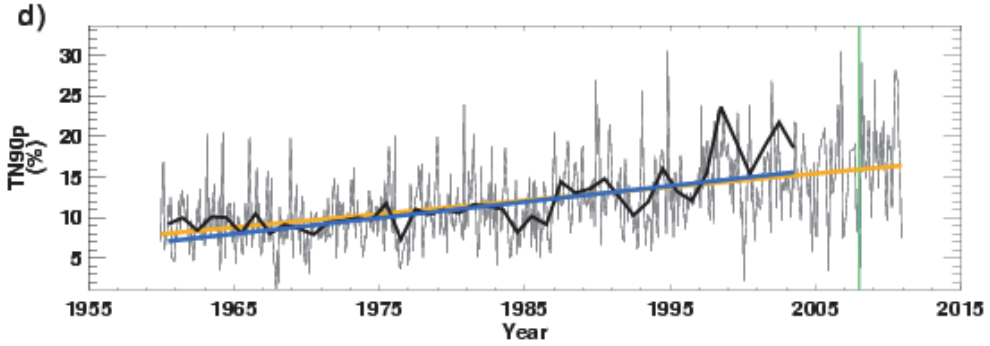

Monthly: 1.66% per decade (1.43 to 1.90)
Total change of 8.28% from 1960 to 2010 (7.14% to 9.48%)

Annual: 1.97% per decade (1.41 to 2.52)
Total change of 7.88% from 1960 to 2003 (5.63% to 10.06%)

e)

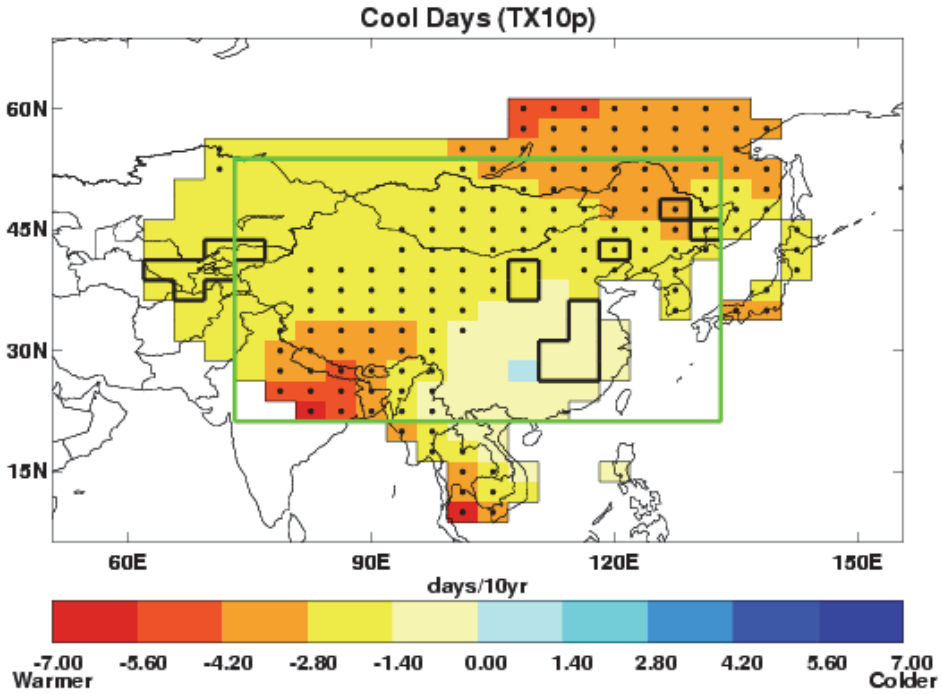

f)

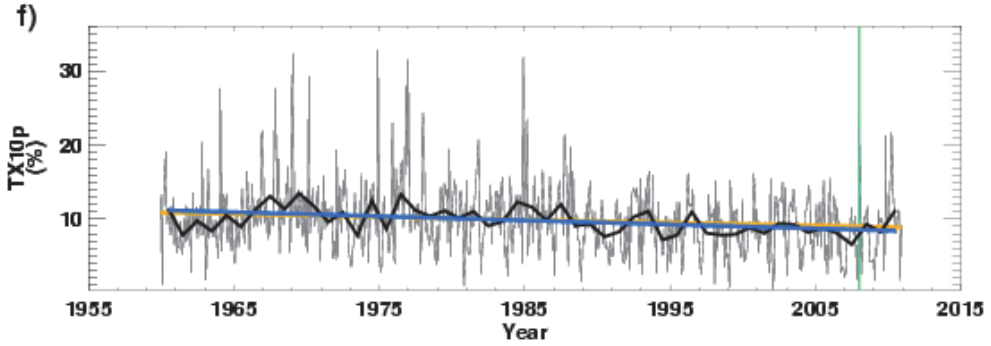

Monthly: -0.39% per decade (-0.63 to -0.17)
Total change of -1.97% from 1960 to 2010 (-3.13% to -0.85%)

Annual: -0.55% per decade (-0.87 to -0.17)
Total change of -2.77% from 1960 to 2010 (-4.35% to -0.84%)

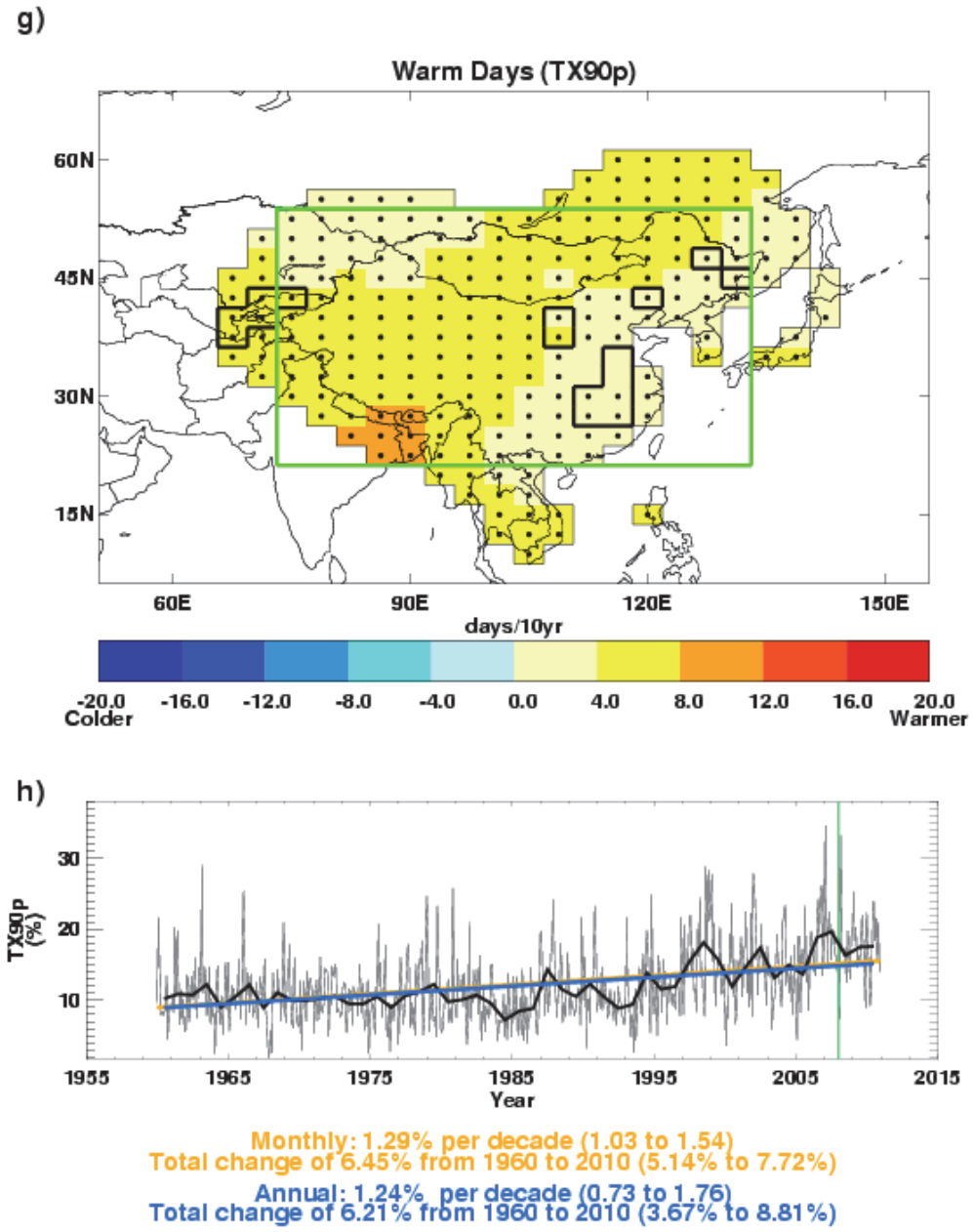

Figure 3. *Change in cool nights (a,b), warm nights (c,d), cool days (e,f) and warm days (g,h) for China over the period 1960 to 2010 relative to 1961-1990 from the GHCND dataset (Durre,et al., 2010). a,c,e,g) Grid box decadal trends. Grid boxes outlined in solid black contain at least 3 stations and so are likely to be more representative of the wider grid box. Trends are fitted using the median of pairwise slopes method (Sen, 1968; Lanzante, 1996). Higher confidence in a long-term trend is shown by a black dot if the 5th to 95th percentile slopes are of the same sign. Differences in spatial coverage occur because each index has its own decorrelation length scale (see the methodology section). b,d,f,h) Area averaged annual time series for 73.125^{o} to 133.12^{o} E and 21.25^{o} to 53.75^{o} N as shown by the green box on the map and red box in Figure 1. Thin and thick black lines show the monthly and annual variation respectively. Monthly (orange) and annual (blue) trends are fitted as described above. The decadal trend and its 5th to 95th percentile confidence intervals are stated along with the change over the period for which data are available. All the trends have higher confidence that they are different from zero as their 5th to 95th percentile slopes are of the same sign. The green vertical lines show the date of the cold spell in January 2008.*

Time-series from the regional averages have been calculated for China, as shown in Figure 3. There is a strong increase with high confidence that the trend is different from zero in the numbers of warm nights and warm days since the 1990s, consistent with the maps. A decrease in the number of cool nights is shown but the signal is smaller for cool day frequency, matching the mixed signal and mixed confidence levels seen in Figure 3. These findings are broadly consistent with previous studies (Zhai and Pan, 2003; You et al., 2010). The severe winter of 2008 can be seen in the cool days and cool nights time-series as a spike corresponding to the green vertical line. The annual regional averages for the nights terminate earlier than for the days because although there are sufficient data to create some monthly regional averages, there are insufficient to create annual ones for these indices.

Attribution of changes in likelihood of occurrence of seasonal mean temperatures

Today's climate covers a range of likely extremes. Recent research has shown that the temperature distribution of seasonal means would likely be different in the absence of anthropogenic emissions (Christidis et al., 2011). Here we discuss the seasonal means, within which the highlighted extreme temperature event occurs, in the context of recent climate and the influence of anthropogenic emissions on that climate. The methods are fully described in the methodology section.

Winter 2007/08

The distributions of the winter mean regional temperatures in recent years in the presence and absence of anthropogenic forcings are shown in Figure 4. Analyses with two independent coupled atmosphere and ocean general circulation models (HadGEM1 and MIROC) suggest that human influences on the climate have shifted the distribution towards higher temperatures than would be expected under natural influences alone. Considering the average over the entire region, the 2007/08 winter is not exceptionally cold, as it lies in the central sector, albeit the cooler half, of the temperature distributions for the climate influenced by anthropogenic forcings. It is also considerably warmer than the winter of 1944/95, which is the coldest in the CRUTEM3 dataset and lies in the cold tail of the both the distribution affected by anthropogenic factors and that with natural factors only. In the absence of human influences on the climate, the 2007/2008 season would be around

average. Notably, the warmest winter in CRUTEM3, 1998/1999, is more consistent with a winter temperature distribution under anthropogenic influences than natural ones.

The attribution results shown here refer to temperature anomalies averaged over the entire region and over an entire season, whereas the actual extreme event highlighted had a shorter duration and affected a smaller region.

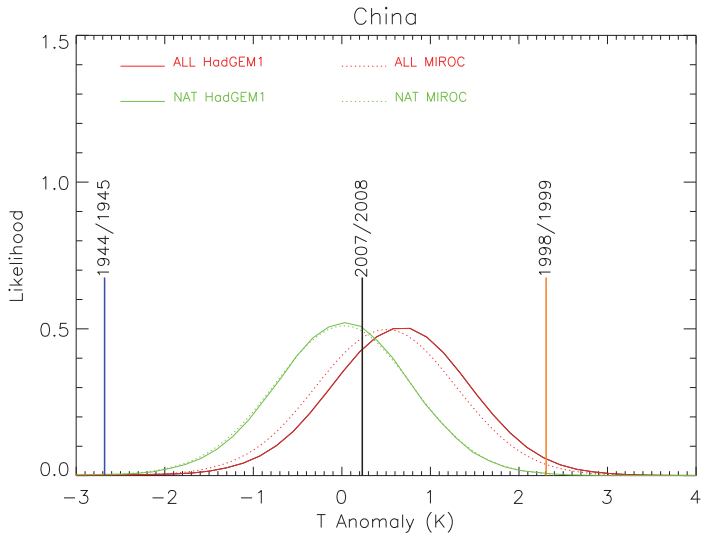

Figure 4. *Distributions of the December-January-February mean temperature anomalies (relative to 1961-1990) averaged over a region centred on China (75-133 °E, 18-50 °N – as shown in Figure 1) including (red lines) and excluding (green lines) the influence of anthropogenic forcings. The distributions describe the seasonal mean temperatures in recent years (2000-2009) and are based on analyses with the HadGEM1 (solid lines) and MIROC (dotted lines) models. The vertical black line marks the observed anomaly in 2007/08 and the vertical orange and blue lines correspond to the maximum and minimum anomaly in the CRUTEM3 dataset since 1900 respectively.*

Precipitation extremes

Precipitation extremes, either excess or deficit, can be hazardous to human health, societal infrastructure, and livestock and agriculture. While seasonal fluctuations in precipitation are normal and indeed important for a number of societal sectors (e.g. tourism, farming etc.), flooding or drought can have serious negative impacts. These are complex phenomena and often the result of accumulated excesses or deficits or other compounding factors such as spring snow-melt, high tides/storm surges or changes in land use. The analysis section below deals purely with precipitation amounts.

Table 2 shows selected extreme events since 2000 that are reported in WMO Statements on Status of the Global Climate and/or BAMS State of the Climate reports. Two events, the drought of 2006 and the flooding in the summer of 2007, are highlighted below as examples of recent extreme precipitation events for China.

Year	Month	Event	Details	Source
2001	Mar-May	Drought	Northern China experienced severe drought and water shortages.	WMO (2002)
2002		Drought	Southeast China experienced drought in winter and spring. Northern China experienced persistent drought.	WMO (2003)
2003	Jul-Aug	Drought	Extremely high temperatures and dry conditions persisted over Southern China; more than 9 million people were confronted with a lack of drinking water.	WMO (2004)
2003	Jun-Oct	Flooding	Heavy monsoon rains brought flooding to China's Yellow River basin and some of its tributaries. The death toll in China reached almost 2000.	WMO (2004)
2004	Sep-Nov	Drought	Southern provinces of China received the lowest rainfall since 1951, resulting in severe drought, affecting agriculture and drinking water.	WMO (2005)
2004	Sept	Flooding	In eastern and southern China, severe flooding and landslides affected more than 100 million people and caused more than 1,000 deaths nationwide.	WMO (2005)
2005	Jun-Jul	Flooding	During the third week of June, consecutive heavy rainstorms in parts of Southern China killed at least 170 people and affected about 21 million people.	WMO (2006)
2005	Sep-Oct	Flooding	Across northern China, heavy rainfall produced extensive flooding in the Hanjiang River and the Weihe River basins, affecting about 5.52 million people.	WMO (2006)
2006	May	Drought	Severe drought in northern China.	WMO (2007)
2006	Jun	Flooding	Heavy rain and severe flooding/landslides.	WMO ((2007)
2006	Aug	Drought	Severe drought in southern China,	WMO (2007)
2007	Mar	Snow	Heaviest snowfall in 56 years.	WMO (2008)
2007	Jun-Jul	Flooding	Persistent heavy rains in late-June and July.	WMO (2008)
2007	Sep-Dec	Drought	Southern China experienced severe drought conditions. Millions of people suffered from water restrictions and crop losses. Some provinces received only 40% of normal rainfall.	WMO (2008)
2009	Feb	Drought	Worst drought in 50 years. Drought conditions affected over 4 million people.	WMO (2010)
2009	Nov	Snow	Heavy snow over parts of northern China; heaviest snowfall in 55 years for the Hebei province and in history for the Shaanxi province.	WMO (2010)
2010	Aug	Flooding	Record rainfall in south-east caused rivers to breach their banks. The worst flooding in this region in over a decade, leading to significant loss of life, directly as well as through landslides, leaving more than 1,700 people dead or missing in Gansu Province.	WMO (2011)

Table 2. *Extreme precipitation events reported in WMO Statements on Status of the Global Climate and/or BAMS State of the Climate reports since 2000.*

Recent extreme precipitation events

Drought, May - November 2006

During May, northern China suffered from severe drought conditions that damaged 12% of the nation's agriculture (WMO, 2007). This was followed by further drought in southern China in August during which 18 million people were affected, causing significant economic losses as well as severe shortages in drinking water (WMO, 2007). From June through to mid November, the Yangtze River valley endured dry conditions as average precipitation was the second lowest since 1951, causing record low river levels (Wang, 2007).

Flooding, June-July 2007

Heavy rains caused devastating floods in the Huaihe River Valley in late June and July (Suda et al., 2008). The BBC reported that Hunan province was placed on high alert after four successive days of rain caused the Xiangjiang River to swell to its highest level in 20 years (BBC, 2007). This flood was believed to be the worst in the region since 1954 (WMO, 2008), killing over 500 people and affecting more than 100 million (CRED, 2007). It was also reported by the BBC that nearly 20,000 hectares of cropland were flooded and 3,000 houses destroyed in the southern province of Guizhou (BBC, 2007). The total cost in damages was estimated at over US$ 4 million (CRED, 2007).

Analysis of long-term features in precipitation

GHCND data (Durre et al., 2010) have been used to update the HadEX extremes analysis for China from 1960 to 2010 for daily precipitation totals. Here we discuss changes in the annual total precipitation, and in the frequency of prolonged (greater than 6 days) wet and dry spells. The methods are fully described in the methodology section.

a)

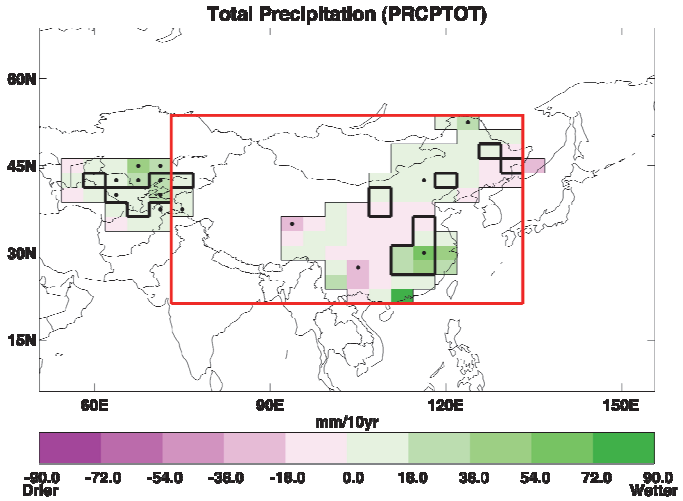

b)

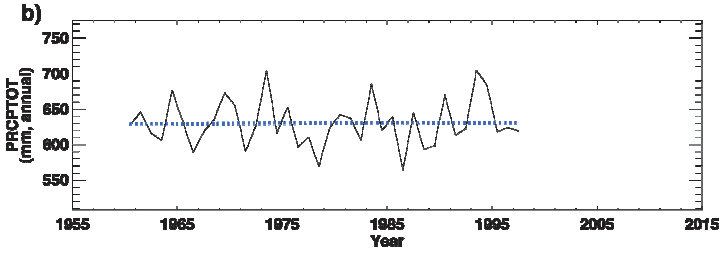

Annual: 0.36mm per decade (-9.67 to 11.04)
Total change of 1.08mm from 1960 to 1997 (-29.02mm to 33.12mm)

c)

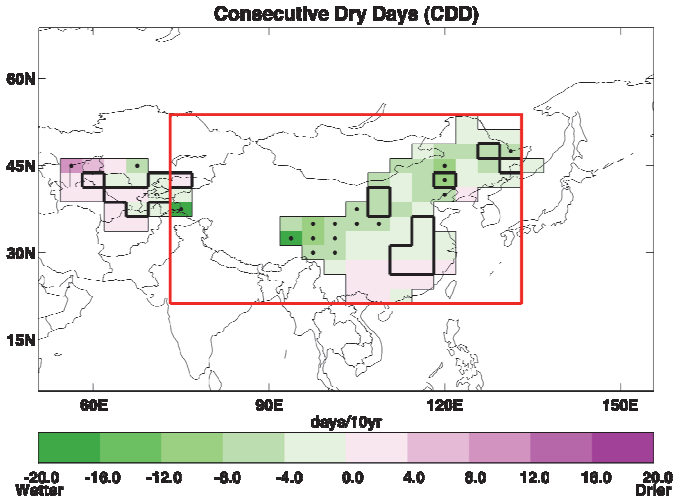

d)

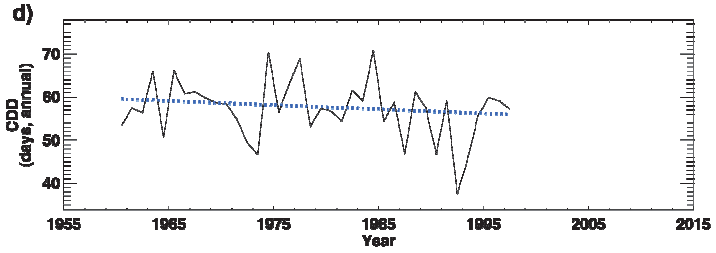

Annual: -0.97days per decade (-3.31 to 0.75)
Total change of -2.90days from 1960 to 1997 (-9.94days to 2.25days)

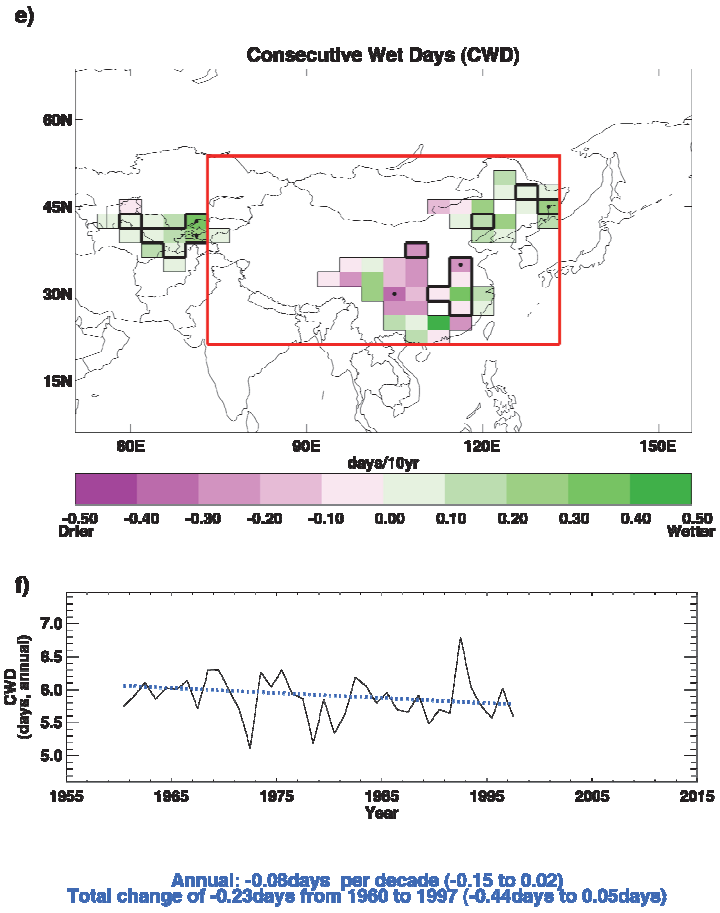

Figure 5. *The change in annual total rainfall (a,b), the annual number of continuous dry days (c,d) and the annual number of continuous wet days (e,f) over the period 1960-2010. The maps and time series have been created in exactly the same way as Figure 3. Only annual regional averages are shown in b,d,f). The dotted lines in b,d,f) indicate that there is lower confidence that the trends are different from zero. The time series for the indices terminate before the notable events for 2006 and 2007 outlined earlier and so no comment can be made about their magnitude compared to past extreme events.*

The signal from the precipitation indices is restricted to the eastern parts of China due to limited station coverage and a shorter decorrelation length scale for these indices (see the methodology section for details). Over the analysed period (1960-2009), using the GHCND dataset as shown in Figure 5, overall the signal for the total precipitation is mixed. There are increasing precipitation totals in the northeast and southeast but decreases centrally. Confidence is low in these signals for the most part. The increase in total precipitation in the south east agrees with the results of Hu et al. (2003) and You et al. (2010). The data presented here have poor coverage in the west and north, preventing any comparisons being made in these regions.

There is a more coherent pattern to the trends in the number of continuous dry days, with the central and north-eastern regions showing a clear decrease with high confidence, agreeing with the study of You et al. (2010). However the number of stations present within these grid boxes is on the whole small.

Recent studies have found some evidence to suggest that annual total precipitation is increasing, as are days with heavy precipitation and a decrease in consecutive dry days. The greatest increases in precipitation have been found in the Yangtze River basin, south-eastern and north-western China, with changes of up to 30%, whilst decreases in precipitation are observed in the Yellow River Basin and in northern China (You et al., 2010; Hu et al., 2003). The strong variation in seasonal rainfall across much of southern and eastern China has weakened. Extreme hazard events, such as floods and mudslides, have increased in frequency, often as a result of rapidly melting glaciers producing large quantities of melt water (Hu et al., 2003).

Storms

Storms can be very hazardous to all sectors of society. They can be small with localised impacts or spread across multiple states. There is no systematic observational analysis included for storms because, despite recent progress (Peterson et al., 2011; Cornes & Jones, 2011), wind data are not yet adequate for worldwide robust analysis (see methodology section). Further progress awaits studies of the more reliable barometric pressure data through the new 20th Century Reanalysis (Compo et al., 2011) and its planned successors.

Table 3 shows selected extreme events since 2000 that are reported in WMO Statements on Status of the Global Climate and/or BAMS State of the Climate reports. Tropical Storm Bilis which made landfall in China in July 2006 is highlighted below as an example of a recent storm event which affected China.

Year	Month	Event	Details	Source
2000	Aug	Storm	Typhoon Bilis	WMO (2001)
2000	Oct	Storm	Typhoon Bebinca	WMO (2001)
2001	Jul	Storm	Typhoon Toraji	WMO (2002)
2001	Jul	Storm	Typhoon Utor	WMO (2002)
2003	Jul	Storm	Typhoon Imbudo	WMO (2004)
2003		Storm	Typhoon Krovanh - 176 km/h peak winds in China.	WMO (2004)
2004		Storm	Typhoon Rananim was the strongest typhoon to affect Zhejiang Province in China since 1956. It caused over US$ 2 billion in damage and 169 deaths.	WMO (2005)
2005	Jul	Storm	Typhoon Haitang made landfall in south-east China	WMO (2006)
2005	Aug	Storm	Typhoon Talim made landfall in south-east China with wind speeds of 195 km/h. At least 150 deaths and serious damage.	WMO (2006)
2006	May	Storm	Typhoon Chanchu was the strongest May hurricane to enter the China sea causing over 50 deaths.	WMO (2007)
2006	Jul	Storm	Tropical Storm Bilis only reached tropical storm intensity, but was responsible for 672 deaths in China and over US$2.5 billion in economic losses due to very heavy rain, flooding, and landslides.	BAMS (Camargo, 2007)
2006	Aug	Storm	Typhoon Saomai had maximum winds at landfall of 260 km/h and was the most powerful typhoon to strike China in 50 years.	WMO (2007)
2007	Oct	Storm	Typhoon Krosa made landfall in south-east China with maximum winds of 162 km/h, the strongest typhoon in this area during the 2007 season.	WMO (2008)
2008	Apr	Storm	Typhoon Neoguri recorded maximum winds of 175 km/h. It was the earliest typhoon to strike China on record.	WMO (2009)
2008	Jun	Storm	Typhoon Fengshen recorded maximum winds of 205 km/h.	WMO (2009)
2008	Sep	Storm	Typhoon Hagupit recorded maximum winds of 220 km/h. It was the worst typhoon to hit China's Guangdong province in more than a decade.	WMO (2009)
2009	Jun	Storms	Violent storms across central China destroyed nearly 9,800 homes and caused up to US$ 39 million in agricultural losses.	WMO (2010)
2009	Aug	Storm	Typhoon Morakot recorded maximum winds of 155 km/h. The deadliest typhoon to hit Taiwan since records began. It caused the worst flooding in 50 years on the island, destroyed over 10,000 homes, caused over 600 deaths and severe damage to agriculture and infrastructure.	WMO (2010)
2010	Oct	Storm	Typhoon Megi recorded maximum winds of 290 km/h. It was the most powerful tropical cyclone in the world since 2005 and strongest in the Western North Pacific since 1983.	WMO (2011)

Table 3. *Extreme storm events reported in WMO Statements on Status of the Global Climate and/or BAMS State of the Climate reports since 2000.*

Recent storm events

Tropical Storm Bilis, July 2006

Bilis made landfall in China on 14th July and, although only reaching tropical storm intensity, was responsible for 672 deaths in China and over US$2.5 billion in economic losses due to very heavy rain, flooding, and landslides (Camargo, 2007). The BBC reported that the Chinese government evacuated over quarter of a million people from the southern province of Fujian in preparation for the storms arrival (BBC, 2006a). There was disruption to transport links and in Guangdong province flooding cut the main Beijing-Guangzhou railway line, stranding thousands of passengers (BBC, 2006b).

Summary

The main features seen in observed climate over China from this analysis are:

- There has been widespread warming over China over the period 1960 to 2010 with greater warming in winter then summer.
- There has been a strong decrease in the frequency of cool nights since 1960 and an increase in the frequency of warm nights.
- There has been a general increase in winter temperatures averaged over the country as a result of human influence on climate, making the occurrence of mild winter temperatures more frequent and cold winter temperatures less frequent.
- Recent studies have found some evidence to suggest that annual total precipitation over China is increasing, as are days with heavy precipitation. Our analysis of trends in the number of continuous dry days, shows a decreasing pattern in the central and north-eastern regions of China.

Methodology annex

Recent, notable extremes

In order to identify what is meant by 'recent' events the authors have used the period since 1994, when WMO Status of the Global Climate statements were available to the authors. However, where possible, the most notable events during the last 10 years have been chosen as these are most widely reported in the media, remain closest to the forefront of the memory of the country affected, and provide an example likely to be most relevant to today's society. By 'notable' the authors mean any event which has had significant impact either in terms of cost to the economy, loss of life, or displacement and long term impact on the population. In most cases the events of largest impact on the population have been chosen, however this is not always the case.

Tables of recent, notable extreme events have been provided for each country. These have been compiled using data from the World Meteorological Organisation (WMO) Annual Statements on the Status of the Global Climate. This is a yearly report which includes contributions from all the member countries, and therefore represents a global overview of events that have had importance on a national scale. The report does not claim to capture all events of significance, and consistency across the years of records available is variable. However, this database provides a concise yet broad account of extreme events per country. This data is then supplemented with accounts from the monthly National Oceanic and Atmospheric Administration (NOAA) State of the Climate reports which outline global extreme events of meteorological significance.

We give detailed examples of heat, precipitation and storm extremes for each country where these have had significant impact. Where a country is primarily affected by precipitation or heat extremes this is where our focus has remained. An account of the impact on human life, property and the economy has been given, based largely on media reporting of events, and official reports from aid agencies, governments and meteorological organisations. Some data has also been acquired from the Centre for Research on Epidemiological Disasters (CRED) database on global extreme events. Although media reports are unlikely to be completely accurate, they do give an indication as to the perceived impact of an extreme event, and so are useful in highlighting the events which remain in the national psyche.

Our search for data has not been exhaustive given the number of countries and events included. Although there are a wide variety of sources available, for many events, an official account is not available. Therefore figures given are illustrative of the magnitude of impact only (references are included for further information on sources). It is also apparent that the reporting of extreme events varies widely by region, and we have, where possible, engaged with local scientists to better understand the impact of such events.

The aim of the narrative for each country is to provide a picture of the social and economic vulnerability to the current climate. Examples given may illustrate the impact that any given extreme event may have and the recovery of a country from such an event. This will be important when considering the current trends in climate extremes, and also when examining projected trends in climate over the next century.

Observational record

In this section we outline the data sources which were incorporated into the analysis, the quality control procedure used, and the choices made in the data presentation. As this report is global in scope, including 23 countries, it is important to maintain consistency of methodological approach across the board. For this reason, although detailed datasets of extreme temperatures, precipitation and storm events exist for various countries, it was not possible to obtain and incorporate such a varied mix of data within the timeframe of this project. Attempts were made to obtain regional daily temperature and precipitation data from known contacts within various countries with which to update existing global extremes databases. No analysis of changes in storminess is included as there is no robust historical analysis of global land surface winds or storminess currently available.

Analysis of seasonal mean temperature

Mean temperatures analysed are obtained from the CRUTEM3 global land-based surface-temperature data-product (Brohan et al. 2006), jointly created by the Met Office Hadley Centre and Climatic Research Unit at the University of East Anglia. CRUTEM3 comprises of more than 4000 weather station records from around the world. These have been averaged together to create 5° by 5° gridded fields with no interpolation over grid boxes that do not contain stations. Seasonal averages were calculated for each grid box for the 1960 to 2010 period and linear trends fitted using the median of pairwise slopes (Sen 1968; Lanzante 1996). This method finds the slopes for all possible pairs of points in the data, and takes their median. This is a robust estimator of the slope which is not sensitive to outlying points.

High confidence is assigned to any trend value for which the 5th to 95th percentiles of the pairwise slopes are of the same sign as the trend value and thus inconsistent with a zero trend.

Analysis of temperature and precipitation extremes using indices

In order to study extremes of climate a number of indices have been created to highlight different aspects of severe weather. The set of indices used are those from the World Climate Research Programme (WCRP) Climate Variability and Predictability (CLIVAR) Expert Team on Climate Change Detection and Indices (ETCCDI). These 27 indices use daily rainfall and maximum and minimum temperature data to find the annual (and for a subset of the indices, monthly) values for, e.g., the 'warm' days where daily maximum temperature exceeds the 90th percentile maximum temperature as defined over a 1961 to 1990 base period. For a full list of the indices we refer to the website of the ETCCDI (http://cccma.seos.uvic.ca/ETCCDI/index.shtml).

Index	Description	Shortname	Notes
Cool night frequency	Daily minimum temperatures lower than the 10th percentile daily minimum temperature using the base reference period 1961-1990	TN10p	---
Warm night frequency	Daily minimum temperatures higher than the 90th percentile daily minimum temperature using the base reference period 1961-1990	TN90p	---
Cool day frequency	Daily maximum temperatures lower than the 10th percentile daily maximum temperature using the base reference period 1961-1990	TX10p	---
Warm day frequency	Daily maximum temperatures higher than the 90th percentile daily maximum temperature using the base reference period 1961-1990	TX90p	---
Dry spell duration	Maximum duration of continuous days within a year with rainfall <1mm	CDD	Lower data coverage due to the requirement for a 'dry spell' to be at least 6 days long resulting in intermittent temporal coverage
Wet spell duration	Maximum duration of continuous days with rainfall >1mm for a given year	CWD	Lower data coverage due to the requirement for a 'wet spell' to be at least 6 days long resulting in intermittent temporal coverage
Total annual precipitation	Total rainfall per year	PRCPTOT	---

Table 4. *Description of ETCCDI indices used in this document.*

A previous global study of the change in these indices, containing data from 1951-2003 can be found in Alexander et al. 2006, (HadEX; see http://www.metoffice.gov.uk/hadobs/hadex/). In this work we aimed to update this analysis to the present day where possible, using the most recently available data. A subset of the indices is used here because they are most easily related to extreme climate events (Table 4).

Use of HadEX for analysis of extremes

The HadEX dataset comprises all 27 ETCCDI indices calculated from station data and then smoothed and gridded onto a 2.5° x 3.75° grid, chosen to match the output from the Hadley Centre suite of climate models. To update the dataset to the present day, indices are calculated from the individual station data using the RClimDex/FClimDex software;

developed and maintained on behalf of the ETCCDI by the Climate Research Branch of the Meteorological Service of Canada. Given the timeframe of this project it was not possible to obtain sufficient station data to create updated HadEX indices to present day for a number of countries: Brazil; Egypt; Indonesia; Japan (precipitation only); South Africa; Saudi Arabia; Peru; Turkey; and Kenya. Indices from the original HadEX data-product are used here to show changes in extremes of temperature and precipitation from 1960 to 2003. In some cases the data end prior to 2003. Table 5 summarises the data used for each country. Below, we give a short summary of the methods used to create the HadEX dataset (for a full description see Alexander et al. 2006).

To account for the uneven spatial coverage when creating the HadEX dataset, the indices for each station were gridded, and a land-sea mask from the HadCM3 model applied. The interpolation method used in the gridding process uses a decorrelation length scale (DLS) to determine which stations can influence the value of a given grid box. This DLS is calculated from the e-folding distance of the individual station correlations. The DLS is calculated separately for five latitude bands, and then linearly interpolated between the bands. There is a noticeable difference in spatial coverage between the indices due to these differences in decorrelation length scales. This means that there will be some grid-box data where in fact there are no stations underlying it. Here we apply black borders to grid-boxes where at least 3 stations are present to denote greater confidence in representation of the wider grid-box area there. The land-sea mask enables the dataset to be used directly for model comparison with output from HadCM3. It does mean, however, that some coastal regions and islands over which one may expect to find a grid-box are in fact empty because they have been treated as sea.

Data sources used for updates to the HadEX analysis of extremes

We use a number of different data sources to provide sufficient coverage to update as many countries as possible to present day. These are summarised in Table 2. In building the new datasets we have tried to use exactly the same methodology as was used to create the original HadEX to retain consistency with a product that was created through substantial international effort and widely used, but there are some differences, which are described in the next section.

Wherever new data have been used, the geographical distributions of the trends were compared to those obtained from HadEX, using the same grid size, time span and fitting method. If the pattern of the trends in the temperature or precipitation indices did not match that from HadEX, we used the HadEX data despite its generally shorter time span.

Differences in the patterns of the trends in the indices can arise because the individual stations used to create the gridded results are different from those in HadEX, and the quality control procedures used are also very likely to be different. Countries where we decided to use HadEX data despite the existence of more recent data are Egypt and Turkey.

GHCND:

The Global Historical Climate Network Daily data has near-global coverage. However, to ensure consistency with the HadEX database, the GHCND stations were compared to those stations in HadEX. We selected those stations which are within 1500m of the stations used in the HadEX database and have a high correlation with the HadEX stations. We only took the precipitation data if its r>0.9 and the temperature data if one of its r-values >0.9. In addition, we required at least 5 years of data beyond 2000. These daily data were then converted to the indices using the *fclimdex* software.

ECA&D and SACA&D:

The European Climate Assessment and Dataset and the Southeast Asian Climate Assessment and Dataset data are pre-calculated indices comprising the core 27 indices from the ETCCDI as well as some extra ones. We kindly acknowledge the help of Albert Klein Tank, the KNMI[1] and the BMKG[2] for their assistance in obtaining these data.

Mexico:

The station data from Mexico has been kindly supplied by the SMN[3] and Jorge Vazquez. These daily data were then converted to the required indices using the *Fclimdex* software. There are a total of 5298 Mexican stations in the database. In order to select those which have sufficiently long data records and are likely to be the most reliable ones we performed a cross correlation between all stations. We selected those which had at least 20 years of data post 1960 and have a correlation with at least one other station with an *r*-value >0.95. This resulted in 237 stations being selected for further processing and analysis.

[1] Koninklijk Nederlands Meteorologisch Instituut – The Royal Netherlands Meteorological Institute

[2] Badan Meteorologi, Klimatologi dan Geofisika – The Indonesian Meteorological, Climatological and Geophysical Agency

[3] Servicio Meteorológico Nacional de México – The Mexican National Meteorological Service

Indian Gridded:

The India Meteorological Department provided daily gridded data (precipitation 1951-2007, temperature 1969-2009) on a 1° x 1° grid. These are the only gridded daily data in our analysis. In order to process these in as similar a way as possible the values for each grid were assumed to be analogous to a station located at the centre of the grid. We keep these data separate from the rest of the study, which is particularly important when calculating the decorrelation length scale, which is on the whole larger for these gridded data.

Country	**Region box** (red dashed boxes in Fig. 1 and on each map at beginning of chapter)	**Data source** (T = temperature, P = precipitation)	**Period of data coverage** (T = temperature, P = precipitation)	**Indices included** (see Table 4 for details)	**Temporal resolution available**	**Notes**
Argentina	73.125 to 54.375 ^{o} W, 21.25 to 56.25 ^{o} S	Matilde Rusticucci (T,P)	1960-2010 (T,P)	TN10p, TN90p, TX10p, TX90p, PRCPTOT, CDD, CWD	annual	
Australia	114.375 to 155.625 ^{o} E, 11.25 to 43.75 ^{o} S	GHCND (T,P)	1960-2010 (T,P)	TN10p, TN90p, TX10p, TX90p, PRCPTOT, CDD, CWD	monthly, seasonal and annual	Land-sea mask has been adapted to include Tasmania and the area around Brisbane
Bangladesh	88.125 to 91.875 ^{o} E, 21.25 to 26.25 ^{o} N	Indian Gridded data (T,P)	1960-2007 (P), 1970-2009 (T)	TN10p, TN90p, TX10p, TX90p, PRCPTOT, CDD, CWD	monthly, seasonal and annual	Interpolated from Indian Gridded data
Brazil	73.125 to 31.875 ^{o} W, 6.25 ^{o} N to 33.75 ^{o} S	HadEX (T,P)	1960-2000 (P) 2002 (T)	TN10p, TN90p, TX10p, TX90p, PRCPTOT, CDD, CWD	annual	Spatial coverage is poor
China	73.125 to 133.125 ^{o} E, 21.25 to 53.75 ^{o} N	GHCND (T,P)	1960-1997 (P) 1960-2003 (T_{min}) 1960-2010 (T_{max})	TN10p, TN90p, TX10p, TX90p, PRCPTOT, CDD, CWD	monthly, seasonal and annual	Precipitation has very poor coverage beyond 1997 except in 2003-04, and no data at all in 2000-02, 2005-11
Egypt	24.375 to 35.625 ^{o} E, 21.25 to 31.25 ^{o} N	HadEX (T,P)	No data	TN10p, TN90p, TX10p, TX90p, PRCPTOT,	annual	There are no data for Egypt so all grid-box values have been interpolated from stations in Jordan, Israel, Libya and Sudan
France	5.625 ^{o} W to 9.375 ^{o} E, 41.25 to 51.25 ^{o} N	ECA&D (T,P)	1960-2010 (T,P)	TN10p, TN90p, TX10p, TX90p, PRCPTOT, CDD, CWD	monthly, seasonal and annual	

Germany	5.625 to 16.875 ^{o} E, 46.25 to 56.25 ^{o} N	ECA&D (T,P)	1960-2010 (T,P)	TN10p, TN90p, TX10p, TX90p, PRCPTOT, CDD, CWD	monthly, seasonal and annual	
India	69.375 to 99.375 ^{o} E, 6.25 to 36.25 ^{o} N	Indian Gridded data (T,P)	1960-2003 (P), 1970-2009 (T)	TN10p, TN90p, TX10p, TX90p, PRCPTOT, CDD, CWD	monthly, seasonal and annual	
Indonesia	95.625 to 140.625 ^{o} E, 6.25 ^{o} N to 11.25 ^{o} S	HadEX (T,P)	1968-2003 (T,P)	TN10p, TN90p, TX10p, TX90p, PRCPTOT,	annual	Spatial coverage is poor
Italy	5.625 to 16.875 ^{o} E, 36.25 to 46.25 ^{o} N	ECA&D (T,P)	1960-2010 (T,P)	TN10p, TN90p, TX10p, TX90p, PRCPTOT, CDD, CWD	monthly, seasonal and annual	Land-sea mask has been adapted to improve coverage of Italy
Japan	129.375 to 144.375 ^{o} E, 31.25 to 46.25 ^{o} N	HadEX (P) GHCND (T)	1960-2003 (P) 1960-2000 (T_{min}) 1960-2010 (T_{max})	TN10p, TN90p, TX10p, TX90p, PRCPTOT,	monthly, seasonal and annual (T), annual (P)	
Kenya	31.875 to 43.125 ^{o} E, 6.25 ^{o} N to 6.25 ^{o} S	HadEX (T,P)	1960-1999 (P)	TN10p, TN90p, TX10p, TX90p, PRCPTOT	annual	There are no temperature data for Kenya and so grid-box values have been interpolated from neighbouring Uganda and the United Republic of Tanzania. Regional averages include grid-boxes from outside Kenya that enable continuation to 2003
Mexico	118.125 to 88.125 ^{o} W, 13.75 to 33.75 ^{o} N	Raw station data from the Servicio Meteorológico Nacional (SMN) (T,P)	1960-2009 (T,P)	TN10p, TN90p, TX10p, TX90p, PRCPTOT, CDD, CWD	monthly, seasonal and annual	237/5298 stations selected. Non uniform spatial coverage. Drop in T and P coverage in 2009.
Peru	84.735 to 65.625 ^{o} W, 1.25 ^{o} N to 18.75 ^{o} S	HadEX (T,P)	1960-2002 (T,P)	TN10p, TN90p, TX10p, TX90p, PRCPTOT, CDD, CWD	annual	Intermittent coverage in TX90p, CDD and CWD

Russia	West Russia 28.125 to 106.875 ° E, 43.75 to 78.75 ° N, East Russia 103.125 to 189.375 ° E, 43.75 to 78.75 ° N	ECA&D (T,P)	1960-2010 (T,P)	TN10p, TN90p, TX10p, TX90p, PRCPTOT, CDD, CWD	monthly, seasonal and annual	Country split for presentation purposes only.
Saudi Arabia	31.875 to 54.375 ° E, 16.25 to 33.75 ° N	HadEX (T,P)	1960-2000 (T,P)	TN10p, TN90p, TX10p, TX90p, PRCPTOT	annual	Spatial coverage is poor
South Africa	13.125 to 35.625 ° W, 21.25 to 36.25 ° S	HadEX (T,P)	1960-2000 (T,P)	TN10p, TN90p, TX10p, TX90p, PRCPTOT, CDD, CWD	annual	---
Republic of Korea	125.625 to 129.375 ° E, 33.75 to 38.75 ° N	HadEX (T,P)	1960-2003 (T,P)	TN10p, TN90p, TX10p, TX90p, PRCPTOT, CDD	annual	There are too few data points for CWD to calculate trends or regional timeseries
Spain	9.375 ° W to 1.875 ° E, 36.25 to 43.75 ° N	ECA&D (T,P)	1960-2010 (T,P)	TN10p, TN90p, TX10p, TX90p, PRCPTOT, CDD, CWD	monthly, seasonal and annual	
Turkey	24.375 to 46.875 ° E, 36.25 to 43.75 ° N	HadEX (T,P)	1960-2003 (T,P)	TN10p, TN90p, TX10p, TX90p, PRCPTOT, CDD, CWD	annual	Intermittent coverage in CWD and CDD with no regional average beyond 2000
United Kingdom	9.375 ° W to 1.875 ° E, 51.25 to 58.75 ° N	ECA&D (T,P)	1960-2010 (T,P)	TN10p, TN90p, TX10p, TX90p, PRCPTOT, CDD, CWD	monthly, seasonal and annual	
United States of America	125.625 to 65.625 ° W, 23.75 to 48.75 ° N	GHCND (T,P)	1960-2010 (T,P)	TN10p, TN90p, TX10p, TX90p, PRCPTOT, CDD, CWD	monthly, seasonal and annual	

Table 5. *Summary of data used for each country.*

Quality control and gridding procedure used for updates to the HadEX analysis of extremes

In order to perform some basic quality control checks on the index data, we used a two-step process on the indices. Firstly, internal checks were carried out, to remove cases where the 5 day rainfall value is less than the 1 day rainfall value, the minimum T_min is greater than the minimum T_max and the maximum T_min is greater than the maximum T_max. Although these are physically impossible, they could arise from transcription errors when creating the daily dataset, for example, a misplaced minus sign, an extra digit appearing in the record or a column transposition during digitisation. During these tests we also require that there are at least 20 years of data in the period of record for the index for that station, and that some data is found in each decade between 1961 and 1990, to allow a reasonable estimation of the climatology over that period.

Weather conditions are often similar over many tens of kilometres and the indices calculated in this work are even more coherent. The correlation coefficient between each station-pair combination in all the data obtained is calculated for each index (and month where appropriate), and plotted as a function of the separation. An exponential decay curve is fitted to the data, and the distance at which this curve has fallen by a factor 1/*e* is taken as the decorrelation length scale (DLS). A DLS is calculated for each dataset separately. For the GHCND, a separate DLS is calculated for each hemisphere. We do not force the fitted decay curve to show perfect correlation at zero distance, which is different to the method employed when creating HadEX. For some of the indices in some countries, no clear decay pattern was observed in some data sets or the decay was so slow that no value for the DLS could be determined. In these cases a default value of 200km was used.

We then perform external checks on the index data by comparing the value for each station with that of its neighbours. As the station values are correlated, it is therefore likely that if one station measures a high value for an index for a given month, its neighbours will also be measuring high. We exploit this coherence to find further bad values or stations as follows. Although raw precipitation data shows a high degree of localisation, using indices which have monthly or annual resolution improves the coherence across wider areas and so this neighbour checking technique is a valid method of finding anomalous stations.

We calculate a climatology for each station (and month if appropriate) using the mean value for each index over the period 1961-1990. The values for each station are then anomalised using this climatology by subtracting this mean value from the true values, so that it is clear if the station values are higher or lower than normal. This means that we do not need to take

differences in elevation or topography into account when comparing neighbours, as we are not comparing actual values, but rather deviations from the mean value.

All stations which are within the DLS distance are investigated and their anomalised values noted. We then calculate the weighted median value from these stations to take into account the decay in the correlation with increasing distance. We use the median to reduce the sensitivity to outliers.

If the station value is greater than 7.5 median-absolute-deviations away from the weighted median value (this corresponds to about 5 standard deviations if the distribution is Gaussian, but is a robust measure of the spread of the distribution), then there is low confidence in the veracity of this value and so it is removed from the data.

To present the data, the individual stations are gridded on a 3.75^{o} x 2.5^{o} grid, matching the output from HadCM3. To determine the value of each grid box, the DLS is used to calculate which stations can reasonably contribute to the value. The value of each station is then weighted using the DLS to obtain a final grid box value. At least three stations need to have valid data and be near enough (within 1 DLS of the gridbox centre) to contribute in order for a value to be calculated for the grid point. As for the original HadEX, the HadCM3 land-sea mask is used. However, in three cases the mask has been adjusted as there are data over Tasmania, eastern Australia and Italy that would not be included otherwise (Figure 6).

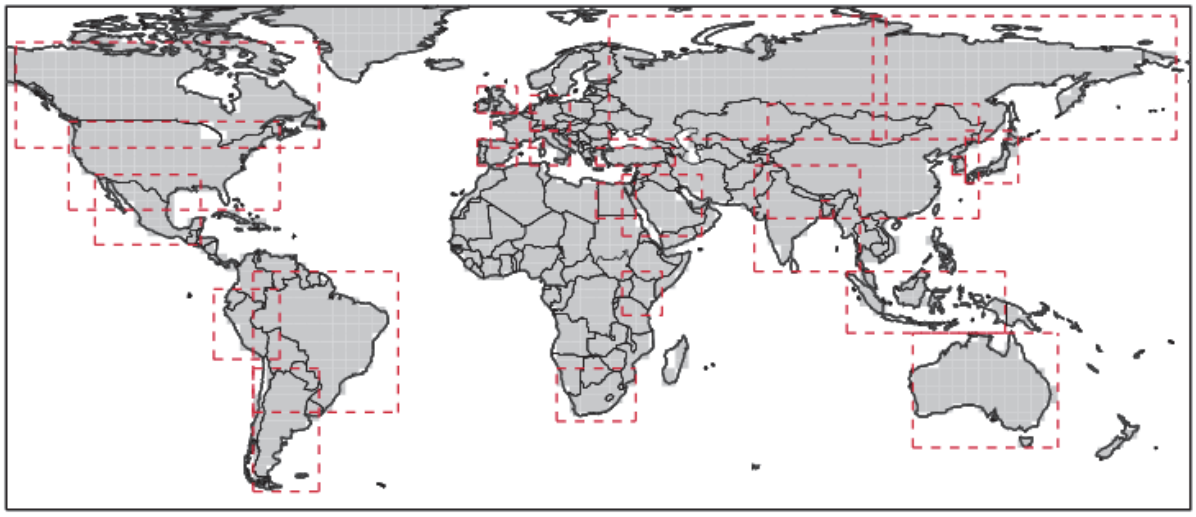

Figure 6. *Land-sea mask used for gridding the station data and regional areas allocated to each country as described in Table 5.*

Presentation of extremes of temperature and precipitation

Indices are displayed as regional gridded maps of decadal trends and regional average time-series with decadal trends where appropriate. Trends are fitted using the median of pairwise slopes method (Sen 1968, Lanzante 1996). Trends are considered to be significantly different from a zero trend if the 5th to 95th percentiles of the pairwise slopes do not encompass zero. This is shown by a black dot in the centre of the grid-box or by a solid line on time-series plots. This infers that there is high confidence in the sign (positive or negative) of the sign. Confidence in the trend magnitude can be inferred by the spread of the 5th to 95th percentiles of the pairwise slopes which is given for the regional average decadal trends. Trends are only calculated when there are data present for at least 50% of years in the period of record and for the updated data (not HadEX) there must be at least one year in each decade.

Due to the practice of data-interpolation during the gridding stage (using the DLS) there are values for some grid boxes when no actually station lies within the grid box. There is more confidence in grid boxes for which there are underlying data. For this reason, we identify those grid boxes which contain at least 3 stations by a black contour line on the maps. The DLS differs with region, season and index which leads to large differences in the spatial coverage. The indices, by their nature of being largely threshold driven, can be intermittent over time which also effects spatial and temporal coverage (see Table 1).

Each index (and each month for the indices for which there is monthly data) has a different DLS, and so the coverage between different indices and datasets can be different. The restrictions on having at least 20 years of data present for each input station, at least 50% of years in the period of record and at least one year in each decade for the trending calculation, combined with the DLS, can restrict the coverage to only those regions with a dense station network reporting reliably.

Each country has a rectangular region assigned as shown by the red dashed box on the map in Figure 1 and listed in Table 2, which is used for the creation of the regional average. This is sometimes identical to the attribution region shown in grey on the map in Figure 1. This region is again shown on the maps accompanying the time series of the regional averages as a reminder of the region and grid boxes used in the calculation. Regional averages are created by weighting grid box values by the cosine of their grid box centre latitude. To ensure consistency over time a regional average is only calculated when there are a sufficient number of grid boxes present. The full-period median number of grid-boxes present is calculated. For regions with a median of more than six grid-boxes there must be at least 80%

of the median number of grid boxes present for any one year to calculate a regional average. For regions with six or fewer median grid boxes this is relaxed to 50%. These limitations ensure that a single station or grid box which has a longer period of record than its neighbours cannot skew the timeseries trend. So sometimes there may be grid-boxes present but no regional average time series. The trends for the regional averages are calculated in the same way as for the individual grid boxes, using the median of pairwise slopes method (Sen 1968, Lanzante 1996). Confidence in the trend is also determined if the 5^{th} to 95^{th} percentiles of the pairwise slopes are of the same sign and thus inconsistent with a zero trend. As well as the trend in quantity per decade, we also show the full change in the quantity from 1960 to 2010 that this fitted linear trend implies.

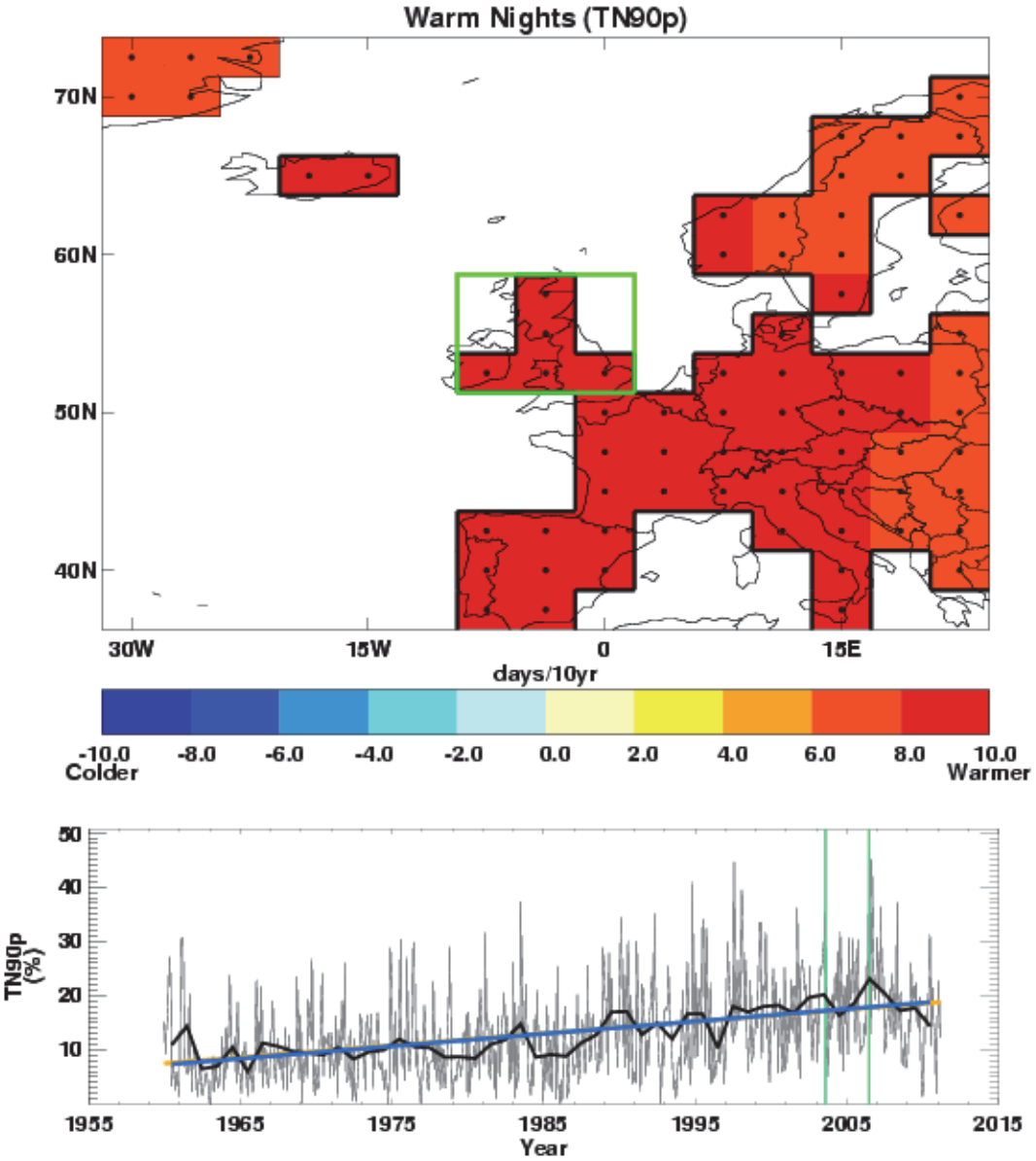

Monthly: 2.20% per decade (1.80 to 2.61)
Total change of 11.02% from 1960 to 2011 (9.00% to 13.06%)

Annual: 2.28% per decade (1.69 to 2.86)
Total change of 11.41% from 1960 to 2010 (8.43% to 14.28%)

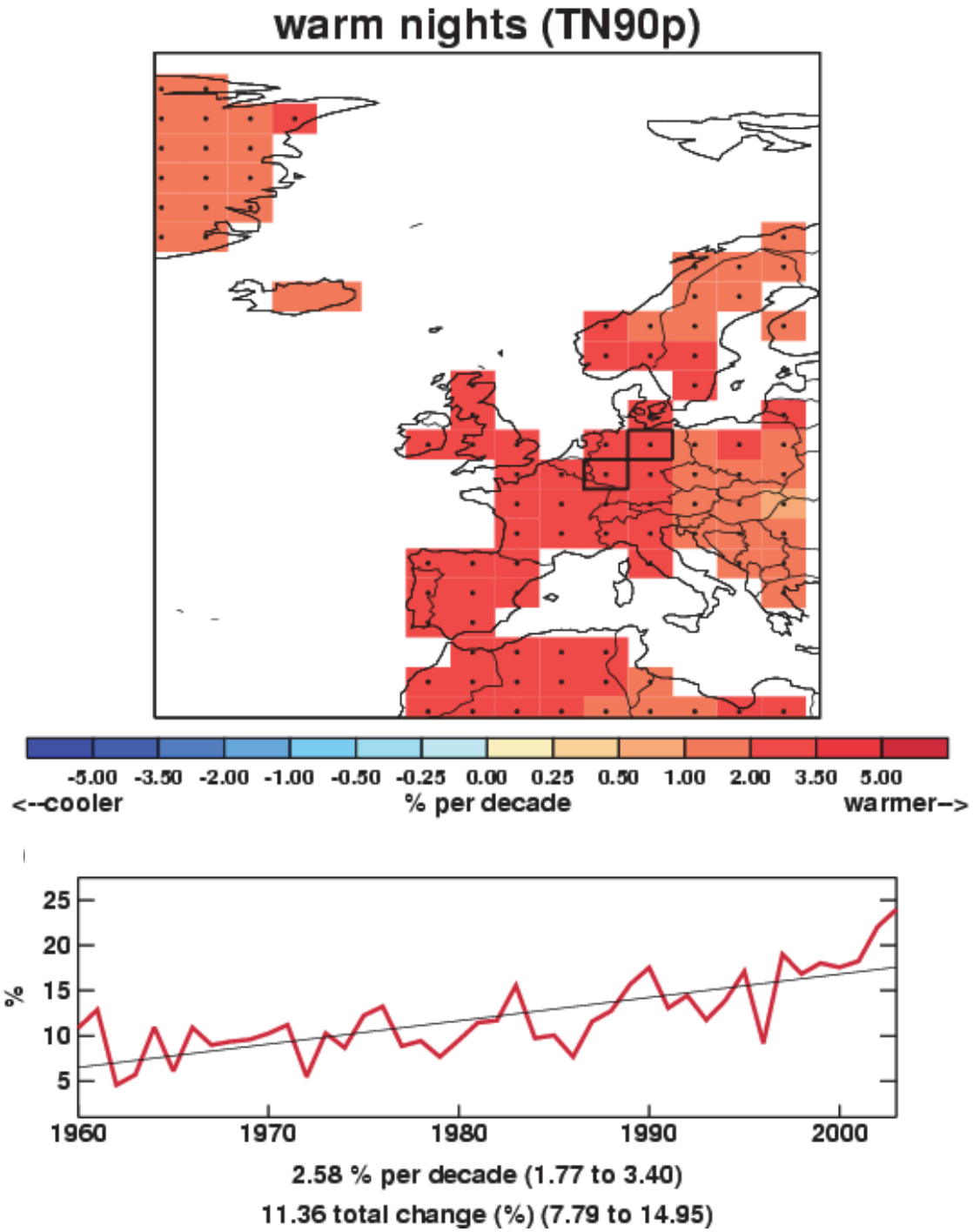

Figure 7. *Examples of the plots shown in the data section. Left: From ECA&D data between 1960-2010 for the number of warm nights, and Right: from HadEX data (1960-2003) for the total precipitation. A full explanation of the plots is given in the text below.*

The results are presented in the form of a map and a time series for each country and index. The map shows the grid box decadal trend in the index over the period for which there are data. High confidence, as determined above, is shown by a black dot in the grid box centre. To show the variation over time, the values for each year (and month if available) are shown in a time series for a regional average. The values of the indices have been normalised to a

base period of 1961-1990 (except the Indian gridded data which use a 1971 to 1990 period), both in HadEX and in the new data acquired for this project. Therefore, for example, the percentage of nights exceeding the 90th percentile for a temperature is 10% for that period.

There are two influences on whether a grid box contains a value or not – the land-sea mask, and the decorrelation length scale. The land-sea mask is shown in Figure 6. There are grid boxes which contain some land but are mostly sea and so are not considered. The decorrelation length scale sets the maximum distance a grid box can be from stations before no value is assigned to it. Grid boxes containing three or more stations are highlighted by a thick border. This indicates regions where the value shown is likely to be more representative of the grid box area mean as opposed to a single station location.

On the maps for the new data there is a box indicating which grid boxes have been extracted to calculate the area average for the time series. This box is the same as shown in Figure 1 at the beginning of each country's document. These selected grid boxes are combined using area (cosine) weighting to calculate the regional average (both annual [thick lines] and monthly [thin lines] where available). Monthly (orange) and annual (blue) trends are fitted to these time series using the method described above. The decadal trend and total change over the period where there are data are shown with 5th to 95th percentile confidence intervals in parentheses. High confidence, as determined above, is shown by a solid line as opposed to a dotted one. The green vertical lines on the time series show the dates of some of the notable events outlined in each section.

Attribution

Regional distributions of seasonal mean temperatures in the 2000s are computed with and without the effect of anthropogenic influences on the climate. The analysis considers temperatures averaged over the regions shown in Figure 8. These are also identified as grey boxes on the maps in Figure 1. The coordinates of the regions are given in Table 6. The methodology combines information from observations and model simulations using the approach originally introduced in Christidis et al., 2010 and later extended in Christidis et al., 2011, where more details can be found. The analysis requires spatial scales greater than about 2,500 km and for that reason the selected regions (Fig.8 and Table 6) are often larger than individual countries, or include several smaller countries in a single region (for example UK, Germany and France are grouped in one region).

Observations of land temperature come from the CRUTEM3 gridded dataset (Brohan et al., 2006) and model simulations from two coupled GCMs, namely the Hadley Centre HadGEM1 model (Martin et al., 2006) and version 3.2 of the MIROC model (K-1 Developers, 2004). The use of two GCMs helps investigate the sensitivity of the results to the model used in the analysis. Ensembles of model simulations from two types of experiments are used to partition the temperature response to external forcings between its anthropogenic and natural components. The first experiment (ALL) simulates the combined effect of natural and anthropogenic forcings on the climate system and the second (ANTHRO) includes anthropogenic forcings only. The difference of the two gives an estimate of the effect of the natural forcings (NAT). Estimates of the effect of internal climate variability are derived from long control simulations of the unforced climate. Distributions of the regional summer mean temperature are computed as follows:

a) A global optimal fingerprinting analysis (Allen and Tett, 1999; Allen and Stott, 2003) is first carried out that scales the global simulated patterns (fingerprints) of climate change attributed to different combinations of external forcings to best match them to the observations. The uncertainty in the scaling that originates from internal variability leads to samples of the scaled fingerprints, i.e. several realisations that are plausibly consistent with the observations. The 2000-2009 decade is then extracted from the scaled patterns and two samples of the decadal mean temperature averaged over the reference region are then computed with and without human influences, which provide the Probability Density Functions (PDFs) of the decadal mean temperature attributable to ALL and NAT forcings.

b) Model-derived estimates of noise are added to the distributions to take into account the uncertainty in the simulated fingerprints.

c) In the same way, additional noise from control model simulations is introduced to the distributions to represent the effect of internal variability in the annual values of the seasonal mean temperatures. The result is a pair of estimated distributions of the annual values of the seasonal mean temperature in the region with and without the effect of human activity on the climate. The temperatures throughout the analysis are expressed as anomalies relative to period 1961-1990.

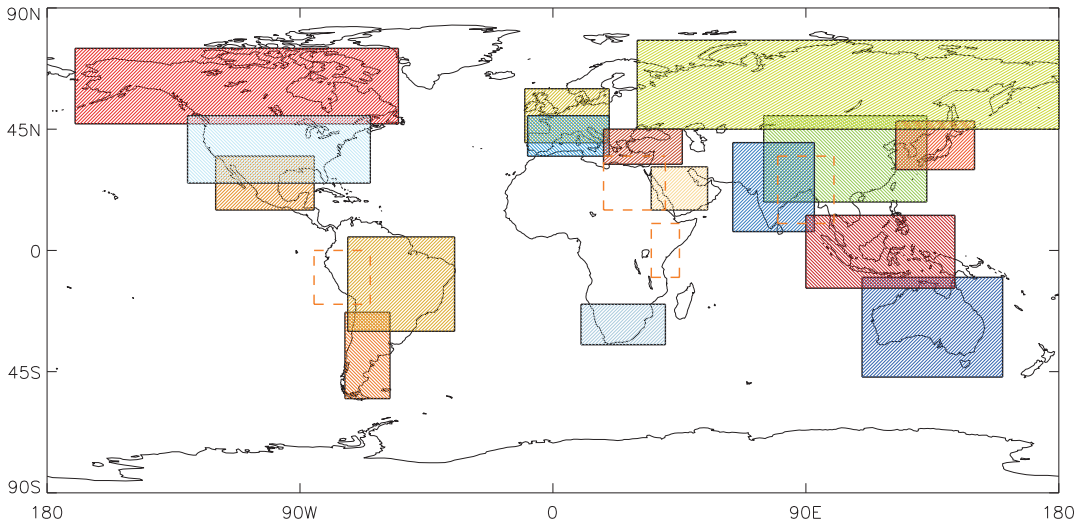

Figure 8. *The regions used in the attribution analysis. Regions marked with dashed orange boundaries correspond to non-G20 countries that were also included in the analysis.*

Region	Region Coordinates
Argentina	74-58W, 55-23S
Australia	110-160E, 47-10S
Bangladesh	80-100E, 10-35N
Brazil	73-35W, 30S-5N
Canada-Alaska	170-55W, 47-75N
China	75-133E, 18-50N
Egypt	18-40E, 15-35N
France-Germany-UK	10W-20E, 40-60N
India	64-93E, 7-40N
Indonesia	90-143E, 14S-13N
Italy-Spain	9W-20E, 35-50N
Japan-Republic of Korea	122-150E, 30-48N
Kenya	35-45E, 10S-10N
Mexico	120-85W, 15-35N
Peru	85-65W, 20-0S
Russia	30-185E, 45-78N
Saudi Arabia	35-55E, 15-31N
South Africa	10-40E, 35-20S
Turkey	18-46E, 32-45N

Table 6. *The coordinates of the regions used in the attribution analysis.*

References

ALEXANDER, L. V., ZHANG. X., PETERSON, T. C., CAESAR, J., GLEASON, B., KLEIN TANK, A. M. G., HAYLOCK, M., COLLINS, D., TREWIN, B., RAHIMZADEH, F., TAGIPOUR, A., RUPA KUMAR, K., REVADEKAR, J., GRIFFITHS, G., VINCENT, L., STEPHENSON, D. B., BURN, J., AGUILAR, E., BRUNET, M., TAYLOR, M., NEW, M., ZHAI, P., RUSTICUCCI, M. and VAZQUEZ-AGUIRRE, J. L. 2006. Global observed changes in daily climate extremes of temperature and precipitation. J. Geophys. Res. 111, D05109. doi:10.1029/2005JD006290

ALLEN, M. R., TETT S. F. B. 1999. Checking for model consistency in optimal fingerprinting. Climate Dynamics 15: 419-434.

ALLEN M. R., STOTT P. A. 2003. Estimating signal amplitudes in optimal fingerprinting, part I: theory. Climate Dynamics 21: 477-491.

BBC NEWS. 2006a. Tropical Storm Bilis takes its final steps. Available online: http://www.bbc.co.uk/weather/world/news/14072006news.shtml accessed on 26 September 2011.

BBC NEWS. 2006b. Chinese storm kills more than 180. Available online: http://news.bbc.co.uk/1/hi/world/asia-pacific/5185314.stm accessed on 26 September 2011.

BBC NEWS. 2007. Flooding in China continues. Available online: http://www.bbc.co.uk/weather/world/news/10062007news.shtml accessed on 26 September 2011.

BROHAN, P., KENNEDY, J.J., HARRIS, I., TETT, S.F.B. and JONES, P.D. 2006. Uncertainty estimates in regional and global observed temperature changes: a new dataset from 1850. J. Geophys. Res. 111, D12106. doi:10.1029/2005JD006548.

CAMARGO S. J. 2007. Western North Pacific Basin in State of the Climate in 2006, Bulletin of the American Meteorological Society 88, S56.

CHRISTIDIS N., STOTT. P A., ZWIERS, F. W., SHIOGAMA, H., NOZAWA, T. 2010. Probabilistic estimates of recent changes in temperature: a multi-scale attribution analysis. Climate Dynamics 34: 1139-1156.

CHRISTIDIS, N., STOTT, P. A., ZWIERS, F. W., SHIOGAMA, H., NOZAWA, T. 2011. The contribution of anthropogenic forcings to regional changes in temperature during the last decade. Climate Dynamics in press.

COMPO, G. P., J.S. WHITAKER, P.D. SARDESHMUKH, N. MATSUI, R.J. ALLAN, X. YIN, B.E. GLEASON, R.S. VOSE, G. RUTLEDGE, P. BESSEMOULIN, S. BRÖNNIMANN, M. BRUNET, R.I. CROUTHAMEL, A.N. GRANT, P.Y. GROISMAN, P.D. JONES, M.C. KRUK, A.C. KRUGER, G.J. MARSHALL, M. MAUGERI, H.Y. MOK, Ø. NORDLI, T.F. ROSS, R.M. TRIGO, X.L. WANG, S.D. WOODRUFF and S.J. WORLEY. 2011. The Twentieth Century Reanalysis Project. Q. J. R.Met.S. 137, 1-28, doi: 10.1002/qj.776.

CORNES, R. C., and P. D. JONES. 2011. An examination of storm activity in the northeast Atlantic region over the 1851–2003 period using the EMULATE gridded MSLP data series. J. Geophys. Res. 116, D16110, doi:10.1029/2011JD016007.

CRED (Centre for Research on the Epidemiology of Disasters) Annual Disaster Statistical Review. 2007. Available online: http://www.cred.be/publication/annual-disaster-statistical-review-numbers-and-trends-2007 accessed 26 September 2011.

CRUZ, R.V., HARASAWA, H., LAL, M., WU, S., ANOKHIN, Y., PUNSALMAA, B., HONDA, Y., JAFARI, M., LI, C. and HUU NINH, N. 2007. Asia. Climate Change 2007: Impacts, Adaptation and Vulnerability. Contribution of Working Group II to the Fourth Assessment Report of the Intergovernmental Panel on Climate Change. M.L. Parry, O.F. Canziani, J.P. Palutikof, P.J. van der Linden and C.E. Hanson, Eds. Cambridge University Press, Cambridge, UK, 469-506.

DURRE, I., MENNE, M.J., GLEASON, B.E., HOUSTON, T.G., VOSE, R.S. 2010. Comprehensive Automated Quality Assurance of Daily Surface Observations. Journal of Applied Meteorology and Climatology 49, 8, 1615-1633

GROVER-KOPEC, E. K. 2004. China in State of the Climate in 2003. Bulletin of the American Meteorological Society 85, S54.

GUO, Y., Y. SAKAI, S. ZHAO, X. WANG, and H. LEE. 2009. East Asia in State of the Climate in 2008. Bulletin of the American Meteorological Society 90, S157.

HU, Z. Z., YANG, S. and WU, R. 2003. Long-term climate variations in China and global warming signals. J. Geophys. Res. 108, 4614. doi:10.1029/2003JD003651.

K-1 MODEL DEVELOPERS. 2004. K-1 coupled GCM (MIROC) description, K-1 Tech Rep, H

Hasumi and S Emori (eds), Centre for Clim Sys Res, Univ of Tokyo.

LANZANTE, J. R. 1996. Resistant, robust and non-parametric techniques for the analysis of climate data: theory and examples, including applications to historical radiosonde station data. Int. J. Clim. 16, 1197–226.

MARTIN G.M., RINGER. M. A., POPE V. D., JONES, A., DEARDEN, C., HINTON, T. 2006. The physical properties of the atmosphere in the new Hadley Centre Global Environmental Model (HadGEM1). Part I: Model description and global climatology. J. Clim. 19: 1274-1301

PETERSON, T.C., VAUTARD, R., McVICAR, T.R., THÉPAUT, J-N. and BERRISFORD, P. 2011. Global Climate, Surface Winds over Land in State of the Climate 2010. Bulletin of the American Meteorological Society 92 (6), S57.

REN, F. and G. GAO. 2006. China in State of the Climate in 2005. Bulletin of the American Meteorological Society 87, S74

ROGERS, M., S. SENSOY, O. BULYGINA, F. RAHIMZADEH, Y. GUO, S. ATTAHER, and A. B. WATKINS. 2009. The Eurasian cold event of January 2008 in State of the Climate in 2008. Bulletin of the American Meteorological Society 90, S156

SANCHEZ-LUGO, A., KENNEDY, J.J. and BERRISFORD, P. 2011. Global Climate Surface Temperatures in State of the Climate 2010. Bulletin of the American Meteorological Society 92 (6), S36-S37.

SEN, P. K. 1968. Estimates of the regression coefficient based on Kendall's tau. J. Am. Stat. Assoc. 63, 1379–89.

SUDA, K., X. ZOU, X. LIANG, Y. CHEN, Y. GUO, J.-E. KIM, and P. GOMBOLUUDEV. 2008. East Asia in State of the Climate in 2007. Bulletin of the American Meteorological Society 89, S133.

WANG, L. and D. YE. 2007. China in State of the Climate in 2006. Bulletin of the American Meteorological Society 88, S97.

WMO WORLD METEOROLOGICAL ORGANIZATION. 2001. Statement on Status of the Global Climate in 2000, WMO-No. 920. http://www.wmo.int/pages/prog/wcp/wcdmp/statement/wmostatement_en.html

WMO WORLD METEOROLOGICAL ORGANIZATION. 2002. Statement on Status of the Global Climate in 2001, WMO-No. 940. http://www.wmo.int/pages/prog/wcp/wcdmp/statement/wmostatement_en.html

WMO WORLD METEOROLOGICAL ORGANIZATION. 2003. Statement on Status of the Global Climate in 2002, WMO-No. 949. http://www.wmo.int/pages/prog/wcp/wcdmp/statement/wmostatement_en.html

WMO WORLD METEOROLOGICAL ORGANIZATION. 2004. Statement on Status of the Global Climate in 2003, WMO-No. 966. http://www.wmo.int/pages/prog/wcp/wcdmp/statement/wmostatement_en.html

WMO WORLD METEOROLOGICAL ORGANIZATION. 2005. Statement on Status of the Global Climate in 2004, WMO-No. 983. http://www.wmo.int/pages/prog/wcp/wcdmp/statement/wmostatement_en.html

WMO WORLD METEOROLOGICAL ORGANIZATION. 2006. Statement on Status of the Global Climate in 2005, WMO-No. 998. http://www.wmo.int/pages/prog/wcp/wcdmp/statement/wmostatement_en.html

WMO WORLD METEOROLOGICAL ORGANIZATION. 2007. Statement on Status of the Global Climate in 2006, WMO-No. 1016. http://www.wmo.int/pages/prog/wcp/wcdmp/statement/wmostatement_en.html

WMO WORLD METEOROLOGICAL ORGANIZATION. 2008. Statement on Status of the Global Climate in 2007, WMO-No. 1031. http://www.wmo.int/pages/prog/wcp/wcdmp/statement/wmostatement_en.html

WMO WORLD METEOROLOGICAL ORGANIZATION. 2009. Statement on Status of the Global Climate in 2008, WMO-No. 1039. http://www.wmo.int/pages/prog/wcp/wcdmp/statement/wmostatement_en.html

WMO WORLD METEOROLOGICAL ORGANIZATION. 2010. Statement on Status of the Global Climate in 2009, WMO-No. 1055. http://www.wmo.int/pages/prog/wcp/wcdmp/statement/wmostatement_en.html

WMO WORLD METEOROLOGICAL ORGANIZATION. 2011. Statement on Status of the Global Climate in 2010, WMO-No. 1074. http://www.wmo.int/pages/prog/wcp/wcdmp/statement/wmostatement_en.html

YOU, Q., KANG, S., AGUILAR, E., PEPIN, N., FLÜGEL, W., YAN, Y. and XU, Y. 2010. Changes in daily climate extremes in China and their connection to the large scale atmospheric circulation during 1961-2003. Climate Dynamics 36, 2399-2417. doi: 10.1007/s00382-009-0735-0.

ZHAI, P. and PAN, X. 2003. Trends in temperature extremes during 1951-1999 in China. Geophys. Res. Lett. 20. doi:10.1029/2003GL018004.

Acknowledgements

Data for this work were taken from the GHCND database (Durre et al., 2010). We thank Lisa Alexander and Markus Donat (University of New South Wales) for their help and advice. We also thank reviewers from China for their valuable input and advice.

Chapter 2 – Climate Change Projections

Introduction

Climate models are used to understand how the climate will evolve over time and typically represent the atmosphere, ocean, land surface, cryosphere, and biogeochemical processes, and solve the equations governing their evolution on a geographical grid covering the globe. Some processes are represented explicitly within climate models, large-scale circulations for instance, while others are represented by simplified parameterisations. The use of these parameterisations is sometimes due to processes taking place on scales smaller than the typical grid size of a climate model (a Global Climate Model (GCM) has a typical horizontal resolution of between 250 and 600km) or sometimes to the current limited understanding of these processes. Different climate modelling institutions use different plausible representations of the climate system, which is why climate projections for a single greenhouse gas emissions scenario differ between modelling institutes. This gives rise to "climate model structural uncertainty".

In response to a proposed activity of the World Climate Research Programme's (WCRP's; http://www.wcrp-climate.org/) Working Group on Coupled Modelling (WGCM), the Program for Climate Model Diagnosis and Intercomparison (PCMDI; http://www-pcmdi.llnl.gov/) volunteered to collect model output contributed by leading climate modelling centres around the world. Climate model output from simulations of the past, present and future climate was collected by PCMDI mostly during the years 2005 and 2006, and this archived data constitutes phase 3 of the Coupled Model Intercomparison Project (CMIP3). In part, the WGCM organised this activity to enable those outside the major modelling centres to perform research of relevance to climate scientists preparing the IPCC Fourth Assessment Report (AR4). This unprecedented collection of recent model output is commonly known as the "CMIP3 multi-model dataset". The GCMs included in this dataset are referred to regularly throughout this review, although not exclusively.

The CMIP3 multi-model ensemble has been widely used in studies of regional climate change and associated impacts. Each of the constituent models was subject to extensive testing by the contributing institute, and the ensemble has the advantage of having been constructed from a large pool of alternative model components, therefore sampling alternative structural assumptions in how best to represent the physical climate system. Being assembled on an opportunity basis, however, the CMIP3 ensemble was not designed to represent model uncertainties in a systematic manner, so it does not, in isolation, support robust estimates of the risk of different levels of future climate change, especially at a regional level.

Since CMIP3, a new (CMIP5) generation of coupled ocean-atmosphere models has been developed, which is only just beginning to be available and is being used for new projections for the IPCC Fifth Assessment Report (AR5).

These newer models typically feature higher spatial resolution than their CMIP3 counterparts, including in some models a more realistic representation of stratosphere-troposphere interactions. The CMIP5 models also benefit from several years of development in their parameterisations of small scale processes, which, together with resolution increases, are expected to result in a general improvement in the accuracy of their simulations of historical climate, and in the credibility of their projections of future changes. The CMIP5 programme also includes a number of comprehensive Earth System Models (ESMs) which explicitly simulate the earth's carbon cycle and key aspects of atmospheric chemistry, and also contain more sophisticated representations of aerosols compared to CMIP3 models.

The CMIP3 results should be interpreted as a useful interim set of plausible outcomes. However, their neglect of uncertainties, for instance in carbon cycle feedbacks, implies that higher levels of warming outside the CMIP3 envelope cannot be ruled out. In future, CMIP5 coupled model and ESM projections can be expected to produce improved advice on future regional changes. In particular, ensembles of ESM projections will be needed to provide a more comprehensive survey of possible future changes and their relative likelihoods of occurrence. This is likely to require analysis of the CMIP5 multi-model ESM projections, augmented by larger ensembles of ESM simulations in which uncertainties in physical and biogeochemical feedback processes can be explored more systematically, for example via ensembles of model runs in which key aspects of the climate model are slightly adjusted. Note that such an exercise might lead to the specification of wider rather than narrower uncertainties compared to CMIP3 results, if the effects of representing a wider range of earth system processes outweigh the effects of refinements in the simulation of physical atmosphere-ocean processes already included in the CMIP3 models.

Climate projections

The Met Office Hadley Centre is currently producing perturbed parameter ensembles of a single model configuration known as HadCM3C, to explore uncertainties in physical and biogeochemical feedback processes. The results of this analysis will become available in the next year and will supplement the CMIP5 multi-model ESM projections, providing a more comprehensive set of data to help progress understanding of future climate change. However, many of the studies covered in the chapter on climate impacts have used CMIP3 model output. For this reason, and because it is still the most widely used set of projections available, the CMIP3 ensemble output for temperature and precipitation, for the A1B emission scenario, for China and the surrounding region is shown below.

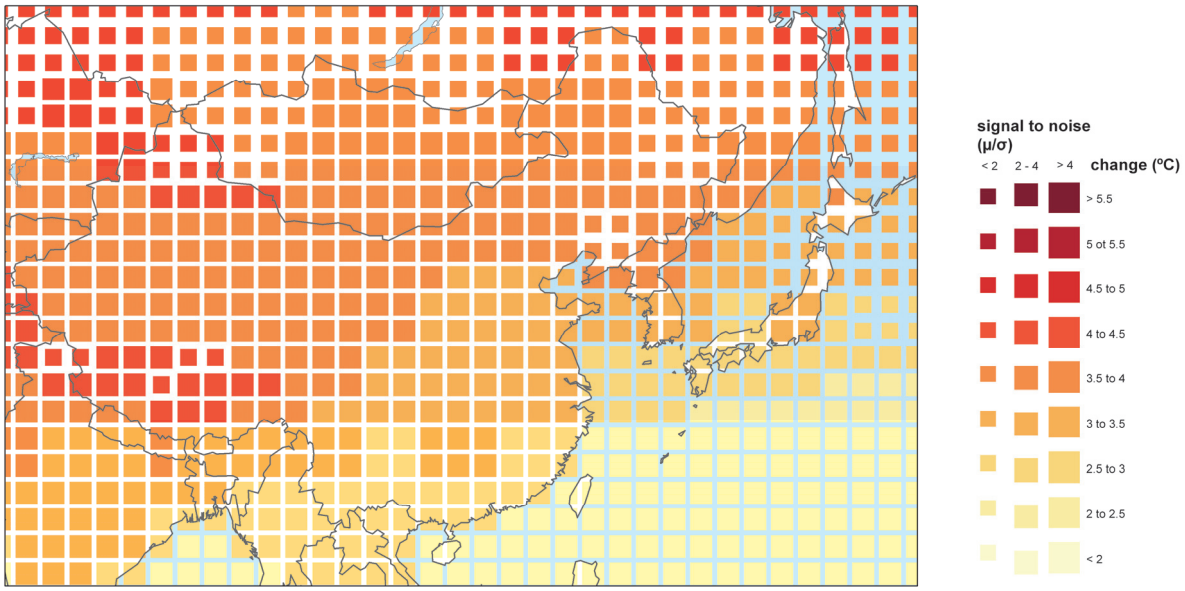

***Figure 1**. Percentage change in average annual temperature by 2100 from 1960-1990 baseline climate, averaged over 21 CMIP3 models. The size of each pixel represents the level of agreement between models on the magnitude of the change.*

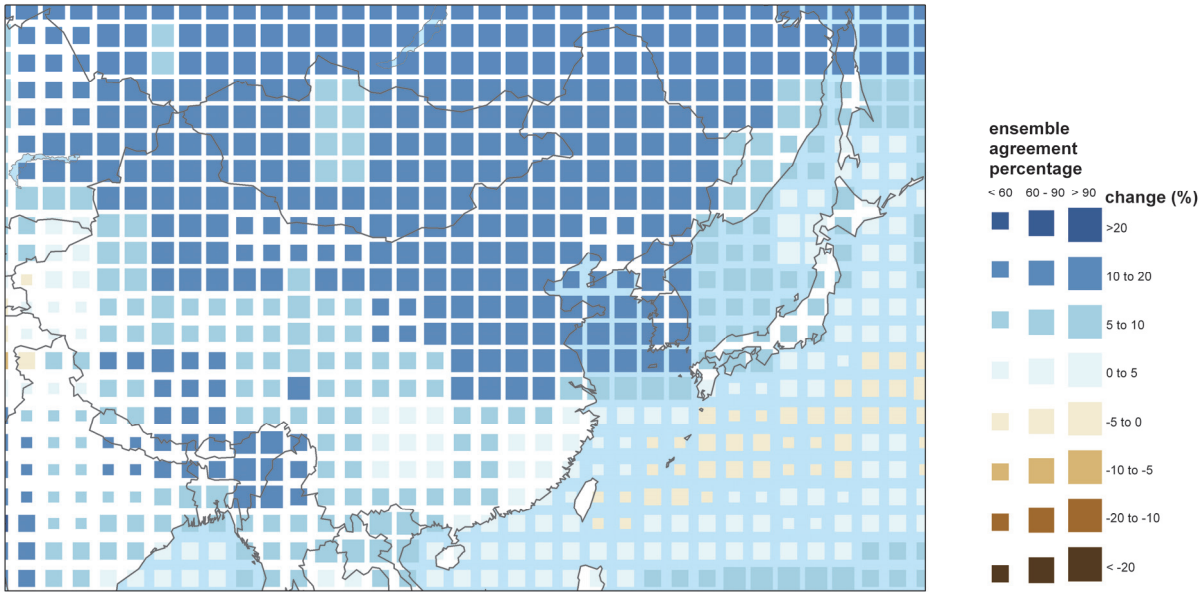

Figure 2. *Percentage change in average annual precipitation by 2100 from 1960-1990 baseline climate, averaged over 21 CMIP3 models. The size of each pixel represents the level of agreement between models on the sign of the change.*

Summary of temperature change in China

Figure 1 shows the percentage change in average annual temperature by 2100 from 1960-1990 baseline climate, averaged over 21 CMIP3 models. All of the models in the CMIP3 ensemble project increased temperatures in the future, but the size of each pixel indicates how well the models agree over the magnitude of the increase.

Projected changes in temperature are higher over northern and western parts of the country, with changes of up to around 4.5°C. In the southeast, projected changes are typically around 3°C. There is good agreement between the models over most of China.

Summary of precipitation change in China

Figure 2 shows the percentage change in average annual precipitation by 2100 from 1960-1990 baseline climate, averaged over 21 CMIP3 models. Unlike for temperature, the models sometimes disagree over whether precipitation is increasing or decreasing over a region, so in this case the size of each pixel indicates the percentage of the models in the ensemble that agree on the sign of the change in precipitation.

Precipitation is projected to increase over almost the entire country. Increases of up to 20% are projected with high ensemble agreement across the northeast of China. Lower increases of between zero and 10% are projected for the southeast of the country, but with less agreement amongst ensemble members.

Chapter 3 – Climate Change Impact Projections

Introduction

Aims and approach

This chapter looks at research on a range of projected climate change impacts, with focus on results for China. It includes projections taken from the AVOID programme, for some of the impact sectors.

The aim of this work is to take a 'top down' approach to assessing global impacts studies, both from the literature and from new research undertaken by the AVOID programme. This project covers 23 countries, with summaries from global studies provided for each of these. This global approach allows some level of comparison between countries, whilst presenting information on a scale most meaningful to inform international policy.

The literature covered in this chapter focuses on research published since the Fourth Assessment Report (AR4) of the Intergovernmental Panel on Climate Change (IPCC) and should be read in conjunction with IPCC AR4 WG1 and WG2 reports. For some sectors considered, an absence of research developments since the IPCC AR4, means earlier work is cited as this helps describe the current level of scientific understanding. This report focuses on assessing scientific research about climate change impacts within sectors; it does not present an integrated analysis of climate change adaptation policies.

Some national and sub-national scale literature is reported to a limited extent to provide some regional context.

Impact sectors considered and methods

This report reviews the evidence for the impact of climate change on a number of sectors, for China. The following sectors are considered in turn in this report:

- Crop yields
- Food security
- Water stress and drought
- Pluvial flooding and rainfall
- Fluvial flooding

- Tropical cyclones (where applicable)
- Coastal regions

Supporting literature

Literature searches were conducted for each sector with the Thomson Reuters Web of Science (WoS., 2011) and Google Scholar academic search engines respectively. Furthermore, climate change impact experts from each of the 23 countries reviewed were contacted. These experts were selected through a combination of government nomination and from experts known to the Met Office. They were asked to provide literature that they felt would be of relevance to this review. Where appropriate, such evidence has been included. A wide range of evidence was considered, including; research from international peer-reviewed journal papers; reports from governments, non-governmental organisations, and private businesses (e.g. reinsurance companies), and research papers published in national journals.

For each impact sector, results from assessments that include a global- or regional-scale perspective are considered separately from research that has been conducted at the national- or sub-national-scale. The consideration of global- and regional-scale studies facilitates a comparison of impacts across different countries, because such studies apply a consistent methodology for each country. While results from national- and sub-national-scale studies are not easily comparable between countries, they can provide a level of detail that is not always possible with larger-scale studies. However, the national- and sub-national scale literature included in this project does not represent a comprehensive coverage of regional-based research and cannot, and should not, replace individual, detailed impacts studies in countries. The review aims to present an up-to-date assessment of the impact of climate change on each of the sectors considered.

AVOID programme results

Much of the work in this report is drawn from modelling results and analyses coming out of the AVOID programme. The AVOID programme is a research consortium funded by DECC and Defra and led by the UK Met Office and also comprises the Walker Institute at the University of Reading, the Tyndall Centre represented through the University of East Anglia,

and the Grantham Institute for Climate Change at Imperial College. The expertise in the AVOID programme includes climate change research and modelling, climate change impacts in natural and human systems, socio-economic sciences, mitigation and technology. The unique expertise of the programme is in bringing these research areas together to produce integrated and policy-relevant results. The experts who work within the programme were also well suited to review the literature assessment part of this report. In this report the modelling of sea level rise impacts was carried out for the AVOID programme by the University of Southampton.

The AVOID programme uses the same emissions scenarios across the different impact sectors studied. These are a business as usual (IPCC SRES A1B) and an aggressive mitigation (the AVOID A1B-2016-5-L) scenario. Model output for both scenarios was taken from more than 20 GCMs and averaged for use in the impact models. The impact models are sector specific, and frequently employ further analytical techniques such as pattern scaling and downscaling in the crop yield models.

Data and analysis from AVOID programme research is provided for the following impact sectors:

- Crop yields
- Water stress and drought
- Fluvial flooding
- Coastal regions

Uncertainty in climate change impact assessment

There are many uncertainties in future projections of climate change and its impacts. Several of these are well-recognised, but some are not. One category of uncertainty arises because we don’t yet know how mankind will alter the climate in the future. For instance, uncertainties in future greenhouse gas emissions depends on the future socio-economic pathway, which, in turn, depends on factors such as population, economic growth, technology development, energy demand and methods of supply, and land use. The usual approach to dealing with this is to consider a range of possible future scenarios.

Another category of uncertainties relate to our incomplete understanding of the climate system, or an inability to adequately model some aspects of the system. This includes:

- Uncertainties in translating emissions of greenhouse gases into atmospheric concentrations and radiative forcing. Atmospheric CO_2 concentrations are currently rising at approximately 50% of the rate of anthropogenic emissions, with the remaining 50% being offset by a net uptake of CO_2 into the oceans and land biosphere. However, this rate of uptake itself probably depends on climate, and evidence suggests it may weaken under a warming climate, causing more CO_2 to remain in the atmosphere, warming climate further. The extent of this feedback is highly uncertain, but it not considered in most studies. The phase 3 of the Coupled Model Intercomparison Project (CMIP3), which provided the future climate projections for the IPCC Fourth Assessment Report (AR4), used a single estimate of CO_2 concentration rise for each emissions scenario, so the CMIP3 projections (which were used in most studies presented here, including AVOID) do not account for this uncertainty.

- Uncertainty in climate response to the forcing by greenhouse gases and aerosols. One aspect of this is the response of global mean temperature ("climate sensitivity"), but a more relevant aspect for impacts studies is the response of regional climates, including temperature, precipitation and other meteorological variables. Different climate models can give very different results in some regions, while giving similar results in other regions. Confidence in regional projections requires more than just agreement between models: physical understanding of the relevant atmospheric, ocean and land surface processes is also important, to establish whether the models are likely to be realistic.

- Additional forcings of regional climate. Greenhouse gas changes are not the only anthropogenic driver of climate change; atmospheric aerosols and land cover change are also important, and unlike greenhouse gases, the strength of their influence varies significantly from place to place. The CMIP3 models used in most impacts studies generally account for aerosols but not land cover change.

- Uncertainty in impacts processes. The consequences of a given changes in weather or climatic conditions for biophysical impacts such as river flows, drought, flooding, crop yield or ecosystem distribution and functioning depend on many other processes which are often poorly-understood, especially at large scales. In particular, the extent to which different biophysical impacts interact with each other has been hardly studied, but may be crucial; for example, impacts of climate change on crop

yield may depend not only on local climate changes affecting rain-fed crops, but also remote climate changes affecting river flows providing water for irrigation.

- Uncertainties in non-climate effects of some greenhouse gases. As well as being a greenhouse gas, CO_2 exerts physiological influences on plants, affecting photosynthesis and transpiration. Under higher CO_2 concentrations, and with no other limiting factors, photosynthesis can increase, while the requirements of water for transpiration can decrease. However, while this has been extensively studied under experimental conditions, including in some cases in the free atmosphere, the extent to which the ongoing rise in ambient CO_2 affects crop yields and natural vegetation functioning remains uncertain and controversial. Many impacts projections assume CO_2 physiological effects to be significant, while others assume it to be non-existent. Studies of climate change impacts on crops and ecosystems should therefore be examined with care to establish which assumptions have been made.

In addition to these uncertainties, the climate varies significantly through natural processes from year-to-year and also decade-to-decade, and this variability can be significant in comparison to anthropogenic forcings on shorter timescales (the next few decades) particularly at regional scales. Whilst we can characterise the natural variability it will not be possible to give a precise forecast for a particular year decades into the future.

A further category of uncertainty in projections arises as a result of using different methods to correct for uncertainties and limitations in climate models. Despite being painstakingly developed in order to represent current climate as closely as possible, current climate models are nevertheless subject to systematic errors such as simulating too little or too much rainfall in some regions. In order to reduce the impact of these, '*bias correction*' techniques are often employed, in which the climate model is a source of information on the *change* in climate which is then applied to the observed present-day climate state (rather than using the model's own simulation of the present-day state). However, these bias-corrections typically introduce their own uncertainties and errors, and can lead to inconsistencies between the projected impacts and the driving climate change (such as river flows changing by an amount which is not matched by the original change in precipitation). Currently, this source of uncertainty is rarely considered

When climate change projections from climate models are applied to climate change impact models (e.g. a global hydrological model), the climate model structural uncertainty carries

through to the impact estimates. Additional uncertainties include changes in future emissions and population, as well as parameterisations within the impact models (this is rarely considered). Figure 1 highlights the importance of considering climate model structural uncertainty in climate change impacts assessment. Figure 1 shows that for 2°C prescribed global-mean warming, the magnitude of, and sign of change in average annual runoff from present, simulated by an impacts model, can differ depending upon the GCM that provides the climate change projections that drive the impact model. This example also shows that the choice of impact model, in this case a global hydrological model (GHM) or catchment-scale hydrological model (CHM), can affect the magnitude of impact and sign of change from present (e.g. see IPSL CM4 and MPI ECHAM5 simulations for the Xiangxi). To this end, throughout this review, the number of climate models applied in each study reviewed, and the other sources of uncertainty (e.g. emissions scenarios) are noted. Very few studies consider the application of multiple impacts models and it is recommended that future studies address this.

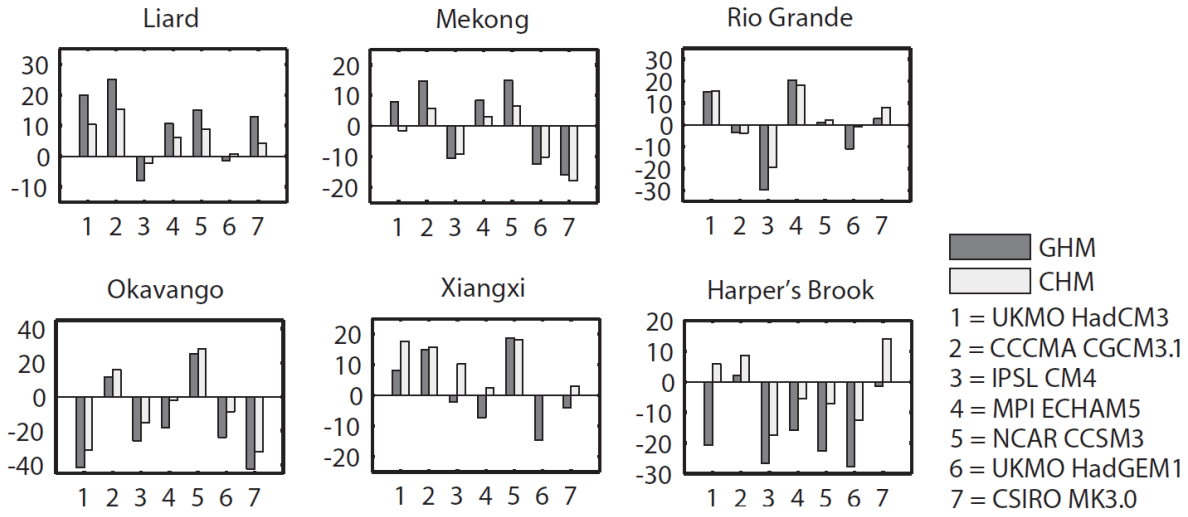

Figure 1. *Change in average annual runoff relative to present (vertical axis; %), when a global hydrological model (GHM) and a catchment-scale hydrological model (CHM) are driven with climate change projections from 7 GCMs (horizontal axis), under a 2°C prescribed global-mean warming scenario, for six river catchments. The figure is from Gosling et al. (2011a).*

The climate of China is affected by large scale circulation patterns. How these change will be a fundamental determinant of climate change impacts, but are highly uncertain. The key processes of: flow over the Tibetan Plateau; the East Asian monsoon and El Niño events are described in the IPCC Fourth Assessment Report (Christensen et al. 2007).

Summary of findings for each sector

Crop yields

- Quantitative crop yield projections under climate change scenarios for China vary across studies due to the application of different models, assumptions and emissions scenarios. As a consequence of the large geographical area of China, projections also vary significantly across the country.

- Although the picture is mixed, a number of global- and regional-scale studies considered here project decreases in the yield of China's major crops: rice, wheat, and most markedly of maize, as a consequence of climate change.

- Some global-scale studies suggest that the magnitude of, and balance between, detrimental ozone effects and CO_2 fertilisation may determine whether crop yield losses or gains are realised under climate change.

- Important knowledge gaps and key uncertainties include the quantification of yield increases due to CO_2 fertilisation, quantification of yield reductions due to ozone damage and the extent to which crop diseases could affect crop yields with climate change.

Food security

- China currently has very low levels of undernourishment. Global-scale studies of food security vary in their conclusions for China, however they generally project that the country will become less food secure with climate change.

- National-scale studies confirm the uncertainty in food security estimates with some suggesting that China could experience large food shortages, while others suggest it may not face pressures on food security with climate change.

- One study concluded that the national economy of China presents a moderate vulnerability to climate change impacts on fisheries by the 2050s. Another projects

that maximum fish catch potential from 2005 to 2055 could decline by up to 7% under SRES A1B.

- The large uncertainty associated with quantifying the effect of climate change on food security for China is an important knowledge gap which future studies should address.

Water stress and drought

- Global-scale studies included here agree that south-eastern China currently suffers from a moderate to high level of water stress.
- Global- and regional-scale studies included here show no consensus as to the sign of change in drought or water stress in China with climate change, due to the application of different climate models and indicators of water stress.
- However some global- and national-scale studies included here project that water stress could increase in China for global-mean warming scenarios of around 2°C, but may decrease under higher warming or higher emission scenarios, due to a projected increase in precipitation and runoff.
- Recent simulations by the AVOID programme project a median increase of 6% of China's population to be exposed to water stress increases, and 20% to water stress decreases under the A1B emissions scenario by 2100. Under a mitigation scenario where global temperature increases are limited to 2°C these values are 2% and 9% respectively.

Pluvial flooding and rainfall

- The IPCC AR4 noted the potential for increased precipitation over East Asia, and also an increase in extreme precipitation in parts of China.
- Results from recent studies suggest that changes in precipitation extremes tend to be larger under higher emissions scenarios.

Fluvial flooding

- Observations show that heavy precipitation events have increased over recent decades in parts of China, and flooding events have become more frequent in a number of river basins.
- Climate change impact studies suggest that this trend could continue, although uncertainties are large, resulting in a wide spread in responses among different climate models.
- Simulations by the AVOID programme show a general tendency towards higher flood risk in China, particularly later in the century and under the A1B scenario.
- Future research must improve regional climate simulations for China, especially of precipitation and extreme events. Hydrological impact studies must take account of the uncertainties in climate scenarios by incorporating ensemble projections, and include relevant processes such as irrigation and land use change.

Tropical cyclones

- There remains large uncertainty in the current understanding of how tropical cyclones might be affected by climate change, including in the western Pacific, as conclusions are based upon a limited number of studies whose projections are from either coarse-resolution global models or from statistical or dynamical downscaling techniques. To this end, caution should be applied in interpreting model-based results, even where the models are in agreement.
- There is relatively less uncertainty regarding the intensity of cyclones in the western Pacific basin, compared to their frequency. A number of global- and regional-scale studies included here project that cyclone intensity could increase considerably in the future in this basin. These increases in intensity could be greatest for the most severe cyclones, which could lead to large increases in cyclone damages in China.
- China is particularly vulnerable to cyclone damages due to its high coastal population density and the valuable economic assets located in coastal regions.

Coastal regions

- Recent global-scale assessments of the impact of sea level rise (SLR) on coasts, which include national estimates for China, suggest that China is one of the countries across the globe that could experience the most severe impacts.

- One study showed that based upon an analysis of 136 port cities, China was the country simulated to have the largest increase in exposure to SLR by 2070 relative to the present day.

- Another study showed that around 17% of China's coastal land area and coastal population could be affected by a 10% intensification of the current 1-in-100-year storm surge combined with a 1m SLR.

Crop yields

Headline

Crop yield projections under climate change scenarios for China vary across studies due to the application of different models, assumptions and emissions scenarios. Moreover, as a consequence of the large geographical area of China, projections vary regionally in China. Generally, simulations suggest yield declines with climate change and for maize in particular. It is uncertain to what degree projections of crop yield losses in current cropping areas take account of changes in cropping area. Some studies show that the magnitude of the CO_2 fertilisation effect may determine whether crop yield losses or gains are realised under climate change.

Results from the AVOID programme for China indicate that the areas of current croplands becoming less suitable for cultivation are projected to be smaller under the mitigation scenario than the A1B scenario, and in both scenarios the area of declining suitability becomes larger than that of increasing suitability (which remains similar over the 21st century in both scenarios).

Supporting literature

Introduction

The impacts of climate change on crop productivity are highly uncertain due to the complexity of the processes involved. Most current studies are limited in their ability to capture the uncertainty in regional climate projections, and often omit potentially important aspects such as extreme events and changes in pests and diseases. Importantly, there is a lack of clarity on how climate change impacts on drought are best quantified from an agricultural perspective, with different metrics giving very different impressions of future risk. The dependence of some regional agriculture on remote rainfall, snowmelt and glaciers adds to the complexity - these factors are rarely taken into account, and most studies focus solely on the impacts of local climate change on rain-fed agriculture. However, irrigated agricultural land produces approximately 40-45 % of the world's food (Doll and Siebert 2002), and the water for irrigation is often extracted from rivers which can depend on climatic conditions far

from the point of extraction. Hence, impacts of climate change on crop productivity often need to take account of remote as well as local climate changes. Indirect impacts via sea-level rise, storms and diseases have also not been quantified. Perhaps most seriously, there is high uncertainty in the extent to which the direct effects of CO_2 rise on plant physiology will interact with climate change in affecting productivity. Therefore, at present, the aggregate impacts of climate change on large-scale agricultural productivity cannot be reliably quantified (Gornall et al, 2010). This section summarises findings from a range of post IPCC AR4 assessments to inform and contextualise the analysis performed by AVOID programme for this project. The results from the AVOID work are discussed in the next section.

Rice, maize and wheat are the three most important staple crops in China but 'fresh vegetables' are also important in terms of the 'Harvested area' and 'Quantity' produce, according to statistics compiled by the FAO (Table 1).

Single cropping is common in northern China, while multi-cropping rotations dominate south of 40°N (Piao et al., 2010). IIASA (1999) describes the distribution of crop production in China. Rice is cultivated predominantly in southern and southeastern provinces, but also in Sichuan. Maize cultivation is concentrated in the north, especially in Jilin and Liaoning provinces. Some maize cultivation also occurs in parts of Beijing, Hebei and Shaanxi provinces, as well as in Sichuan and Guizhou provinces. Wheat cultivation is concentrated in the East China plane (Hebei, Shandong, Henan), in the East-Central provinces of Shaanxi and Gansu but also in parts of Heilongjiang province in the north. There are also relatively small areas of intense wheat cultivation in the west (Xinjiang). Soybean cultivation is concentrated in the north-east of China - in Heilongjiang, Jilin and Liaoning. Significant cultivation also occurs in the northern parts of Shaanxi province.

Harvested area (ha)		**Quantity (Metric ton)**		**Value ($1000)**	
Maize	29800000	Rice, paddy	193000000	Rice, paddy	36500000
Rice, paddy	29400000	Maize	166000000	Fresh Vegetables	23800000
Wheat	23600000	Fresh Vegetables	147000000	Wheat	15800000
Soybeans	9120000	Sugar cane	124000000	Cotton lint	11100000
Fresh Vegetables	8660000	Wheat	112000000	Asparagus	10100000
Rapeseed	6590000	Sweet potatoes	78400000	Garlic	9700000
Seed cotton	5760000	Potatoes	70800000	Apples	8570000

Table 1. *The top 7 crops by harvested area, quantity and value according to the FAO (2008) in China. Crops that feature in all lists are shaded green; crops that feature in two top 7 lists are shaded amber. Data is from FAO (2008) and is rounded down to three significant figures.*

A number of impact model studies looking at crop yield which include results for some of the main crops in China have been conducted. They apply a variety of methodological approaches, including using different climate model inputs and treatment of other factors that might affect yield, such as impact of increased CO_2 in the atmosphere on plant growth and adaption of agricultural practises to changing climate conditions. These different models, assumptions and emissions scenarios mean that there are a range of crop yield projections for China.

To this end, important knowledge gaps, which are applicable to China as well as at the global-scale, include; the quantification of yield increases due to CO_2 fertilisation and yield reductions due to ozone damage (Ainsworth and McGrath, 2010; Iglesias et al., 2009), and the extent crop diseases could affect crop yields with climate change (Luck et al., 2011).

Most crop simulation models do not include the direct effect of extreme temperatures on crop development and growth, thus only changes in mean climate conditions are considered to affect crop yields for the studies included here.

Assessments that include a global or regional perspective

Recent past

Crop yield changes could be due to a variety of factors, which might include, but not be confined to, a changing climate. In order to assess the impact of recent climate change (1980-2008) on maize, rice, wheat and soybean yields, Lobell et al. (2011) looked at how the impacts of recent climate change (1980-2008) on maize, rice, wheat and soybean yields at the global-scale and national estimates for China were calculated. For China, negative impacts were estimated for maize yield, with no substantial effects estimated for rice, wheat or soybean yields (see Table 2).

Crop	Trend
Maize	-0.2 to -0.1
Rice	0.0 to 0.1
Wheat	-0.1 to 0.0
Soybean	-0.1 to 0.0

***Table 2**. The estimated net impact of climate trends for 1980-2008 on crop yields in China. Climate-induced yield trend divided by overall yield trend. Data is from Lobell et al. (2011).*

Climate change studies

Global studies on changes in crop yield due to climate change covered in this report are derived mainly from applying Global Climate Model (GCM) output to crop models. The results for China are presented.

Included in this report are recent studies have applied climate projections from GCMs to crop yield models to assess the global-scale impact of climate change on crop yields, and which include impact estimates at the national-scale for China (Iglesias and Rosenzweig, 2009; Lobell et al., 2008; Masutomi et al., 2009). The process of CO_2 fertilisation of some crops is usually included in most climate impact studies of yields. However, other gases can influence crop yield and are not always included in impacts models. An example of this is ozone (O_3) and so a study which attempts to quantify the potential impact on crop yield of changes in ozone in the atmosphere is also included (Avnery et al. 2011). In addition to these studies, the AVOID programme analysed the patterns of climate change for 21 GCMs, to establish an index of 'climate suitability' of agricultural land. Climate suitability is not directly equivalent to crop yields, but is a means of looking at a standard metric across all the countries included in this project, and of assessing the level of agreement on variables that affect crop production, between all 21 GCMs.

Iglesias and Rosenzweig (2009) repeated an earlier study presented by Parry et al. (2004) by applying climate projections from the HadCM3 GCM (instead of HadCM2, which was applied by Parry et al. (2004)), under seven SRES emissions scenarios and for three future time periods This study used consistent crop simulation methodology and climate change scenarios globally, and weighted the model site results by their contribution to regional and national, and rain-fed and irrigated production. The study also applied a quantitative estimation of physiological CO_2 effects on crop yields and considered the affect of adaptation by assessing the country or regional potential for reaching optimal crop yield. The results from the study are presented in Table 3 and Table 4. Three out of seven emission scenarios were associated with wheat yield below baseline (1970-2000) levels by 2020 but this was reduced by 2050 and 2080 to zero and one emission scenarios, indicating an increase in wheat yield between 2020 and 2080. A rice yield deficit was projected by 2020 but rice yield increases were simulated between 2020 and 2080, which resulted in rice yield gains relative to baseline levels by 2050 and 2080. Maize yield deficits were projected for 2020, 2050 and 2080 but between 2050 and 2080 maize yield was projected to increase.

Scenario	Year	Wheat	Rice	Maize
A1FI	2020	-0.22	-0.92	-3.30
	2050	6.10	3.67	-5.97
	2080	-0.87	7.12	-0.16
A2a	2020	-1.17	-1.18	-5.05
	2050	7.26	3.65	-6.96
	2080	8.31	8.71	-2.85
A2b	2020	3.80	-0.24	-3.54
	2050	7.83	3.00	-5.96
	2080	5.75	8.91	-2.45
A2c	2020	-2.31	-1.31	-5.31
	2050	6.10	-0.13	-7.43
	2080	6.60	7.55	-4.11
B1a	2020	3.32	-0.67	-3.35
	2050	5.26	0.82	-6.62
	2080	5.69	-0.63	-7.81
B2a	2020	0.75	-1.68	-5.56
	2050	4.23	0.44	-7.46
	2080	6.84	3.83	-6.22
B2b	2020	0.08	-1.78	-5.73
	2050	5.00	0.81	-7.41
	2080	7.56	4.29	-5.46

Table 3. *Wheat, rice and maize yield changes (%) relative to baseline scenario (1970-2000) for different emission scenarios and future time periods for China. Some emissions scenarios were run in an ensemble simulation (e.g. A2a, A2b, A2c). Data is from Iglesias and Rosenzweig (2009)*.

	Wheat		Rice		Maize	
	Up	Down	Up	Down	Up	Down
Baseline to 2020	4	3	0	7	0	7
Baseline to 2050	7	0	6	1	0	7
Baseline to 2080	6	1	6	1	0	7
2020 to 2050	7	0	7	0	0	7
2050 to 2080	5	2	6	1	6	1

Table 4. *The number of emission scenarios that predict yield gains ("Up") or yield losses ("Down") for wheat, rice and maize between two points in time for China. Data is from Iglesias and Rosenzweig (2009).*

Lobell et al. (2008) conducted an analysis of climate risks for the major crops in 12 food-insecure regions to identify adaptation priorities. Statistical crop models were used in combination with climate projections for 2030 from 20 GCMs that have contributed to the World Climate Research Programme's Coupled Model Intercomparison Project phase 3 (CMIP3). The results from the study for China are presented in Figure 2. In China by 2030, a negative climate change impact on maize yield was simulated (at least 75% of projections

were associated with yield losses) but positive impacts were projected for groundnut, soybean and wheat (at least 75% of projections were associated with yield increases.

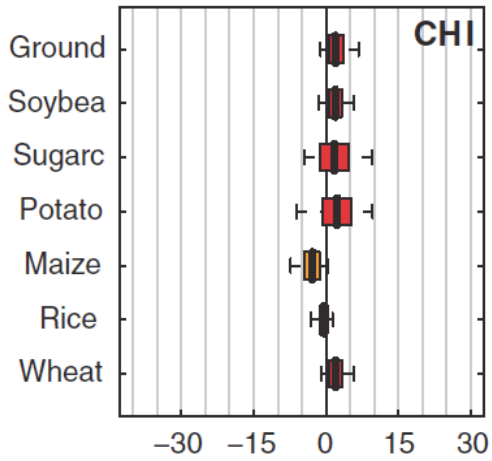

***Figure 2**. Probabilistic projections of production impacts in 2030 from climate change (expressed as a percentage of 1998 to 2002 average yields) for China. Red, orange, and yellow indicate a Hunger Importance Ranking of 1 to 30 (more important), 31 to 60 (important), and 61 to 94 (less important), respectively. Dashed lines extend from 5th to 95th percentile of projections, boxes extend from 25th to 75th percentile, and the middle vertical line within each box indicates the median projection. Figure is from Lobell et al. (2008).*

Masutomi et al. (2009) comprehensively assessed the impact of climate change on rice production in Asia considering the process/parameter uncertainty in GCMs. The authors created climate scenarios based on the projections of GCMs for three emissions scenarios (18 GCMs for A1B, 14 GCMs for A2, and 17 GCMs for B1). The climate scenarios were then used as input to the M-GAEZ crop model to calculate the average change in production (ACP) and other parameters taking into account the effect of CO_2 fertilisation. Since land-use change was not considered in the study, changes in crop production actually equate to changes in crop yield and the country-level results for China are presented in Table 5.

1990s - 2020s			1990s - 2050s			1990s - 2080s		
A2	**A1B**	**B1**	**A2**	**A1B**	**B1**	**A2**	**A1B**	**B1**
-7.1	-5.8	-3.4	-3.8	-5.2	-2.1	-13.2	-10.0	-5.7

***Table 5.** Average change in rice production (%) taking CO_2 effect into consideration, for China. The values represent the average across all GCMs considered in the analysis (individual GCM results are not presented in the study). Data is from Masutomi et al. (2009).*

Other recent studies have assessed the impact of climate change on a global-scale and include impact estimates for Northwest Pacific and/or East Asia as a whole (Arnell et al.,

2010a; Tatsumi et al., 2011; Arnell et al., 2010b; Nelson et al., 2009). Whilst these studies provide a useful indicator of crop yields under climate change for the *region*, it should be noted that the crop yields presented in such cases are not definitive *national* estimates. This is because the yields are averaged over the entire region, which includes other countries as well as China.

Tatsumi et al. (2011) applied an improved version of the GAEZ crop model (iGAEZ) to simulate crop yields on a global scale for wheat, potato, cassava, soybean, rice, sweet potato, maize, green beans. The impact of global warming on crop yields from the 1990s to 2090s was assessed by projecting five GCM outputs under the SRES A1B scenario and comparing the results for crop yields as calculated using the iGAEZ model for the period of 1990-1999. The results for East Asia, which includes China, are displayed in Table 6.

Wheat	Potato	Cassava	Soybean	Rice	Sweet	Maize	Green
4.35	6.33	-29.35	16.35	-5.60	8.96	7.23	20.31

Table 6. *Average change in yield (%), during 1990s-2090s in South Asia. Data is from Tatsumi et al. (2011).*

Arnell et al. (2010a) used 5 GCMs to assess the effects of climate scenarios on crop productivity. Specifically, the crop simulation model GLAM-maize was used to simulate the effect of climate change on maize productivity. For NW Pacific and East Asia a loss of between approximately 32% and 41% of yield by 2050 was estimated relative to the baseline (1961-1990) in the absence of adaptation and mitigation strategies. Implementing a climate change mitigation scenario that reduced global emissions from 2016 onwards at a rate of 5%/year reduced the negative impact by approximately 20% and 30% in 2050 and 2100 respectively.

Arnell et al. (2010b) applied the same crops model used by Arnell et al. (2010a) to assess the potential impacts on water and food security avoided by a set of defined climate policies. One of the metrics of impact included was the regional change of yield. For wheat, only changes at the global-scale were reported but for soybean projected yield changes at the region or country level were published as bar charts. The results showed all models projected a decrease in yield throughout the 21st century under the SRES A1B emission scenario. When the mitigation scenarios of 2-5% reduction in CO_2 per year were applied to two of the models, the change in yield from A1B was both positive and negative, depending

on the model and the mitigation scenario, demonstrating no benefit from mitigation in this case. The results for NW Pacific and East Asia are displayed in Table 7.

	2050	2085	2100
No mitigation	-15 to -5	-33 to -14	-38 to -18
2050 IPSL	-6 to 11	n/a	n/a
2050 CGCM31	-16 to 8	n/a	n/a

Table 7. *Range of yield change (%) for the NW Pacific and East Asia region, at three different times in the future as estimated by five GCMs under the SRES A1B emission scenario (Row 1; values show range across the 5 GCMs) and avoided impact on regional soybean production (expressed as % of A1B impact) by 2050 for several mitigation scenarios as simulated with two GCMs (Row 2 and 3). The mitigations scenarios included reductions in emissions from 2016 or 2030 onwards, at rates of 2-5%/year. Data is from Arnell et al. (2010b).*

Nelson et al. (2009) applied two GCMs in combination with the DSSAT crop model under the SRES A2 emissions scenario to project future yields of rice, maize, soybean, wheat and groundnut with and without CO_2 enrichment, and for rain-fed and irrigated lands, for several regions across the globe. Table 8 represents the results for East Asia and the Pacific, the World Bank regional grouping in which China is included.

GCM and CO_2 fertilisation	**Rice**		**Maize**		**Soybean**		**Wheat**		**Groundnut**	
	Rf.	Irr.	Rf.	Irr.	Rf.	Irr.	Rf.	Irr.	Rf.	Irr.
CSIRO NoCF	-4.5	-13.0	1.5	-1.3	-3.6	-8.2	-14.8	-2.7	-5.1	-11.1
NCAR NoCF	-5.8	-19.8	-3.9	-2.6	-8.6	-13.4	-16.1	-7.1	-6.5	-13.7
CSIRO CF	2.5	4.4	3.7	-0.8	17.0	9.1	-5.4	3.7	11.3	3.6
NCAR CF	1.8	-1.1	-2.0	-1.9	11.5	3.6	-9.2	-0.6	9.7	1.2

Table 8. *Projected yield changes (%) by 2050 for East Asia and the Pacific region, compared to baseline (yields with 2000 climate) using two GCMs with (CF) and without CO_2 fertilisation effect (NoCF). Rain-fed (Rf.) and Irrigated (Irr.) crop lands were assessed separately. Data is from Nelson et al. (2009).*

In addition to the studies looking at the effect of changes in climate and CO_2 concentrations on crop yield, Avnery et al. (2011) investigated the effects of ozone surface exposure on crop yield losses for soybeans, maize and wheat under the SRES A2 and B1 scenarios respectively. Two metrics of ozone exposure were investigated; seasonal daytime (08:00-19:59) mean O_3 (M12) and accumulated O_3 above a threshold of 40 ppbv (AOT40). The results for China are presented in Table 9.

	A2		B1	
	M12	**AOT40**	**M12**	**AOT40**
Soybeans	30-45	30-45	30-45	30-45
Maize	10-15	6-8	10-15	4-6
Wheat	2-4	25-30	2-4	15-20

Table 9*. National relative crop yield losses (%) for 2030 under A2 and B1 emission scenarios according to the M12 (seasonal daytime (08:00–19:59) mean) and AOT40 (accumulated O_3 above a threshold of 40 ppbv) metrics of O_3 exposure. Data is from Avnery et al. (2011).*

National-scale or sub-national scale assessments

Recent past

A study conducted by Welch et al. (2010) look at the impacts of daily minimum and maximum temperatures and solar radiation on rice yields using meteorological observations and yield data for a five year period (1994-1999). This study concluded that rice yield at Jinhua and other main rice producing locations in South Asia was negatively affected by higher minimum temperatures during the vegetative and ripening phases of growth. Higher maximum temperatures on the other hand, though still below the optimum during these phases, increased yield. Effects of solar radiation were negative during vegetative growth but positive during ripening. Combined, these effects of radiation and temperature suggested that if observed weather trends at the end of the 20th century had not occurred, annual rice growth rate could have actually been 4.1 kg ha^{-1} $yr^{—1}$ lower during the shorter, lower yielding cropping season due to the negative impact of maximum temperatures outweighing the positive impact of minimum temperatures.

AVOID programme

To further quantify the impact of climate change on crops, the AVOID programme simulated the effect of climate change on the suitability of land for crop cultivation for all countries reviewed in this literature assessment based upon the patterns of climate change from 21 GCMs (Warren et al., 2010). This ensures a consistent methodological approach across all countries and takes consideration of climate modelling uncertainties.

Methodology

The effect of climate change on the suitability of land for crop cultivation is characterised here by an index which defines the percentage of cropland in a region with 1) a decrease in suitability or 2) an increase in suitability. A threshold change of 5% is applied here to

characterise decrease or increase in suitability. The crop suitability index is calculated at a spatial resolution of 0.5°x0.5°, and is based on climate and soil properties (Ramankutty et al., 2002). The baseline crop suitability index, against which the future changes are measured, is representative conditions circa 2000. The key features of the climate for the crop suitability index are temperature and the availability of water for plants, and changes in these were derived from climate model projections of future changes in temperature and precipitation, with some further calculations then being used to estimate actual and potential evapotranspiration as an indicator of water availability. It should be noted that changes in atmospheric CO_2 concentrations can decrease evapotranspiration by increasing the efficiency of water use by plants (Ramankutty et al., 2002), but that aspect of the index was not included in the analysis here. Increased CO_2 can also increase photosynthesis and improve yield to a small extent, but again these effects are not included. Exclusion of these effects may lead to an overestimate of decreases in suitability.

The index here is calculated only for grid cells which contain cropland circa 2000, as defined in the global crop extent data set described by Ramankutty et al. (2008) which was derived from satellite measurements. It is assumed that crop extent does not change over time. The crop suitability index varies significantly for current croplands across the world (Ramankutty et al., 2002), with the suitability being low in some current cropland areas according to this index. Therefore, while climate change clearly has the potential to decrease suitability for cultivation if temperature and precipitation regimes become less favourable, there is also scope for climate change to increase suitability in some existing cropland areas if conditions become more favourable in areas where the suitability index is not at its maximum value of 1. It should be noted that some areas which are not currently croplands may already be suitable for cultivation or may become suitable as a result of future climate change, and may become used a croplands in the future either as part of climate change adaptation or changes in land use arising for other reasons. Such areas are not included in this analysis.

Results

Crop suitability was estimated under the pattern of climate change from 21 GCMs with two emissions scenarios; 1) SRES A1B and 2) an aggressive mitigation scenario where emissions follow A1B up to 2016 but then decline at a rate of 5% per year thereafter to a low emissions floor (denoted A1B-2016-5-L). The application of 21 GCMs is an attempt to quantify the uncertainty due to climate modelling, although it is acknowledged that only one crop suitability impacts model is applied. Simulations were performed for the years 2030, 2050, 2080 and 2100. The results for China are presented in Figure 3.

Under all the climate projections, some existing cropland areas in China become less suitable for cultivation while other existing cropland areas become more suitable. The areas of increased and decreased suitability differ considerably according to the climate model used, but some common trends can be discerned. The areas experiencing declining suitability become larger through the 21st century in both the A1B and mitigation scenario, but the increase is larger in A1B. The difference between model projections of this quantity also becomes larger over time, and also becomes larger under A1B than the mitigation scenario.

However, the range of areas projected to experience increased suitability is similar in both scenarios and does not change significantly over time in either scenario. This may be because only current croplands are considered – although over a wider area there may be differences in suitability between different scenarios and different times, this would not appear in the current analysis if such changes occurred outside current cropland areas.

The mean projection for areas of declining suitability is the same as that for increasing suitability in 2030 (15% of current cropland in China, for both scenarios), but the difference between models is larger for declining suitability (again suggesting that the cropland area itself may be a limiting factor for increasing suitability). By 2100, up to 60% of current croplands in China are projected to become less suitable under A1B, but only up to 43% under the mitigation scenario.

So, for China, the areas of current croplands becoming less suitable for cultivation are projected to be smaller under the mitigation scenario than the A1B scenario, and in both scenarios the area of declining suitability becomes larger than that of increasing suitability (which remains similar over the 21st century in both scenarios).

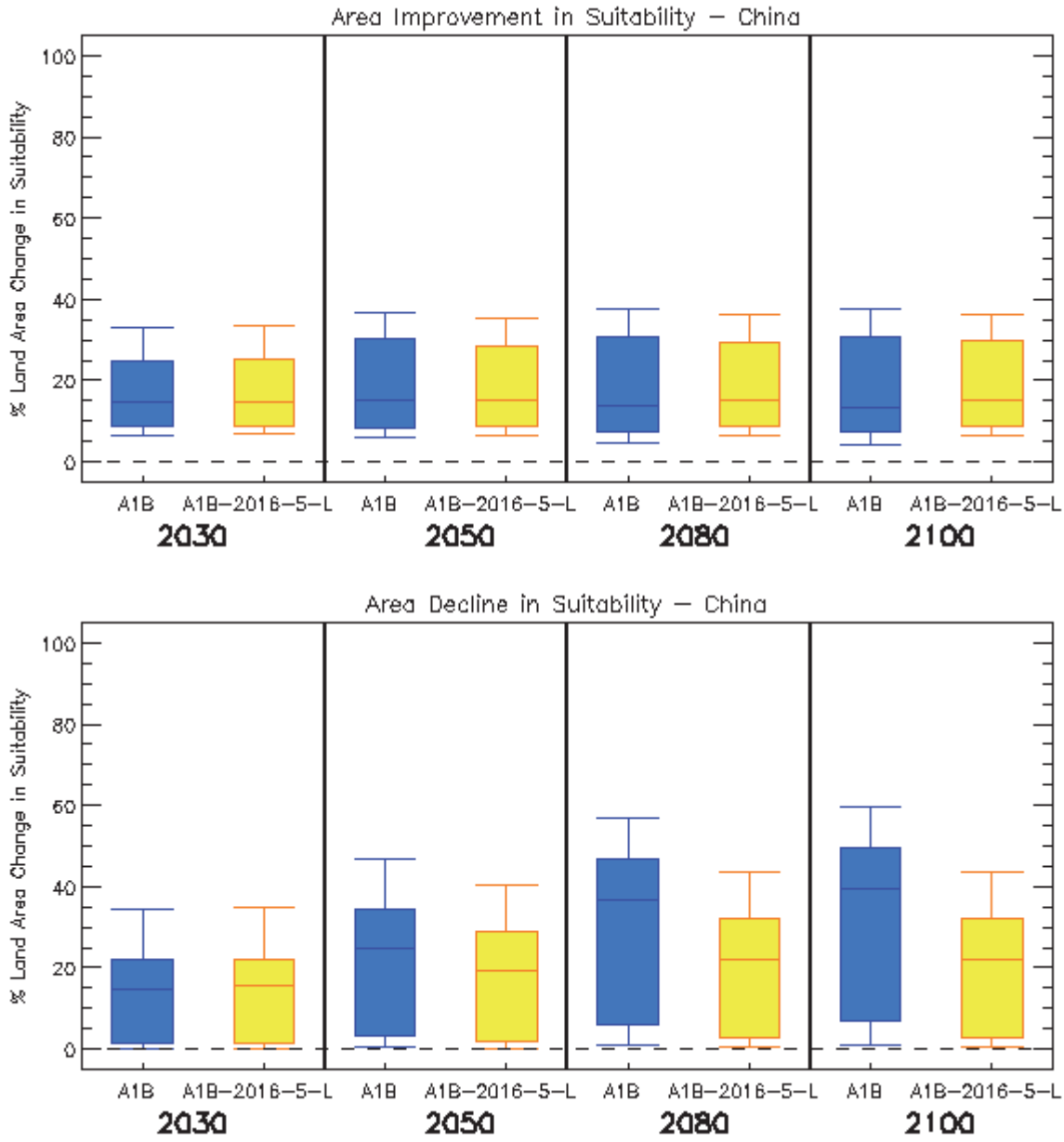

***Figure 3**. Box and whisker plots for the impact of climate change on increased crop suitability (top panel) and decreased crop suitability (bottom panel) for China, from 21 GCMs under two emissions scenarios (A1B and A1B-2016-5-L), for four time horizons. The plots show the 25th, 50th, and 75th percentiles (represented by the boxes), and the maximum and minimum values (shown by the extent of the whiskers).*

Food security

Headline

Large uncertainty is associated with quantifying the effect of climate change on food security for China. Some studies suggest that China may not face pressures on food security under climate change, and others suggesting that China could face severe food security issues.

Supporting literature

Introduction

Food security is a concept that encompasses more than just crop production, but is a complex interaction between food availability and socio-economic, policy and health factors that influence access to food, utilisation and stability of food supplies. In 1996 the World Food Summit defined food security as existing 'when all people, at all times, have physical and economic access to sufficient, safe and nutritious food to meet their dietary needs, and their food preferences are met for an active and healthy life'.

As such this section cannot be a comprehensive analysis of all the factors that are important in determining food security, but does attempt to assess a selection of the available literature on how climate change, combined with projections of global and regional population and policy responses, may influence food security.

Assessments that include a global or regional perspective

China is not a country of high concern in terms of food security, particularly in a global context. According to FAO statistics China has a very low level of undernourishment, (between 5% and 9% of the population).

Climate change studies

The results presented by Wu et al. (2011) suggest an optimistic future for China's food security situation. Wu et al. (2011) simulated crop yields with the GIS-based Environmental Policy Integrated Climate (EPIC) model. This was combined with crop areas simulated by a crop choice decision model to calculate total food production and per capita food availability across the globe, which was used to represent the status of food availability and stability.

The study focussed on the SRES A1 scenario and applied climate change simulations for the 2000s (1991–2000) and 2020s (2011–2020). The climate simulations were performed by MIROC (Model for Interdisciplinary Research on Climate) version 3.2., which means the effects of climate model uncertainty were not considered. Downscaled population and GDP data from the International Institute for Applied Systems Analysis (IIASA) were applied in the simulations. Wu et al. (2011) conclude that China is not likely to face severe food insecurity in the next 20 years. Similarly, Lobell et al. (2008) explored climate risks for crops in 12 food-insecure regions, based on statistical crop models and climate projections for 2030 from 20 GCMs. The study found that, based upon a number of probabilistic projections for various crops, China is unlikely to suffer food insecurity because although crop yields do decline under climate change, the crops grown in China present a relatively lower "Hunger Importance Rating" (HIR) than for other regions.

However, Falkenmark et al. (2009) present a global analysis of food security under climate change scenarios for the 2050s that considers the importance of water availability for ensuring global food security and obtains less optimistic results. The study presents an analysis of water constraints and opportunities for global food production on current croplands and assesses five main factors:

1) how far improved land and water management might go towards achieving global food security,

2) the water deficits that would remain in regions currently experiencing water scarcity and which are aiming at food self-sufficiency,

3) how the water deficits above may be met by importing food,

4) the cropland expansion required in low income countries without the needed purchasing power for such imports, and

5) the proportion of that expansion pressure which will remain unresolved due to potential lack of accessible land.

Similar to the study presented by Wu et al. (2011), there is no major treatment of modelling uncertainty; simulations were generated by only the LPJml dynamic global vegetation and water balance model (Gerten et al. 2004) with population growth and climate change under the SRES A2 emission scenario. Falkenmark et al. (2009) summarise the impacts of future improvements (or lack thereof) in water productivity for each country across the globe and show that this generates either a deficit or a surplus of water in relation to food water

requirements in each country. These can be met either by trade or by horizontal expansion (by converting other terrestrial ecosystems to crop land). The study estimated that in 2050 around one third of the world's population could live in each of three regions: those that export food, those that import food, and those that have to expand their croplands at the expense of other ecosystems because they do not have enough purchasing power to import their food. The simulations demonstrated that China could be a food importing country in 2050.

The results presented by Arnell et al. (2010b) are also less optimistic. Arnell et al. (2010b) considered the impacts of global climate change and mitigation on food security for eleven countries. The study applied climate change patterns from the HadCM3 GCM and explored food security under two emissions scenarios; a business as usual scenario (SRES A1B) and four mitigations scenarios where emissions peak in 2030 and subsequently reduce at 2% per year to a high emissions floor (referred to as 2030-2-H) or 5% per year to a low emissions floor (2030-5-L), or where they peak in 2016 and subsequently reduce at 2% per year to a high emissions floor (referred to as 2016-2-H) or 5% per year to a low emissions floor (2016-5-L). The study also considered a series of structural adjustments that could be made in the future to adapt to food security issues, including that 1) if there is a shortfall of any per-capita food availability due to crop yield and/or population changes, then original (baseline) food amounts are made up by reducing or removing export amounts; and 2) if, after the above adjustments, there is still a shortfall, then the amount of crops going to animal feed is reduced or removed to try to make up to the original (baseline) food amounts. The model simulations presented by Arnell et al. (2010b) characterise the numbers of people *exposed to undernourishment* in the absence of increased crop production and imports, not actual numbers of undernourished people. The results are presented in Figure 4. Arnell et al. (2010b) calculated that undernourishment increases in China up until 2050, after which it begins to decline. The principle initial causal factor is a 28% increase in population up to 2050. This is followed by a decline in population which reduces population below current levels by 2100. Despite this decline, decreasing crop yields under all scenarios mean that undernourishment could remain higher than levels are in the present, with all mitigation scenarios (plus structural adjustments) giving similar results of 40-50% of total population undernourished by 2100, as compared to 70% with no mitigation.

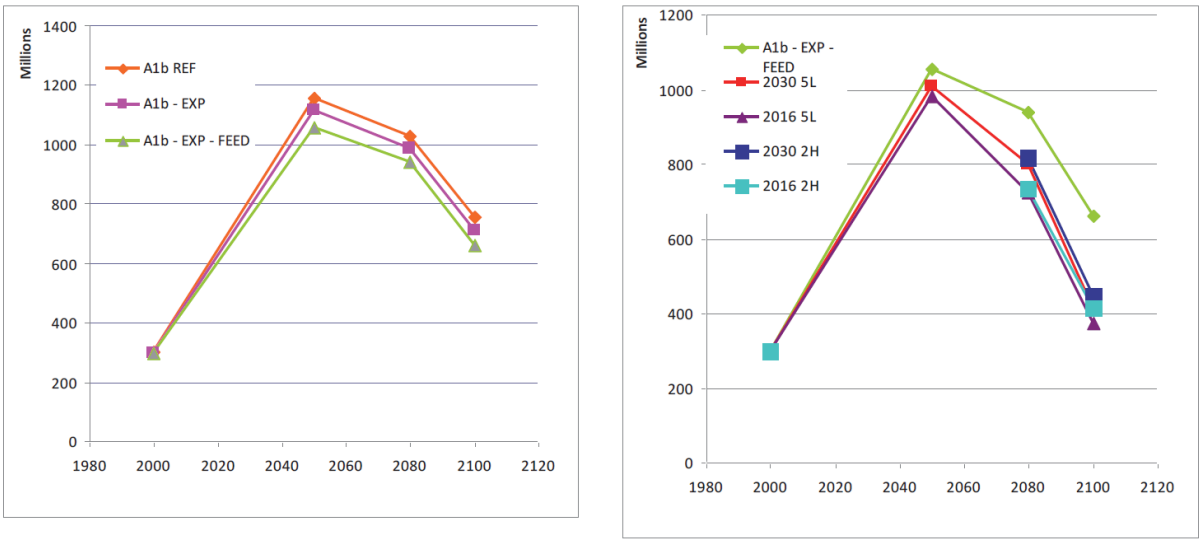

Figure 4. *Total projected population exposed to undernourishment in China. The left panel shows total exposure under the A1B emissions scenario ("A1b REF"), plus the A1B scenario with exports reduced or removed ("A1b–EXP") and the A1B scenario with exports removed and allocation to feed reduced or removed ("A1b–EXP–FEED"). The right panel shows the total exposure under the A1b–EXP–FEED and three mitigation scenarios. The figure is from Arnell et al. (2010b).*

The International Food Policy Research Institute (IFPRI) have produced a report and online tool that describes the possible impact of climate change on two major indicators of food security; 1) the number of children aged 0-5 malnourished, and 2) the average daily kilocalorie availability (Nelson et al., 2010; IFPRI, 2010)**.** The study considered three broad socio-economic scenarios; 1) a 'pessimistic' scenario, which is representative of the lowest of the four GDP growth rate scenarios from the Millennium Ecosystem Assessment GDP scenarios and equivalent to the UN high variant of future population change, 2) a 'baseline' scenario, which is based on future GDP rates estimated by the World Bank and a population change scenario equivalent to the UN medium variant, and 3) an 'optimistic' scenario that is representative of the highest of the four GDP growth rate scenarios from the Millennium Ecosystem Assessment GDP scenarios and equivalent to the UN low variant of future population change. Nelson et al. (2010) also considered climate modelling and emission uncertainty and included a factor to account for CO_2 fertilisation in their work. The study applied two GCMs, the CSIRO GCM and the MIROC GCM, and forced each GCM with two SRES emissions scenarios (A1B and B1). They also considered a no climate change emissions scenario, which they called 'perfect mitigation' (note that in most other climate change impact studies that this is referred to as the baseline). The changes shown the combination of both climate change and socio-economic changes. Estimates for both indicators of food security from 2010 to 2050, for China, are presented in Table 10 and Table

11. Figure 5 displays the effect of climate change, calculated by comparing the 'perfect mitigation' scenario with each baseline, optimistic and pessimistic scenario. The results show that for most scenarios the number of children malnourished in China declines considerably from 2010 to 2050. There are also large increases in average kilocalorie availability over this time. However, these improvements are largely due to socio-economic factors and not due to a positive climate change effect. To the contrary, by 2050, climate change is attributable for up to a 10% decline in kilocalorie availability, and over a 200% increase in child malnourishment (baseline scenario). This suggests that climate change could have a serious impact on food security in China, unless adequate adaptation measures are taken, which is largely supportive of conclusions reached by Falkenmark et al. (2009) and Arnell et al. (2010b). Figure 6 and Figure 7 show how the changes projected for China compare with the projections for the rest of the globe (IFPRI, 2010).

Scenario	2010	2050
Baseline CSI A1B	2992	3160
Baseline CSI B1	2996	3190
Baseline MIR A1B	2975	3089
Baseline MIR B1	2984	3141
Baseline Perfect Mitigation	3043	3418
Pessimistic CSI A1B	2928	2671
Pessimistic CSI B1	2932	2696
Pessimistic MIR A1B	2911	2609
Pessimistic MIR B1	2919	2649
Pessimistic Perfect Mitigation	2977	2891
Optimistic CSI A1B	2968	3502
Optimistic CSI B1	2971	3521
Optimistic MIR A1B	2949	3408
Optimistic MIR B1	2957	3454
Optimistic Perfect Mitigation	3016	3771

Table 10. *Average daily kilocalorie availability simulated under different climate and socioeconomic scenarios, for China (IFPRI, 2010)*

Scenario	2010	2050
Baseline CSI A1B	7.41	2.16
Baseline CSI B1	7.38	1.98
Baseline MIR A1B	7.54	2.57
Baseline MIR B1	7.47	2.27
Baseline Perfect Mitigation	7.05	0.72
Pessimistic CSI A1B	7.88	5.97
Pessimistic CSI B1	7.85	5.77
Pessimistic MIR A1B	8.01	6.46
Pessimistic MIR B1	7.95	6.15
Pessimistic Perfect Mitigation	7.52	4.32
Optimistic CSI A1B	7.59	0.24
Optimistic CSI B1	7.57	0.16
Optimistic MIR A1B	7.73	0.68
Optimistic MIR B1	7.67	0.46
Optimistic Perfect Mitigation	7.24	No data

Table 11. *Number of malnourished children (aged 0-5; millions) simulated under different climate and socioeconomic scenarios, for China (IFPRI, 2010).*

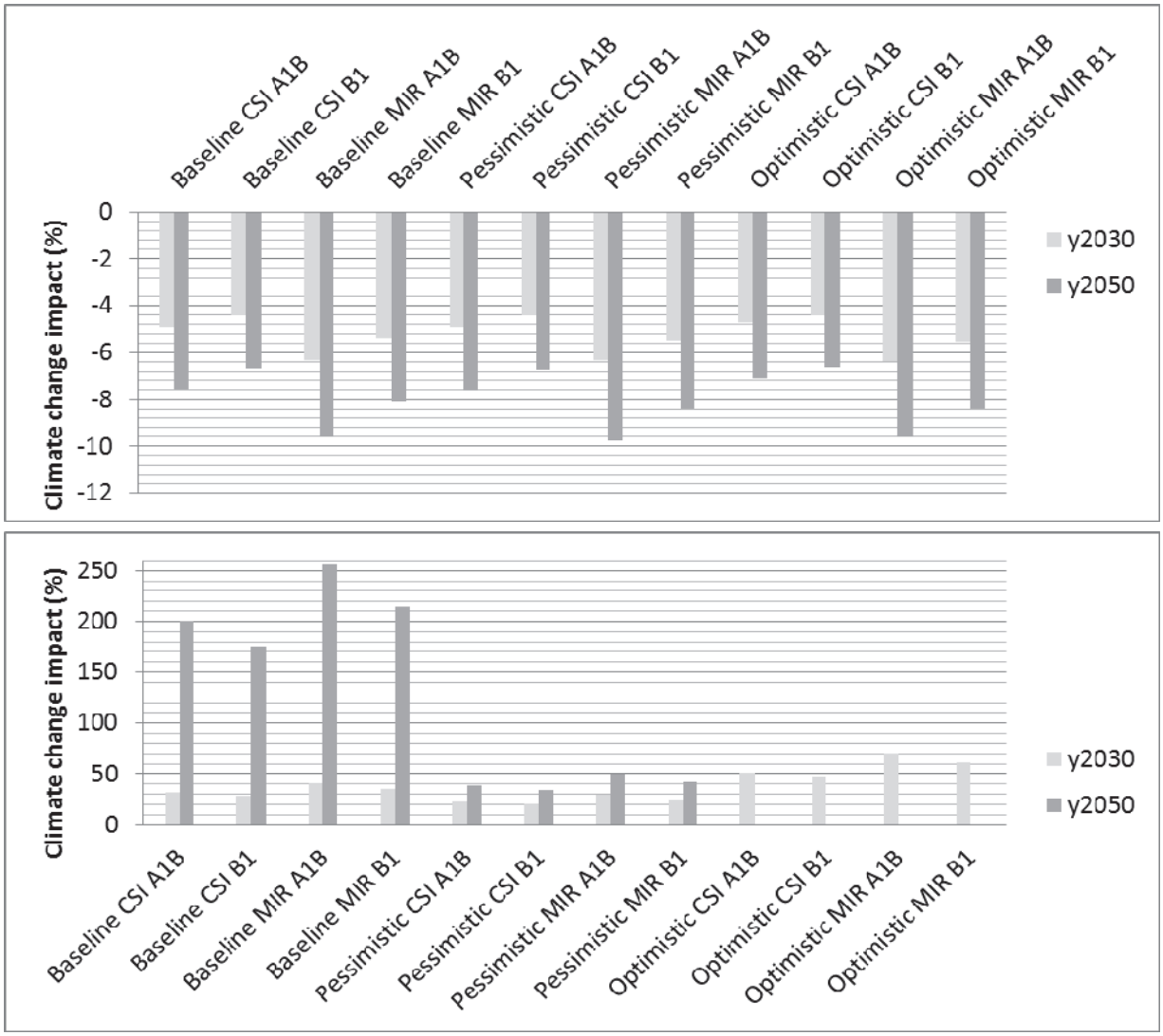

Figure 5. *The impact of climate change on average daily kilocalorie availability (top panel) and number of malnourished children (bottom) (IFPRI, 2010).*

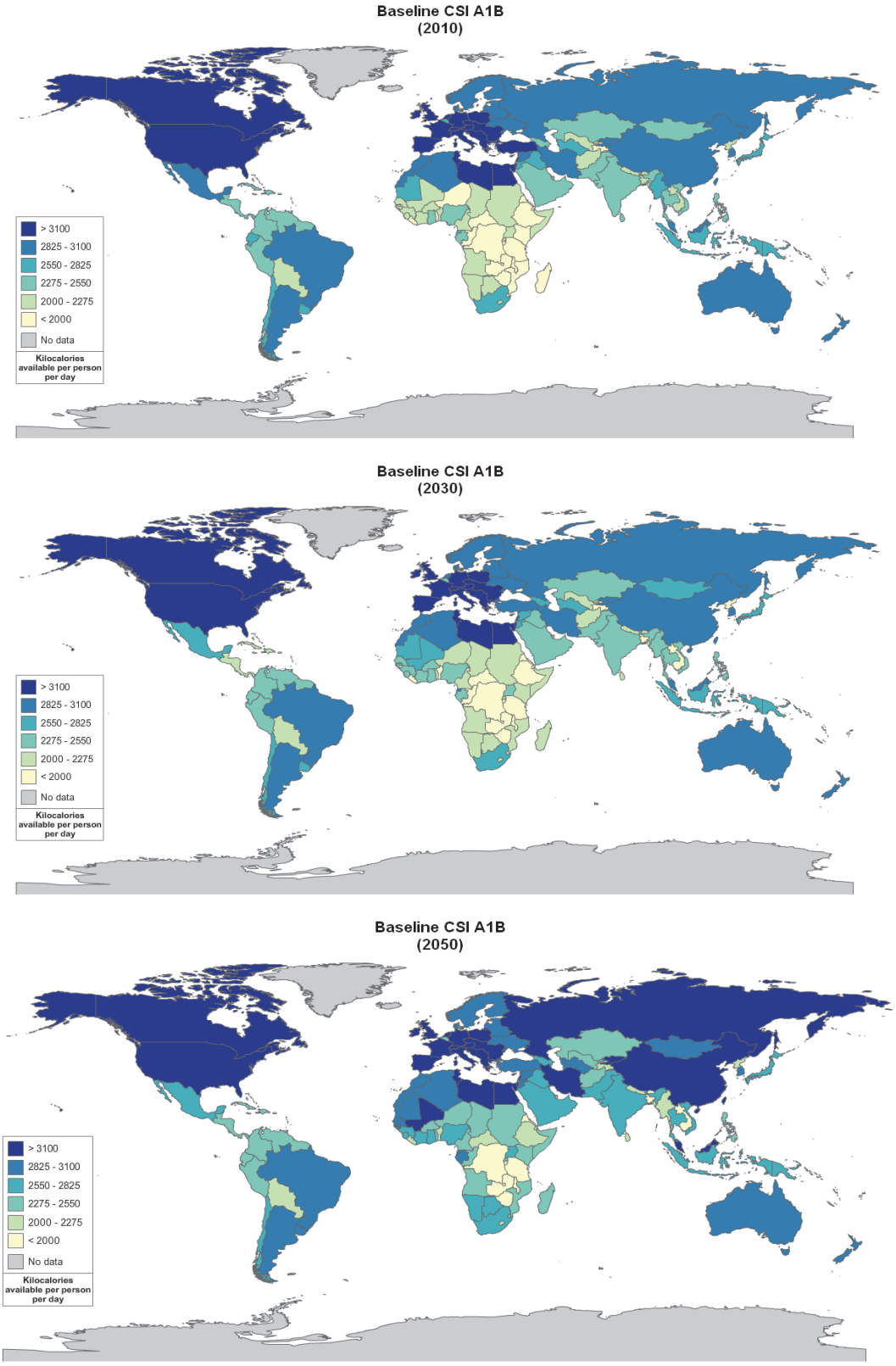

Figure 6. *Average daily kilocalorie availability simulated by the CSIRO GCM (CSI) under an A1B emissions scenario and the baseline socioeconomic scenario, for 2010 (top panel), 2030 (middle panel) and 2050 (bottom panel). The figure is from IFPRI (IFPRI, 2010). The changes show the combination of both climate change and socio-economic changes.*

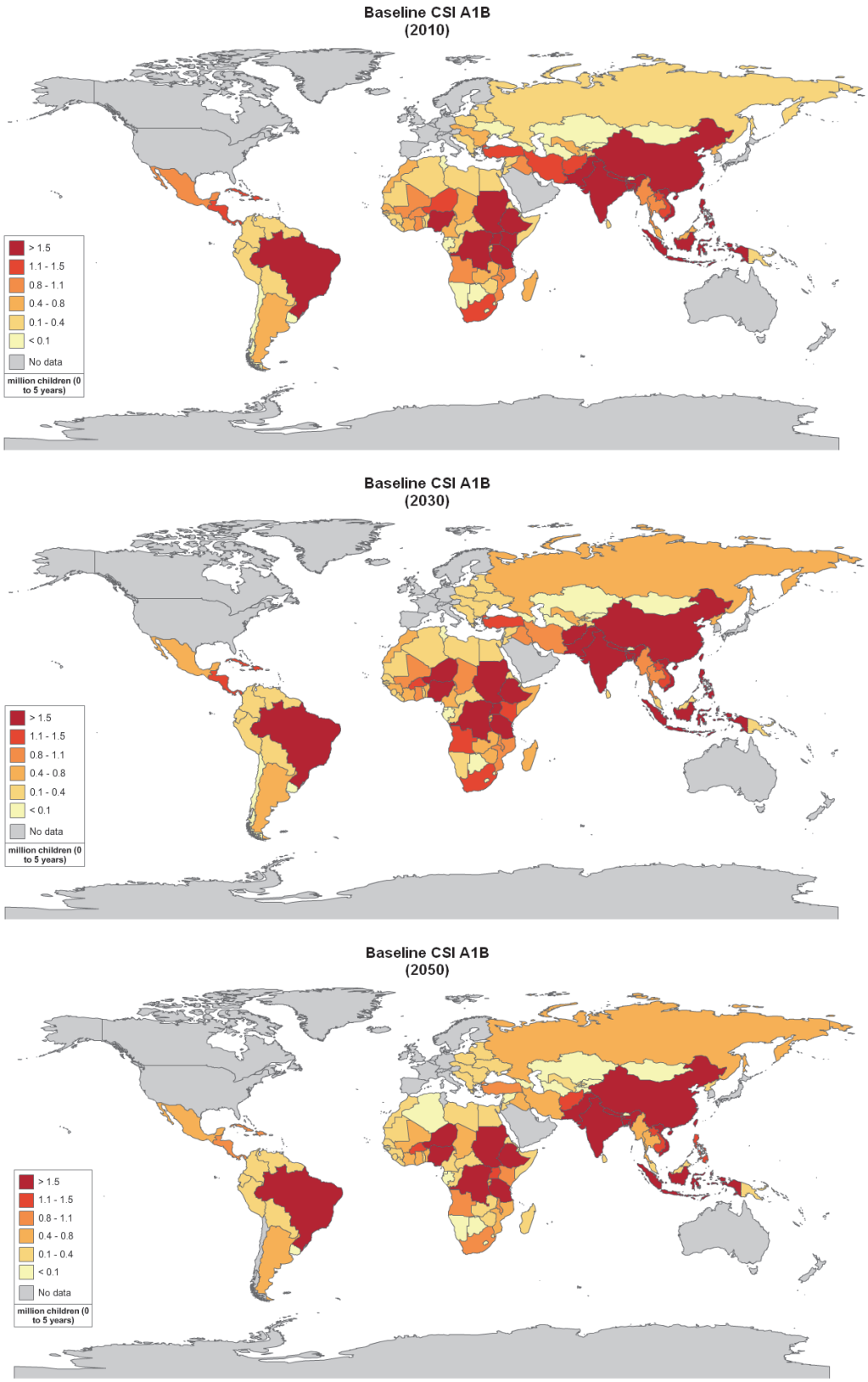

Figure 7. *Number of malnourished children (aged 0-5; millions) simulated by the CSIRO GCM (CSI) under an A1B emissions scenario and the baseline socioeconomic scenario, for 2010 (top panel), 2030 (middle panel) and 2050 (bottom panel). The figure is from IFPRI (IFPRI, 2010). The changes show the combination of both climate change and socio-economic changes.*

It is important to note that up until recently, projections of climate change impacts on global food supply have tended to focus solely on production from terrestrial biomes, with the large contribution of animal protein from marine capture fisheries often ignored. However, recent studies have addressed this knowledge gap (Allison et al. 2009, Cheung et al., 2010). In addition to the direct affects of climate change, changes in the acidity of the oceans, due to increases in CO_2 levels, could also have an impact of marine ecosystems, which could also affect fish stocks. However, this relationship is complex and not well understood, and studies today have not been able to begin to quantify the impact of ocean acidification on fish stocks. For example, Allison et al. (2009) present a global analysis that compares the vulnerability of 132 national economies to potential climate change impacts on their capture fisheries by 2050. The study considered a country's vulnerability to be a function of the combined effect of projected climate change, the relative importance of fisheries to national economies and diets, and the national societal capacity to adapt to potential impacts and opportunities. Climate change projections from a single GCM under two emissions scenarios (SRES A1FI and B2) were used in the analysis. Allison et al. (2009) concluded that the national economy of China presented a moderate vulnerability to climate change impacts on fisheries. In contrast, countries in Central and Western Africa (e.g. Malawi, Guinea, Senegal, and Uganda), Peru and Colombia in north-western South America, and four tropical Asian countries (Bangladesh, Cambodia, Pakistan, and Yemen) were identified as most vulnerable (see Figure 8). It should be noted, however, that results from studies that have applied only a single climate model or climate change scenario should be interpreted with caution. This is because they do not consider other possible climate change scenarios which could result in a different impact outcome, in terms of magnitude and in some cases sign of change.

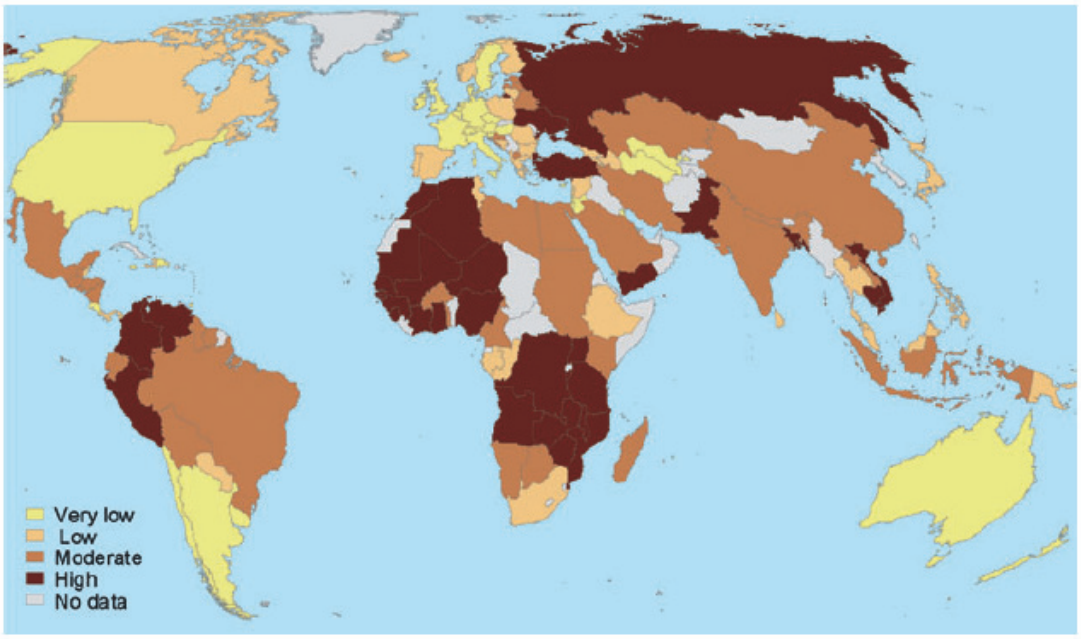

Figure 8. *Vulnerability of national economies to potential climate change impacts on fisheries under SRES B2 by 2050 (Allison et al., 2009). Colours represent quartiles with dark brown for the upper quartile (highest index value), yellow for the lowest quartile, and grey where no data were available.*

Cheung et al. (2010) also consider marine capture fisheries at the global scale for several countries. The study projected changes in global catch potential for 1066 species of exploited marine fish and invertebrates from 2005 to 2055 under climate change scenarios. Cheung et al. (2010) found that climate change may lead to large-scale redistribution of global catch potential, with an average of 30–70% increase in high-latitude regions and a decline of up to 40% in the tropics. The simulations were based climate simulations from a single GCM (GFDL CM2.1) under a SRES A1B emissions scenario (CO_2 concentration at 720ppm in 2100) and a stable-2000 level scenario (CO_2 concentration maintains at year 2000 level of 365 ppm). For China, the projected change in the 10-year averaged maximum catch potential from 2005 to 2055 was around a 7% reduction under A1b and a 3% reduction under the stabilisation scenario, based upon 101 exploited species included in the analysis. Figure 9 demonstrates how this compares with projected changes for other countries across the globe. The limitations of applying a single GCM have been noted previously.

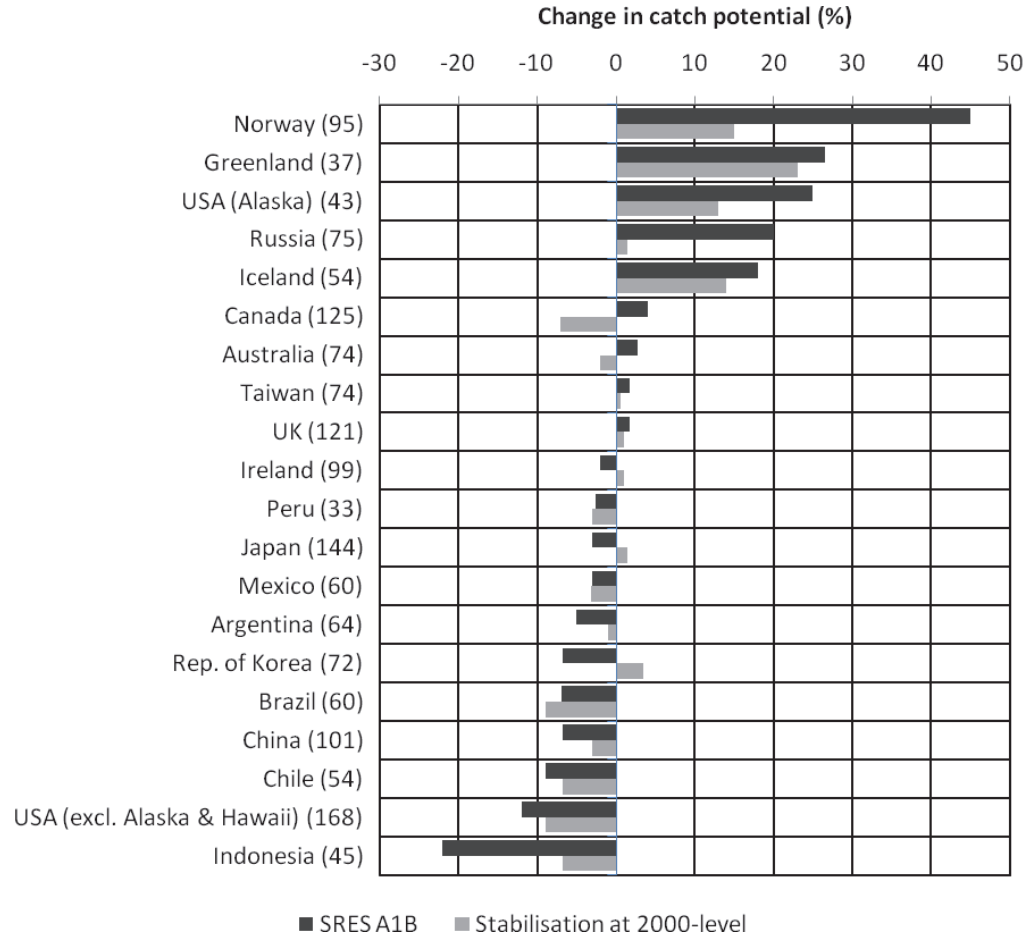

Figure 9. *Projected changes in the 10-year averaged maximum catch potential from 2005 to 2055. The numbers in parentheses represent the numbers of exploited species included in the analysis. Adapted from Cheung et al. (2010).*

National-scale or sub-national scale assessments

Climate change studies

A number of national-scale studies confirm the uncertainty that surrounds the issue of whether China could experience food security problems under climate change scenarios. Some studies suggest China could experience large food shortages (Mu and Khan, 2009), whilst others suggest the opposite (Tao et al., 2009; Xiong et al., 2007).

Mu and Khan (2009) applied estimates of future irrigation demands and crop production to estimate food surpluses and deficits in the years 2000, 2030 and 2050. The simulations indicated that total grain demand in China could increase from 427 million tons in 2000 to 609 million tons by 2030 and 714 million tons by 2050. The simulations also estimated that food production in 2030 and 2050 could be 521 million tons and 629 million tons, which is 121 million tons and 229 million tons higher than in 2000, respectively. To this end, Mu and

Khan (2009) conclude that the 27 million ton grain deficit that was estimated for China in the year 2000 is projected to rise to 88 million tons and 85 million tons, respectively, in 2030 and 2050 in the medium population growth and irrigation area development scenarios. To meet the total food demand in 2030 and 2050, 46% and 75% of surface water and groundwater irrigation efficiencies in the year 2030 and 45% and 72% of surface water and groundwater irrigation efficiencies in the year 2050 could be required.

Xiong et al. (2007) considered the combined effects of technological advances, trade and climate change from a single Regional Climate Model (RCM), developed by the Met Office, called PRECIS, including the CO_2 fertilisation effect, to estimate future (year 2080) food availability in China. The study observed that when technology progress and international trade were incorporated into simulations, without the CO_2 fertilization effect, the per capita grain supply could meet future basic demand (300 kg/capita) for direct human consumption in China under an SRES B2 scenario. However, it could not be met under an A2 emissions scenario. When the CO_2 fertilization effect was included, the basic food demand could be satisfied under both A2 and B2 scenarios, and the additional food requirement for sustained economic growth (400 kg/capita) could be met under the B2 scenario. Xiong et al. (2007) conclude that overall, the impact of climate change on China's main crops production could have more positive than negative impacts if the direct effects of CO_2 are included. Nevertheless, the authors note the limiting factors of their study, mainly that the effects of pests and diseases are not considered, in addition the response of plants to elevated levels of CO_2 is not well understood. It should be noted, also, that results from studies that have applied only a single climate model or climate change scenario should be interpreted with caution. This is because they do not consider other possible climate change scenarios which could result in a different impact outcome, in terms of magnitude and in some cases sign of change.

Tao et al. (2009) demonstrate the importance of the proportion of the total cropland in a country that is used to grow cereals (an index they denote "H/C"), for determining future food security in China. Tao et al. (2009) argue that H/C could be higher than 100% in the future because harvest area could be larger than cropland area in a given region, with double or triple cropping systems that allow multiple harvests per year. The study defines food security as meaning that China can meet the food demand for the whole population (using 95% domestic production and 5% imports) according to a living standard they base on per capita GDP in the projected year. By assuming that H/C increases from 20% to 100% as a result of technological advances and innovation, the study shows that China's food demand could be satisfied in the 2020s, 2050s and 2080s, and moreover that China could have food surplus.

The food surplus is equivalent amount of food demand of 221 to 708 million people in 2020s, of 44 to 1,251 million people in 2050s, and of 125 to 1,906 million people in 2080s. However, the limitations of assuming that H/C could increase from 20% to 100% should be noted, and Tao et al. (2009) highlight that if H/C were only 20%, the number of people at risk of under nutrition could be 955-1,107 million in the 2020s, 750-1,356 million in the 2050s, and 381-1,823 million in 2080s, which is far less optimistic than when H/C equal to 100% is assumed.

Water stress and drought

Headline

Studies indicate that south-eastern China is currently vulnerable to water stress. Simulations from global-scale and national-scale assessments suggest that water stress could increase in China for global-mean warming scenarios of around 2°C. However, under higher emissions scenarios and global-mean warming, simulations show that water stress may decrease relative to present in China, due to an increase in precipitation and runoff – this is supported by recent research by the AVOID programme. Nevertheless, there is no consensus across all studies, with some suggesting deceased water stress with climate change and some an increase. This is due to the application of different climate models, indicators of water stress, hydrological models, emissions scenarios, time horizons, and the large geographical area of China.

Supporting literature

Introduction

For the purposes of this report droughts are considered to be extreme events at the lower bound of climate variability; episodes of prolonged absence or marked deficiency of precipitation. Water stress is considered as the situation where water stores and fluxes (e.g. groundwater and river discharge) are not replenished at a sufficient rate to adequately meet water demand and consumption.

A number of impact model studies looking at water stress and drought for the present (recent past) and future (climate change scenario) have been conducted. These studies are conducted at global or national scale and include the application of global water 'availability' or 'stress' models driven by one or more climate change scenario from one or more GCM. The approaches variously include other factors and assumptions that might affect water availability, such as the impact of changing demographics and infrastructure investment, etc. These different models (hydrological and climate), assumptions and emissions scenarios mean that there are a range of water stress projections for China. This section summarises findings from these studies to inform and contextualise the analysis performed by the AVOID

programme for this project. The results from the AVOID work and discussed in the next section.

Important knowledge gaps and key uncertainties which are applicable to China as well as at the global-scale, include; the appropriate coupling of surface water and groundwater in hydrological models, including the recharge process, improved soil moisture and evaporation dynamics, inclusion of water quality, inclusion of water management (Wood et al. 2011) and further refinement of the down-scaling methodologies used for the climate driving variables (Harding et al. 2011).

Assessments that include a global or regional perspective

Recent Past

Recent research presented by Vörösmarty et al. (2010) describes the calculation of an '*Adjusted Human Water Security Threat'* (HWS) indicator. The indicator is a function of the cumulative impacts of 23 biophysical and chemical drivers simulated globally across 46,517 grid cells representing 99.2 million km^2. With a digital terrain model at its base, the calculations in each of the grid boxes of this model take account of the multiple pressures on the environment, and the way these combine with each other, as water flows in river basins. The level of investment in water infrastructure is also considered. This infrastructure measure (the *investment benefits factor*) is based on actual existing built infrastructure, rather than on the financial value of investments made in the water sector, which is a very unreliable and incomplete dataset. The analysis described by Vörösmarty et al. (2010) represents the current state-of-the-art in applied policy-focussed water resource assessment. In this measure of water security, the method reveals those areas where this is lacking, which is a representation of human water stress. One drawback of this method is that no analysis is provided in places where there is 'no appreciable flow', where rivers do not flow, or only do so for such short periods that they cannot be reliably measured. This method also does not address places where water supplies depend wholly on groundwater or desalination, being piped in, or based on wastewater reuse. It is based on what is known from all verified peer reviewed sources about surface water resources as generated by natural ecosystem processes and modified by river and other hydraulic infrastructure (Vörösmarty et al., 2010).

Here, the present day HWS is mapped for China. The model applied operates at 50km resolution, so, larger countries appear to have smoother coverage than smaller countries, but all are mapped and calculated on the same scale, with the same data and model, and thus comparisons between places are legitimate. It is important to note that this analysis is a

comparative one, where each place is assessed *relative* to the rest of the globe. In this way, this presents a realistic comparison of conditions across the globe. As a result of this, however, some places may seem to be less stressed than may be originally considered. One example is Australia, which is noted for its droughts and long dry spells, and while there are some densely populated cities in that country where water stress is a real issue, for most of the country, *relative to the rest of the world*, the measure suggests water stress (as measured by HWS defined by Vörösmarty et al. (2010)), is not a serious problem.

Figure 10 presents the results of this analysis for China. The holistic systems approach of this analysis shows the serious state of water resources in China. Only in the south-west of the country, where the great rivers rise and population is lower, is there a moderate degree of water security. Elsewhere, pollution, abstraction, water storage and land degradation have all combined to place a high level of threat to water security for the majority of the population.

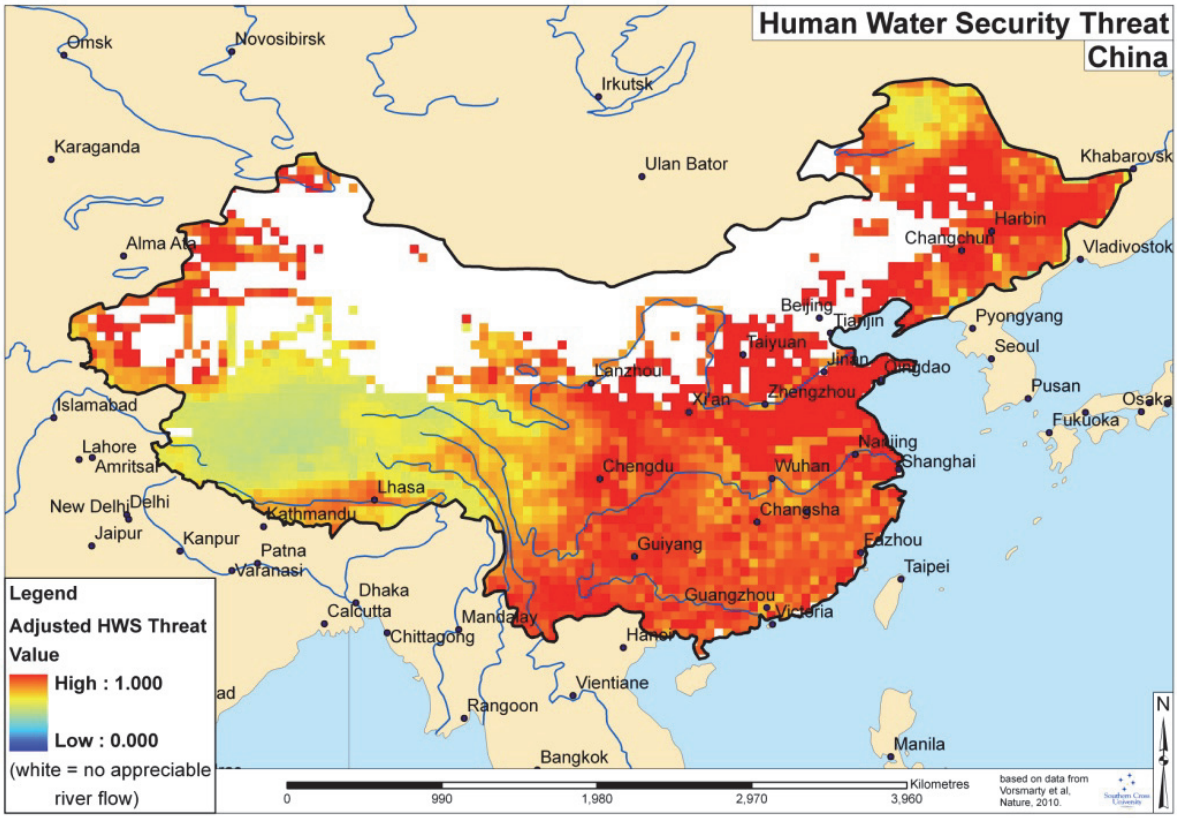

***Figure 10**. Present Adjusted Human Water Security Threat (HWS) for China, calculated following the method described by Vörösmarty et al. (2010).*

Smakhtin et al. (2004) present a first attempt to estimate the volume of water required for the maintenance of freshwater-dependent ecosystems at the global scale. This total

environmental water requirement (EWR) consists of ecologically relevant low-flow and high-flow components. The authors argue that the relationship between water availability, total use and the EWR may be described by the water stress indicator (WSI). If WSI exceeds 1.0, the basin is classified as “environmentally water scarce”. In such a basin, the discharge has already been reduced by total withdrawals to such levels that the amount of water left in the basin is less than EWR. Smaller index values indicate progressively lower water resources exploitation and lower risk of “environmental water scarcity.” Basins where WSI is greater than 0.6 but less than 1.0 are arbitrarily defined as heavily exploited or “environmentally water stressed” and basins where WSI is greater than 0.3 but less than 0.6 are defined as moderately exploited. In these basins, 0-40% and 40-70% of the utilizable water respectively is still available before water withdrawals come in conflict with the EWR. Environmentally “safe” basins are defined as those where WSI is less than 0.3. The global distribution of WSI for the 1961-1990 time horizon is shown in Figure 11.

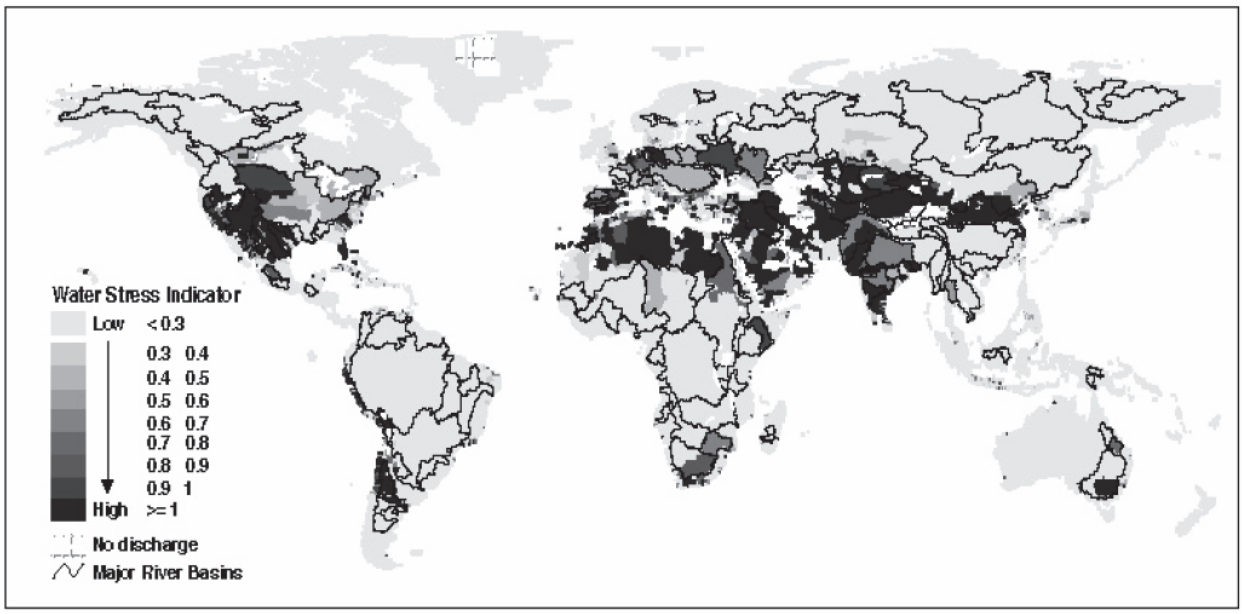

Figure 11. *A map of the major river basins across the globe and the water stress indicator (WSI) for the 1961-1990 time horizon. The figure is from Smakhtin et al. (2004).*

Climate change studies

Rockstrom et al. (2009) applied the LPJml vegetation and water balance model (Gerten et al. 2004) to assess green-blue water (irrigation and infiltrated water) availability and requirements. The authors applied observed climate data from the CRU TS2.1 gridded dataset for a present-day simulation, and climate change projections from the HadCM2 GCM under the SRES A2 scenario to represent the climate change scenario for the year 2050. The study assumed that if water availability was less than 1,300m^3/capita/year,

then the country was considered to present insufficient water for food self-sufficiency. The simulations presented by Rockstrom et al. (2009) should not be considered as definitive, however, because the study only applied one climate model, which means climate modelling uncertainty was overlooked. The results from the two simulations are presented in Figure 12. Rockstrom et al. (2009) found that globally in 2050 and under the SRES A2 scenario, around 59% of the world's population could be exposed to "blue water shortage" (i.e. irrigation water shortage), and 36% exposed to "green water shortages" (i.e. infiltrated rain shortage). For China, Rockstrom et al. (2009) found that blue-green water availability was well above the 1,300m^3/capita/year threshold in the present but that with climate change by 2050, China's population could be on the verge of exposure to green-blue water shortages.

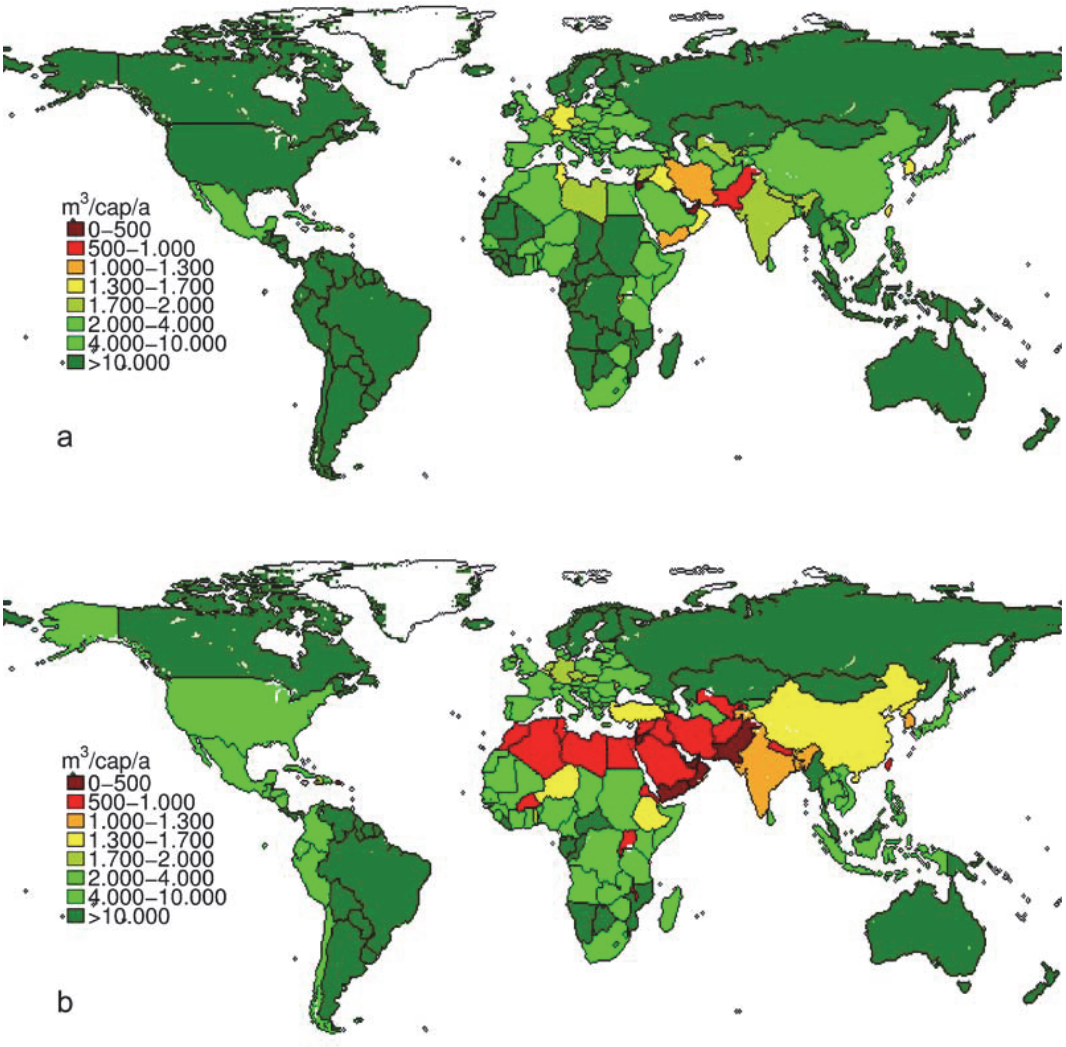

***Figure 12**. Simulated blue-green water availability (m^3/capita/year) for present climate (top panel) and including both demographic and climate change under the SRES A2 scenario in 2050 (bottom panel). The study assumed that if water availability was less than 1,300m^3/capita/year, then the country was considered to present insufficient water for food self-sufficiency. The figure is from Rockstrom et al. (2009).*

Doll (2009) presents updated estimates of the impact of climate change on groundwater resources by applying a new version of the WaterGAP hydrological model. The study accounted for the number of people affected by changes in groundwater resources under climate change relative to present (1961-1990). To this end, the study provides an assessment of the vulnerability of humans to decreases in available groundwater resources (GWR). This indicator was termed the “Vulnerability Index” (VI), defined as; VI = -% change GWR * Sensitivity Index (SI). The SI component was a function of three more specific sensitivity indicators that include an indicator of water scarcity (calculated from the ratio between consumptive water use to low flows), an indicator for the dependence upon groundwater supplies, and an indicator for the adaptive capacity of the human system. Doll (2009) applied climate projections from two GCMs (ECHAM4 and HadCM3) to WaterGAP, for two scenarios (SRES A2 and B2), for the 2050s. Figure 13 presents each of these four simulations respectively. For China, the simulations with HadCM3 suggest that China is not vulnerable to groundwater stress under climate change. However, with the ECHAM4 GCM and under the B2 scenario, south-east China is simulated to present low to moderate vulnerability – this is lower under the A2 emissions scenario because GWR was slightly lower with this scenario. The relatively low vulnerability of China suggested by Doll (2009) is likely due to the ratio of groundwater withdrawals to total water withdrawals being very low in China (Doll, 2009), relative to other countries considered in their analysis.

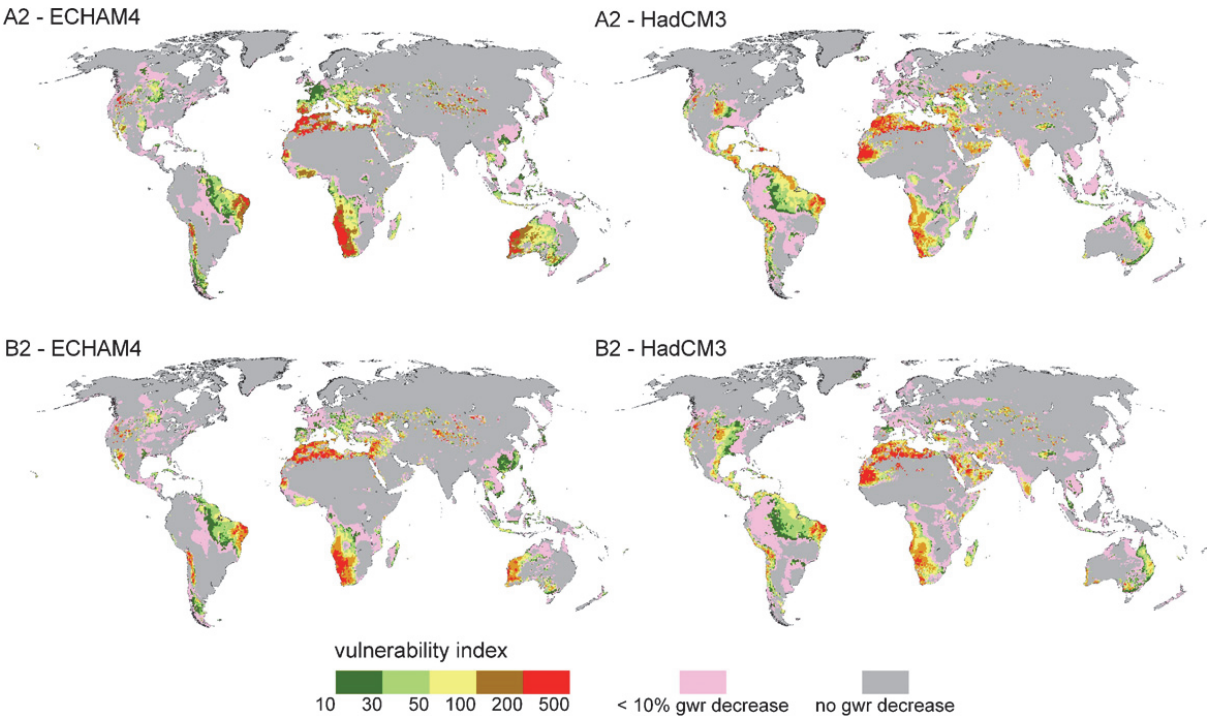

***Figure 13**. Vulnerability index (VI) showing human vulnerability to climate change induced decreases of renewable groundwater resources (GWR) by the 2050s under two emissions scenarios for two GCMs. VI is only defined for areas with a GWR decrease of at least 10% relative to present (1961-1990). The figure is from Doll (2009).*

Fung et al. (2011) applied climate change scenarios for prescribed global-mean warming of 2°C and 4°C respectively, from two ensembles; 1) an ensemble of 1518 (2°C world) and 399 (4°C) members from the ClimatePrediction.net (CPDN) experiments, and 2) an ensemble of climate projections from 22 GCMs included in the CMIP3 multi-model dataset. The climate projections were applied to the MacPDM global hydrological model (Gosling and Arnell, 2011) and population projections followed the UNPOP60 population scenario. Fung et al. (2011) calculated a water stress index (WSI) based upon resources per capita, similar to the method applied by Rockstrom et al.(2009). Results from the simulations are presented in Figure 14. There was consensus across models that water stress increases with climate change in south-eastern China with a 2°C global-mean warming. However, with 4°C warming, water availability increased relative to present in this region, in part, due to an increase in precipitation and runoff at the higher temperature.

It should also be noted that the estimates of drying across the globe that are presented by Fung et al. (2011) could be over-estimated slightly. This is because the MacPDM hydrological model is an offline model; i.e. it is not coupled to an ocean-atmosphere GCM. Therefore the dynamical effects of vegetation changes in response to water availability are not simulated. Recent work has highlighted that increased plant water use efficiency under

higher CO_2 may ameliorate future increased drought to some extent, but not completely (Betts et al. 2007).

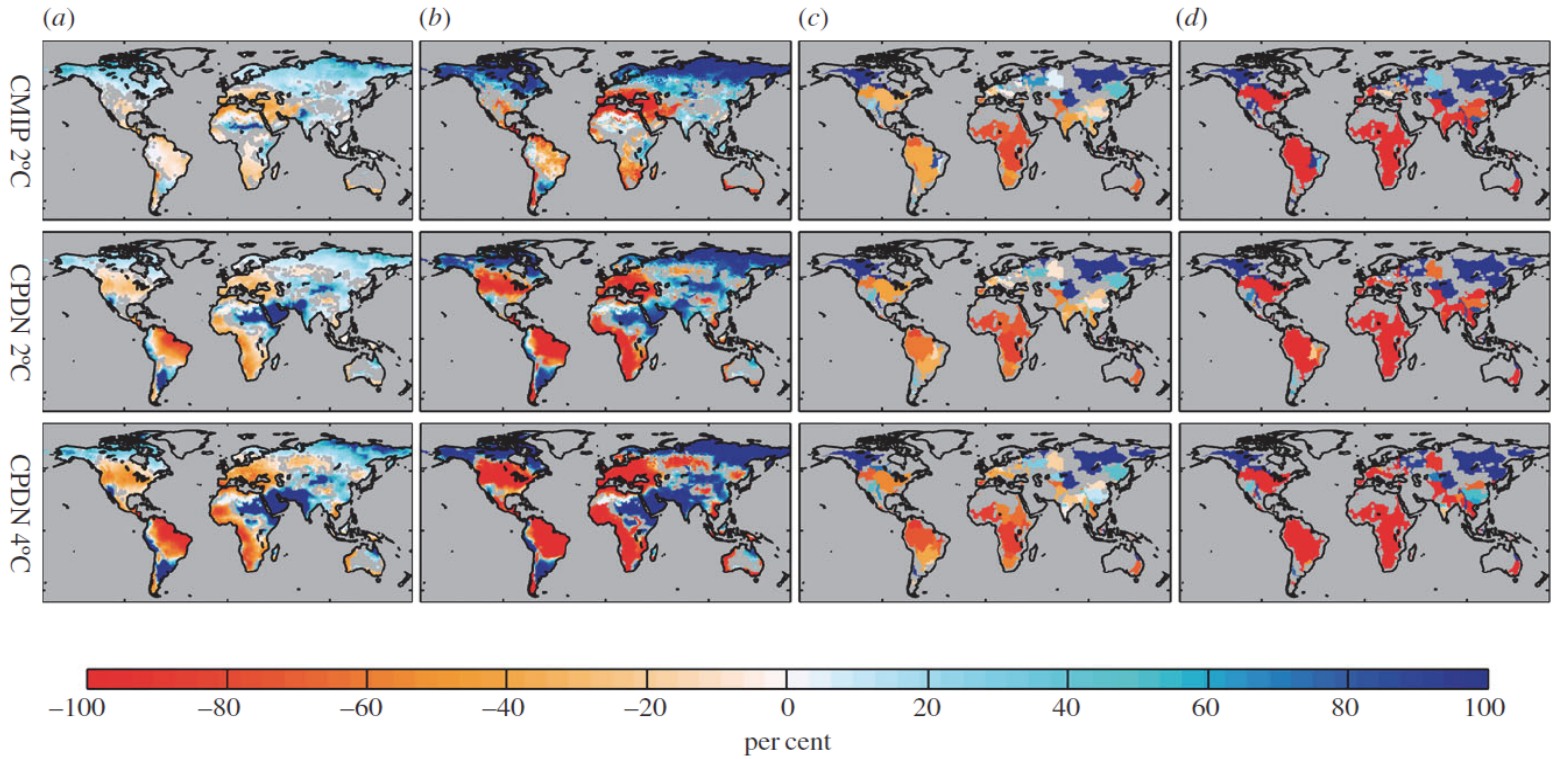

***Figure 14**. For a 2°C and 4°C rise in temperature and UNPOP60 population scenario compared with the baseline period (1961-1990); (a) spatial pattern of ensemble-average changes in mean annual run-off (DMAR), (b) model consensus on direction of change in run-off, (c) ensemble-average change in water stress (DWSI) and (d) model consensus on the direction of change in water stress. For the model consensus, red and therefore negative values represent the percentage of models showing a negative change in the respective parameter and for blue, positive values, represent the percentage of models showing a positive change. For DMAR and DWSI, colour classification spans from −100% to greater than 100% (this means that high positive values of DMAR and DWSI are effectively filtered out in these plots), whereas for consensus, colour classification spans from −100% to 100%. For plots of DMAR and consensus for the direction of change in run-off, grey land areas represent where DMAR is less than natural variability. For DWSI and consensus for direction of change in water stress, only 112 major river basins are plotted (Greenland has been excluded from the analysis). The figure is from Fung et al. (2011).*

National-scale or sub-national scale assessments

Recent past

The IPCC AR4 (2007a) noted an increase over recent decades in the area affected by drought, and that this has now exceeded 6.6Mha since 2000 in Beijing, Hebei Province, Shanxi Province, Inner Mongolia, and North China.

Shen et al. (2007) investigated severed historical droughts over the past five centuries in China. They identified three exceptional drought events (1586-89, 1638-41, and 1965-66) which all developed first in North China. In the most recent event (1965-66) the significant reduction in summer rainfall was due to a weakening of the summer monsoon and an anomalous displacement of the western Pacific subtropical high pressure. Other potential factors in these events are volcanic eruptions, which may trigger or amplify drought events, and El Niño events.

Cui et al. (2009) considered the evidence of changing river runoff and groundwater levels in the Yellow River basin since the mid 20th century. Runoff in the upper reaches was found to have increased, perhaps due to glacier melt, while in lower reaches the flow was much reduced. Water tables in Beijing have fallen, and per capita availability has dropped. Moreover, Ringler et al. (2010) estimated annual per capita water resources in the Yellow River basin to be around 430m^3, significantly less than the 1000m^3 value used to define chronic water scarcity by the Falkenmark Index. Furthermore, given that demand within the basin exceeds 75% of the of the renewable water resources available, management approaches are now focusing on demand rather than supply, and the need for more investment. Wang et al. (2006) analysed datasets of river discharge, precipitation and water demand for the Huanghe River in China and assessed the connections between decreasing river flows, global ENSO events and human impacts. Anthropogenic impacts were found to be as great as natural factors, accelerating losses from the hydrological cycle. Dams and reservoirs were observed to allow more use of the flow in the river, and this combined with ENSO events has resulted in serious declines in the water available. Increased losses from higher evapotranspiration as a result of climate change could however be offset by glacier melt in the near future.

Climate change studies

Jiang et al. (2011) notes that China is influenced by the East Asian monsoon system and that ensemble GCM simulations for the end of the 21st century indicate more frequent and intense precipitation events, particularly in the middle and lower reaches of the Yangtze River, the Southeast coastal region, western Northwest China, and the Tibetan Plateau. In

the Northeast and Northwest, a decrease in the number of consecutive dry days could reduce drought risk in these regions. The authors calculated several extreme precipitation indices for China; see Table 12. For an index of consecutive dry days (CDD), Jiang et al. (2011) noted that GCMs tend to underestimate the index in northern and western China where drought occurs more frequently, but overestimate it in the south where drought occurs less frequently. The authors conclude that GCMs do have a good ability to simulate the spatial distributions of the main extreme precipitation indices except the CDD index. The results demonstrate that precipitation generally increases with climate change for China and this increase is higher under higher emissions scenarios (e.g. A2) than lower scenarios (e.g. B1). The consecutive dry days averaged over the whole of China have small and inconsistent variation. They decrease under the lower emission (B1) scenario, but increase under mid-range (A1B) and higher (A2) emission scenarios. The small change in CDD is in fact the result of spatial cancellation from different regions of China. CDDs show a weak decreasing trend of 9.9 day/100-year in the past (1961-2000), with trends in the twenty-first century of 1.4, 1.0 and -0.4 day/100-year for the A2, A1B and B1 scenarios, respectively.

	Scenario	R10 (day)	CDD (day)	R5d (mm)	SDII (mm/day)	R95T (%)
Trend/100 years	**A2**	3.4	1.4	18.8	0.9	6.3
	A1B	3.2	1.0	15.0	0.7	5.9
	B1	1.9	-0.4	8.0	0.4	2.9
2071-2100 deviation (% difference)	**A2**	2.3 (22%)	1.4 (4%)	15.0 (18%)	0.7 (12%)	6.0 (31%)
	A1B	2.3 (22%)	0.7 (2%)	12.8 (16%)	0.6 (11%)	5.4 (28%)
	B1	1.8 (17%)	-0.7 (-2%)	8.7 (11%)	0.4 (7%)	3.9 (21%)

Table 12. *Linear trend for the twenty-first century and changes for the end of the twenty-first century (in comparison to the period 1961–1990) for various extreme precipitation indices averaged over China. Results are given for the three emission scenarios A2, A1B and B1 separately. Numbers in parenthesis are relative changes. R10 = Raindays with over 10mm, CDD = Consecutive Dry Days, R5d = Maximum 5-day rainfall, SDII = Simple Daily Intensity Index, R95T = Fraction of precipitation above the 95th percentile. Data is from Jiang et al. (2011).*

Tao et al. (2011) applied climate change scenarios from the HadCM3 GCM under SRES A2 and B2 emissions scenarios to assess changes in water stress for agriculture across China. The Water Stress Index (WSI) was calculated as an indicator of changes to water resources available for agriculture across China. Results showed that areas of the North and Northeast

China Plain were identified as suffering from severe water stress (WSI<0.5). For the 2020s and 2050s, under both scenarios, the area of critical water stress expanded to the Northeast China Plain, with some areas experiencing 80-100% occurrence at such levels, thus requiring irrigation. In contrast, Liu et al. (2010) applied climate change scenarios under the A2 and B2 emissions scenarios to assess the impacts of climate change on flows within the headwater catchment of the Tarim River. Mean annual runoff between the 2000-2005 and 2020-2025 time horizons was not found to change significantly. Intra annual runoff was found to change, with winter runoff exhibiting a decreasing trend. Little difference between the two scenarios was found. Similarly, Xiong et al. (2010) applied climate scenarios from the PRECIS RCM to drive water simulation models under SRES A2 and B2 socio-economic pathways. Results suggested an increase of 20% for total annual availability by the 2020s, and 18% for the 2040s. The effects of climate change on water availability for agriculture were small compared to the effects of socio-economic development.

AVOID Programme Results

To further quantify the impact of climate change on water stress and the inherent uncertainties, the AVOID programme calculated water stress indices for all countries reviewed in this literature assessment based upon the patterns of climate change from 21 GCMs, following the method described by Gosling et al. (2010) and Arnell (2004). This ensures a consistent methodological approach across all countries and takes consideration of climate modelling uncertainties.

Methodology

The indicator of the effect of climate change on exposure to water resources stress has two components. The first is the number of people within a region with an *increase in exposure to stress*, calculated as the sum of 1) people living in water-stressed watersheds with a significant reduction in runoff due to climate change and 2) people living in watersheds which become water-stressed due to a reduction in runoff. The second is the number of people within a region with a *decrease in exposure to stress*, calculated as the sum of 1) people living in water-stressed watersheds with a significant increase in runoff due to climate change and 2) people living in watersheds which cease to be water-stressed due to an increase in runoff. It is not appropriate to calculate the net effect of “increase in exposure” and “decrease in exposure”, because the consequences of the two are not equivalent. A

water-stressed watershed has an average annual runoff less than 1000m^3/capita/year, a widely used indicator of water scarcity.

Average annual runoff (30-year mean) is simulated at a spatial resolution of 0.5x0.5^o using a global hydrological model, MacPDM (Gosling and Arnell, 2011), and summed to the watershed scale. Climate change has a "significant" effect on average annual runoff when the change from the baseline is greater than the estimated standard deviation of 30-year mean annual runoff: this varies between 5 and 10%, with higher values in drier areas.

The pattern of climate change from 21 GCMs was applied to MacPDM, under two emissions scenarios; 1) SRES A1B and 2) an aggressive mitigation scenario where emissions follow A1B up to 2016 but then decline at a rate of 5% per year thereafter to a low emissions floor (denoted A1B-2016-5-L). Both scenarios assume that population changes through the 21st century following the SRES A1 scenario as implemented in IMAGE 2.3 (van Vuuren et al., 2007). The application of 21 GCMs is an attempt to quantify the uncertainty due to climate modelling, although it is acknowledged that only one impacts model is applied (MacPDM). Simulations were performed for the years 2030, 2050, 2080 and 2100.

Results

The results for China are presented in Figure 15. The percentage of China's population exposed to water stress increases with climate change to around a median of 6% in 2100 under A1B emissions (2% under the mitigation scenario). For the same time horizon, the median estimate for population exposed to a decrease in water stress is around 20% (A1B) and 9% (A1B-2016-5-L).

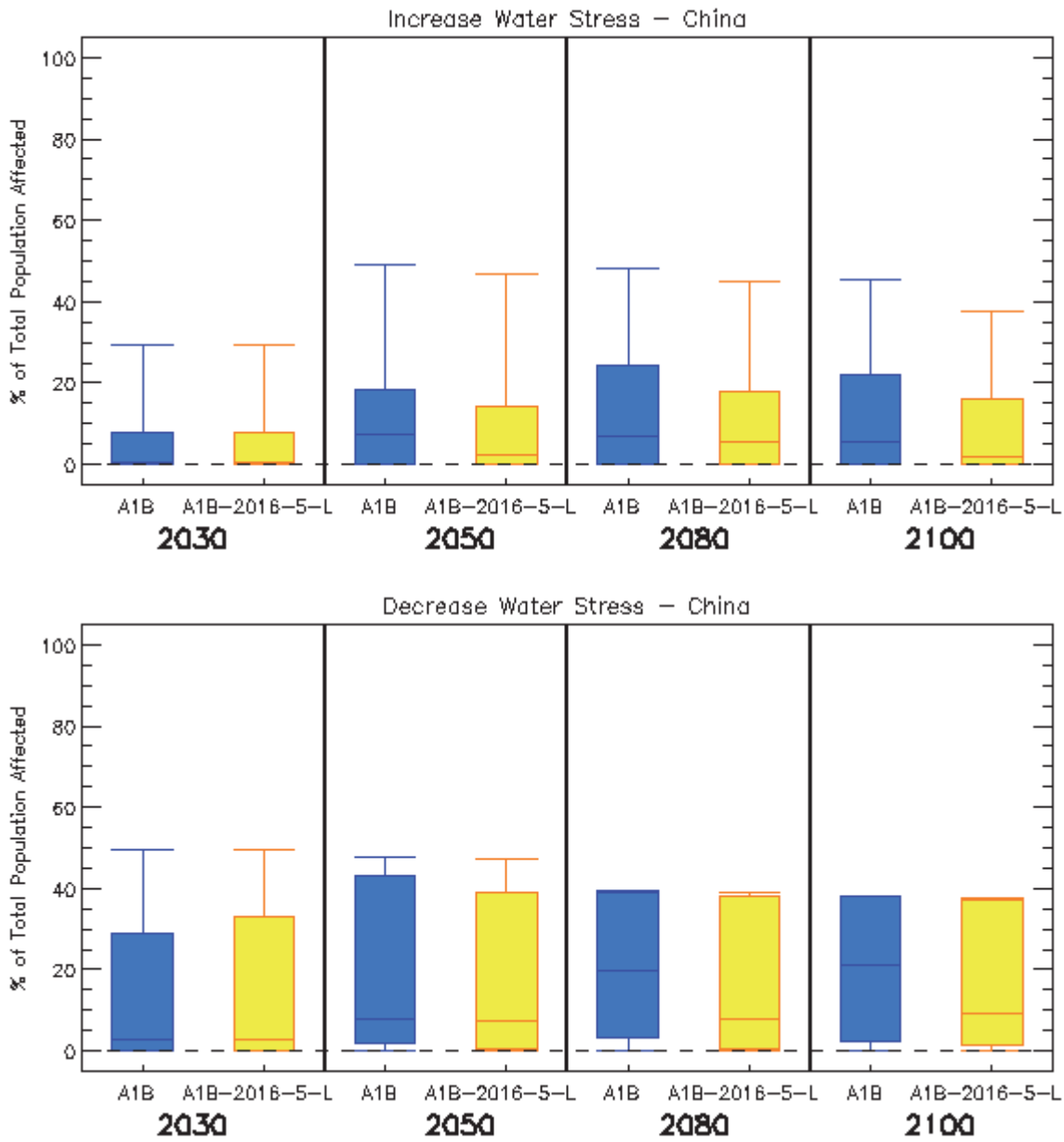

Figure 15. *Box and whisker plots for the impact of climate change on increased water stress (top panel) and decreased water stress (bottom panel) in China, from 21 GCMs under two emissions scenarios (A1B and A1B-2016-5-L), for four time horizons. The plots show the 25th, 50th, and 75th percentiles (represented by the boxes), and the maximum and minimum values (shown by the extent of the whiskers).*

Pluvial flooding and rainfall

Headline

The IPCC AR4 noted the potential for increased precipitation over East Asia, and also an increase in extreme precipitation in parts of China. More recent research has generally confirmed this, and shows that changes in extremes tend to be larger under higher emissions scenarios.

Supporting literature

Introduction

Pluvial flooding can be defined as flooding derived directly from heavy rainfall, which results in overland flow if it is either not able to soak into the ground or exceeds the capacity of artificial drainage systems. This is in contrast to fluvial flooding, which involves flow in rivers either exceeding the capacity of the river channel or breaking through the river banks, and so inundating the floodplain. Pluvial flooding can occur far from river channels, and is usually caused by high intensity, short-duration rainfall events, although it can be caused by lower intensity, longer-duration events, or sometimes by snowmelt. Changes in mean annual or seasonal rainfall are unlikely to be good indicators of change in pluvial flooding; changes in extreme rainfall are of much greater significance. However, even increases in daily rainfall extremes will not necessarily result in increases in pluvial flooding, as this is likely to be dependent on the sub-daily distribution of the rainfall as well as local factors such as soil type, antecedent soil moisture, land cover (especially urbanisation), capacity and maintenance of artificial drainage systems etc. It should be noted that both pluvial and fluvial flooding can potentially result from the same rainfall event.

Assessments that include a global or regional perspective

Recent past

The IPCC AR4 (2007a) noted an observed increasing frequency of extreme rain in western and southern parts, and decreases in northern regions. There were more floods in Changjiang river during the past decade, and more frequent floods in NE China since the 1990s, along with more intense summer rains in East China. Choi et al. (2009) showed that

observed trends in total precipitation for China for the period 1955-2007 display an increase in annual precipitation of 3.3mm/decade, with 1.5mm/decade in winter, and 1.6mm/decade in summer These trends were not statistically significant at the 95% level, however.

Climate change studies

The IPCC AR4 (2007b) noted that all members of the multi-model dataset under the SRES A1B emissions scenario projected an increase in precipitation in East Asia for all seasons. The median change at the end of the 21st Century was +9% in the annual mean, with little seasonal difference, but a large model spread in December-February. Qualitative agreement was good, but there were large quantitative variations. The IPCC AR4 also noted that intense precipitation events over East Asia are very likely to increase, consistent with historical trends for the region. Xu et al. (2006) found more extreme precipitation events over China with climate change and Gao et al. (2002) found an increase in the number of rainy days in NW China, and a decrease in rain days, but an increase in days with heavy rain, over South China. Sillmann and Roeckner (2008) suggested that the trends of recent past could continue with climate change based upon their global modelling experiments; the authors found large increases for much of China in heavy precipitation indices during the 21st century, with larger changes under the A1B emissions scenario than under the B2 scenario. Washington et al. (2009) investigated climate change projections from an aggressive mitigation scenario (CO_2 stabilisation in 2100 at around 450ppm) compared with a non-mitigation scenario (CO_2 concentrations around 740ppm in 2100) at the global-scale. In terms of precipitation, an increase of around 10-20% was avoided under mitigation relative no-mitigation, for northeast China, but with smaller avoided changes over the remainder of the country.

Li et al. (2010a) investigated changes in the East Asian monsoon system by applying 14 GCMs under an A1B emissions scenario. They demonstrated that regional-mean East Asian Summer Monsoon (EASM) rainfall is dominated by large inter-annual to decadal fluctuations. Li et al. (2010a) showed that the EASM strength does not respond with any pronounced trend to the A1B scenario during the 21st century. They suggest that the response of the EASM to a warming climate may be through the form of a change in position rather than a change in intensity, which could lead to the spatial coexistence of floods and droughts in east Asia than has been observed over recent decades.

National-scale or sub-national scale assessments

Climate change studies

Jiang et al. (2011) found that ensemble GCM results for the end of the 21st century indicate more frequent and intense precipitation events, particularly in the middle and lower reaches of the Yangtze River, the Southeast coastal region, western Northwest China, and the Tibetan Plateau. They calculated various extreme precipitation indices averaged over China, under climate change (see Table 13). The authors found that the models tend to underestimate indices such as R10 (number of days with over 10mm precipitation), R5d (maximum 5-day precipitation) and R95T (precipitation above the 95th percentile) in southern China where heavy precipitation is frequent and intense, but overestimate them in northern and western China where heavy precipitation events are rare. All precipitation indices except the consecutive dry days showed increasing trends for all scenarios. The indices R10, R5d, SDII and R95T under A1B emissions increased by 22%, 16%, 11% and 28%, respectively, for the late twenty-first century. Higher emission scenarios were associated with larger changes. In terms of relative changes, R95T demonstrated the most important variation for most scenarios. This implies that future rainfall extremes could increase, especially in the late twenty-first century with enhanced intensity of heavy precipitation. These simulations are consistent with observed trends. Comparing observed and projecting trends in extremes indices over China in the multi-model ensemble, Jiang et al. (2011) found that projected trends shared a consistent sign with observations, with the exception of consecutive dry days. Other indices showed enhanced strength during the 21st century, and larger trends with higher emissions scenarios. As an example, maximum 5-day rainfall increased from 2.1 mm/100-year (1961-2000) to 18.8, 15.0 and 8.0 mm/100-year in the twenty-first century for the A2, A1B and B1 scenarios, respectively. In terms of spatial patterns of change there was a general increase, in most regions, of the number of days with precipitation greater than 10mm. Increases were also observed for R5d and R95T, which describe heavy precipitation, and precipitation intensity (SDII). The largest increases mainly occur in the south Tibetan Plateau, in the west part of Northwest China and in the regions along the Yangtze River (about 30N) and the Huai River (about 35N). To this end, an increasing risk of pluvial flooding is possible for most regions of China with climate change.

Fluvial flooding

Headline

Observations show that heavy precipitation events have increased over recent decades in parts of China, and flooding events have become more frequent in a number of river basins. Several climate change impact studies have suggested that this trend could continue, although uncertainties are large, resulting in a wide spread in responses among different climate models. Simulations by the AVOID programme confirm this but show a general tendency towards higher flood risk in China, particularly later in the century and under the A1B scenario. Future research must improve regional climate simulations over China, especially of precipitation and extreme events. Also, hydrological impact studies must take account of the uncertainties in climate scenarios by incorporating ensemble projections, and include relevant processes such as irrigation and land use change.

Supporting literature

Introduction

This section summarises findings from a number of post IPCC AR4 assessments on river flooding in China to inform and contextualise the analysis performed by the AVOID programme for this project. The results from the AVOID work are discussed in the next section.

Fluvial flooding involves flow in rivers either exceeding the capacity of the river channel or breaking through the river banks, and so inundating the floodplain. A complex set of processes is involved in the translation of precipitation into runoff and subsequently river flow (routing of runoff along river channels). Some of the factors involved are; the partitioning of precipitation into rainfall and snowfall, soil type, antecedent soil moisture, infiltration, land cover, evaporation and plant transpiration, topography, groundwater storage. Determining whether a given river flow exceeds the channel capacity, and where any excess flow will go, is also not straightforward, and is complicated by the presence of artificial river embankments and other man-made structures for example. Hydrological models attempt to simplify and conceptualise these factors and processes, to allow the simulation of runoff and/or river flow under different conditions. However, the results from global-scale

hydrological modelling need to be interpreted with caution, especially for smaller regions, due to the necessarily coarse resolution of such modelling and the assumptions and simplifications this entails (e.g. a 0.5^{o} grid corresponds to landscape features spatially averaged to around 50-55km for mid- to low-latitudes). Such results provide a consistent, high-level picture, but will not show any finer resolution detail or variability. Smaller-scale or catchment-scale hydrological modelling can allow for more local factors affecting the hydrology, but will also involve further sources of uncertainty, such as in the downscaling of global climate model data to the necessary scale for the hydrological models. Furthermore, the application of different hydrological models and analysis techniques often makes it difficult to compare results for different catchments.

In the past few decades, China has repeatedly experienced devastating floods. The 1998 floods in the Yangtze River (Cháng Jiāng) basin, which inundated 21 million hectares of land and destroyed five million houses with an estimated economic loss of over US$ 20 billion (Zong and Chen, 2000), are often noted as the most damaging river flood event ever (Kundzewicz et al., 2009). Although many authors have investigated recent trends in the occurrence of river floods across China, few studies have assessed the impacts of future climate change on flood hazards.

Assessments that include a global or regional perspective

Climate change studies

Projections of changes in precipitation over China are highly uncertain, but climate models generally simulate a more intense hydrological cycle and an increase in annual runoff in the major rivers of China (Piao et al., 2010).

A global modelling study presented by Hirabayashi et al. (2008), under the A1B emissions scenario, projected localised increases in flood frequency in China in the next few decades (2001-2030). In some places, the return period of what was a 100-year flood event in the 20^{th} century was projected to decrease to 40 years or less, except for the south coast where a slight increase in the return period was simulated. By the end of the century (2071-2100) the authors found a widespread decrease in the return period of a 100-year flood to 30 years or less throughout the country, implying an increase in the frequency of severe floods. Only in the Guangxi Province and Pearl River basin was a decrease in flood hazard projected, with the return period of a 100-year flood lengthening to 140 years or more. In the Yangtze, the return period of a 20^{th} century 100-year flood was projected to reduce to 45 years, in the Amur to 20 years and in the Yellow River to less than 3 years. The latter number could mean that by the end of the century extreme and currently rare floods could be expected to occur

every few years. Furthermore, in northern China and Mongolia a shift in the timing of peak flow by about 3 to 4 months was simulated, indicating a change in the flood regime from snowmelt in spring to rainfall-dominated flooding in summer.

However, a study presented by Nohara et al. (2006), which applied 19 GCMs under the A1B emissions scenario for the end of the 21st century (2081-2100), found a wide spread in the response of river discharge in the Yangtze, Yellow and Amur rivers among the different climate models. This suggested large climate modelling uncertainty. Furthermore the model performance was poor in the Yellow River Basin because irrigation and water extraction were not taken into account.

Future research must therefore improve regional climate simulations over China, especially of precipitation and extreme events (Piao et al., 2010). Hydrological impact studies must take account of the uncertainties in climate scenarios by incorporating ensemble projections, and include relevant processes such as irrigation. Land use change, particularly a loss of forest cover, may further exacerbate an increase in flooding potential due to climate change (Guo et al., 2008) and must therefore be taken into account as well.

National-scale or sub-national scale assessments

Recent past

Observations suggest that heavy rainfall events appear to have become more frequent over north-western China and the middle and lower reaches of the Yangtze River, but less frequent in north-eastern China and the north-western reaches of the Yangtze (Zhai et al., 2005; Su et al., 2008). Over the Yangtze Basin, more precipitation tends to fall in heavy rainfall events at the expense of moderate and light events (Jiang et al., 2008). As a consequence, discharge during the summer flood season has risen significantly, which has been associated with an increase in the number of flooding events over the past 40 years (Jiang et al., 2007; Zhang et al., 2006; Zhang et al., 2009). A similar trend has been observed in the lower reaches of the Pearl River (Zhū Jiāng) further south (Piao et al., 2010). In the arid, continental Tarim basin in western China and other areas in the northwest the number of flood events has risen sharply due to glacier melting and more rapid snowmelt (Shi et al., 2007; Shen et al., 2006). In stark contrast, the Yellow River (Huang He) has shown a persistent decline in runoff in recent decades (Piao et al., 2010).

AVOID programme results

To quantify the impact of climate change on fluvial flooding and the inherent uncertainties, the AVOID programme calculated an indicator of flood risk for all countries reviewed in this literature assessment based upon the patterns of climate change from 21 GCMs (Warren et al., 2010). This ensures a consistent methodological approach across all countries and takes consideration of climate modelling uncertainties.

Methodology

The effect of climate change on fluvial flooding is shown here using an indicator representing the percentage change in average annual flood risk within a country, calculated by assuming a standardised relationship between flood magnitude and loss. The indicator is based on the estimated present-day (1961-1990) and future flood frequency curve, derived from the time series of runoff simulated at a spatial resolution of 0.5°x0.5° using a global hydrological model, MacPDM (Gosling and Arnell, 2011). The flood frequency curve was combined with a generic flood magnitude–damage curve to estimate the average annual flood damage in each grid cell. This was then multiplied by grid cell population and summed across a region, producing in effect a population-weighted average annual damage. Flood damage is thus assumed to be proportional to population in each grid cell, not the value of exposed assets, and the proportion of people exposed to flood is assumed to be constant across each grid cell (Warren et al., 2010).

The national values are calculated across major floodplains, based on the UN PREVIEW Global Risk Data Platform (preview.grid.unep.ch). This database contains gridded estimates, at a spatial resolution of 30 arc-seconds (0.00833°x0.00833°), of the estimated frequency of flooding. From this database the proportion of each 0.5°x0.5° grid cell defined as floodplain was determined, along with the numbers of people living in each 0.5°x0.5° grid cell in flood-prone areas. The floodplain data set does not include “small” floodplains, so underestimates actual exposure to flooding. The pattern of climate change from 21 GCMs was applied to MacPDM, under two emissions scenarios; 1) SRES A1B and 2) an aggressive mitigation scenario where emissions follow A1B up to 2016 but then decline at a rate of 5% per year thereafter to a low emissions floor (denoted A1B-2016-5-L). Both scenarios assume that population changes through the 21st century following the SRES A1 scenario as implemented in IMAGE 2.3 (van Vuuren et al., 2007). The application of 21 GCMs is an attempt to quantify the uncertainty due to climate modelling, although it is acknowledged that only one impacts model is applied (MacPDM). Simulations were performed for the years

2030, 2050, 2080 and 2100. The result represents the change in flood risk due to climate change, not the change in flood risk relative to present day (Warren et al., 2010).

Results

The results for China are presented in Figure 16. By the 2030s, the models project a range of changes in mean fluvial flooding risk over China in both scenarios, with some models projecting decreases and others increases. However, the balance is more towards higher flood risk, with 75% of models projecting an increase. The largest decrease projected for the 2030s is a 20% decline in the average annual flood risk, and the largest increase is around 80%. The mean across all projections is approximately a 10% increase in flood risk.

By 2100 the balance shifts even more towards increased flood risk in both scenarios, and the difference in projections from the different models also becomes greater. Both these aspects of the results are more pronounced for the A1B scenario than the mitigation scenario. Under the mitigation scenario, about a quarter of the models still project a decrease in flood risk down to −20%, but around three quarters of the models project an increase in flood risk compared to present day. The mean of all projections is a 20% increase, and the highest increase is nearly 150%. Under the A1B scenario, most models project an increased flood risk, but still some project a decrease in flood risk (down to −50%). The largest projected increase is approximately 500% of the present-day annual average flood risk, with the mean across all projections being approximately a 50% increase.

So for China, the models show a much greater tendency for increasing flood risk, particularly later in the century and particularly under the A1B scenario. Differences between the model projections are also greater later in the century and particularly for A1B.

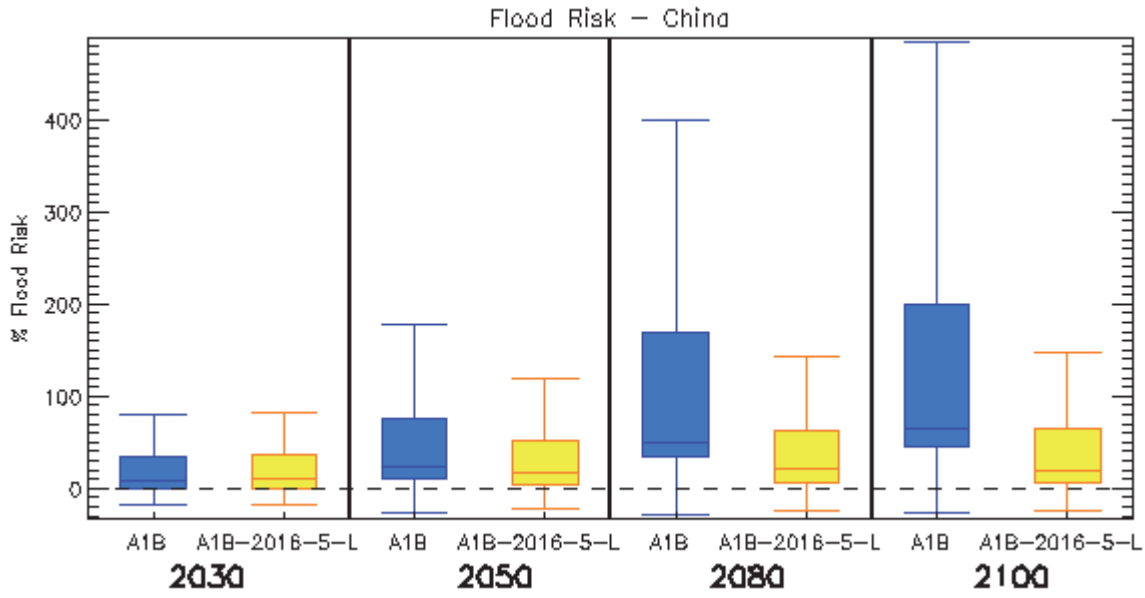

Figure 16. *Box and whisker plots for the percentage change in average annual flood risk within China, from 21 GCMs under two emissions scenarios (A1B and A1B-2016-5-L), for four time horizons. The plots show the 25th, 50th, and 75th percentiles (represented by the boxes), and the maximum and minimum values (shown by the extent of the whiskers).*

Tropical cyclones

Headline

There still remains, since the IPCC AR4, considerable uncertainty in projections of tropical-cyclone *frequency* changes in the western Pacific under climate change scenarios. There is relatively less uncertainty regarding the *intensity* of cyclones in this basin, which a number of studies show could increase considerably. These increases in intensity could be greatest for the most severe cyclones, which could lead to large increases in cyclone damages in China. China is particularly vulnerable to cyclone damages due to its high coastal population density and the valuable economic assets located in coastal regions.

Supporting literature

Introduction

Tropical cyclones are different in nature from those that exist in mid-latitudes in the way that they form and develop. There remains an overall large uncertainty in the current understanding of how tropical cyclones might be affected by climate change because conclusions are based upon a limited number of studies. Moreover, the majority of tropical-cyclone projections are from either coarse-resolution global models or from statistical or dynamical downscaling techniques. The former are unable to represent the most-intense storms, whereas the very patterns used for the downscaling may change in itself under climate change. To this end, caution should be applied in interpreting model-based results, even where the models are in agreement.

Assessments that include a global or regional perspective

Assessments of cyclone frequency

Projections of changes in tropical-cyclone frequency in the West Pacific basin under climate change scenarios, remain highly uncertain, even on the sign of the change. Bengtsson et al. (2007) conducted timeslice experiments (experiments over a short period of time to enable ensemble simulations using reasonable amounts of computational power) with the atmospheric component of the ECHAM5 GCM at 60km and 40km resolutions respectively. The model was driven by the SSTs and sea ice simulated by the a lower-resolution version of the GCM under the A1B emissions scenario, using the 2071-2100 time horizon for the

60km simulation and 2081-2100 for the 40km simulation. The 2081-2100 period was compared to the present-day simulation using the SSTs and sea ice for the 1980-2000 period. The simulations are summarised in Figure 17. The two climate-change experiments projected a decrease in western Pacific tropical cyclones, with a 20% decrease in the 60km model and a 28% decrease in the 40km model. The authors attributed the decrease to a more stable atmosphere in the West Pacific, as measured by dry static stability, as well as reduced upward motion.

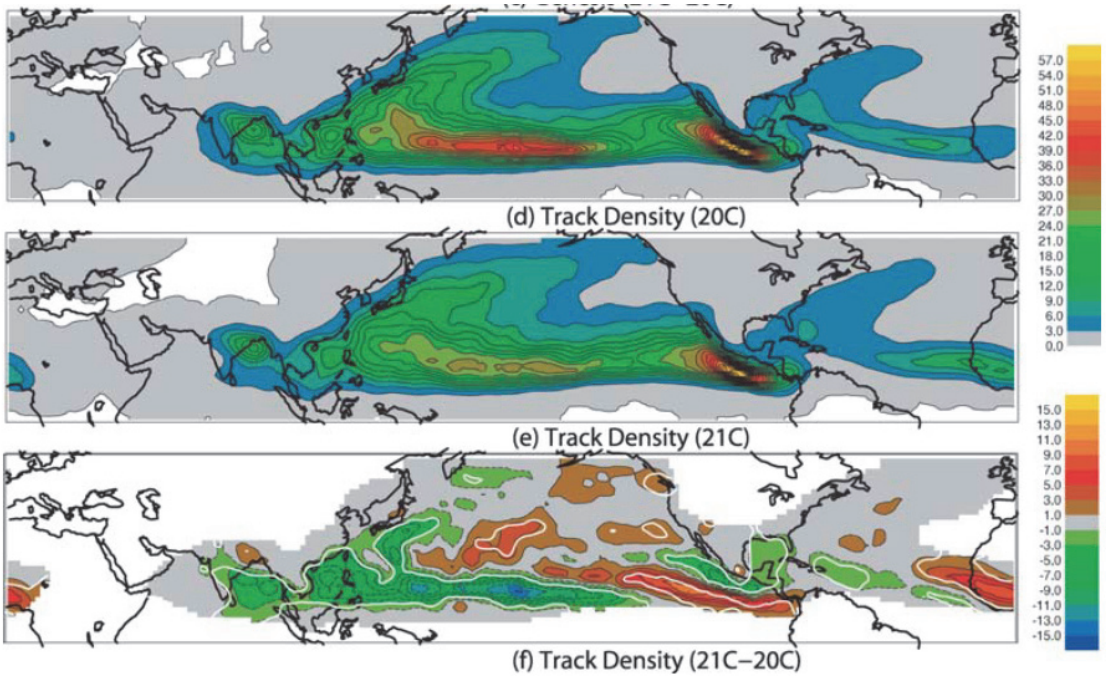

Figure 17. *Tracks of tropical cyclones simulated by the 60km resolution ECHAM5 GCM for the present-day climate (top panel; 1980-2000), under the A1B emissions scenario for the 2071-2100 time horizon (middle), and the difference between the two (bottom panel). The units are cyclones per year per unit area, where the unit area is approximately 10^6 km^2. The prominent features are the shift in tropical-cyclone tracks away from the western coast of Mexico and the decrease in tracks in the South China Sea and near Japan. The figure is adapted from Bengtsson et al. (2007).*

In an even finer-resolution experiment, Oouchi et al. (2006) applied the JMA climate model at 20km resolution for ten years, using mean SSTs and sea ice projections from the MRI GCM for 2080-2099 under the A1B emission scenario. The results from the simulations are presented in Figure 18. The authors found that the number of West Pacific tropical cyclones declined by 38%, relative to a present-day simulation using the mean SSTs and sea ice for 1982-1993. In agreement with Bengtsson et al. (2007), the authors concluded that the decreases were due to increased atmospheric stability in a warmer world; the model simulated a 10% increase in the dry static stability, defined as the difference in potential

temperature between the 250hPa level of the atmosphere and the surface. Modest decreases in West Pacific cyclone frequency were also found by Gualdi et al. (2008), based on an application of the 120km resolution SINTEX-G model in a 30-year simulation under a $2xCO_2$ emissions scenario.

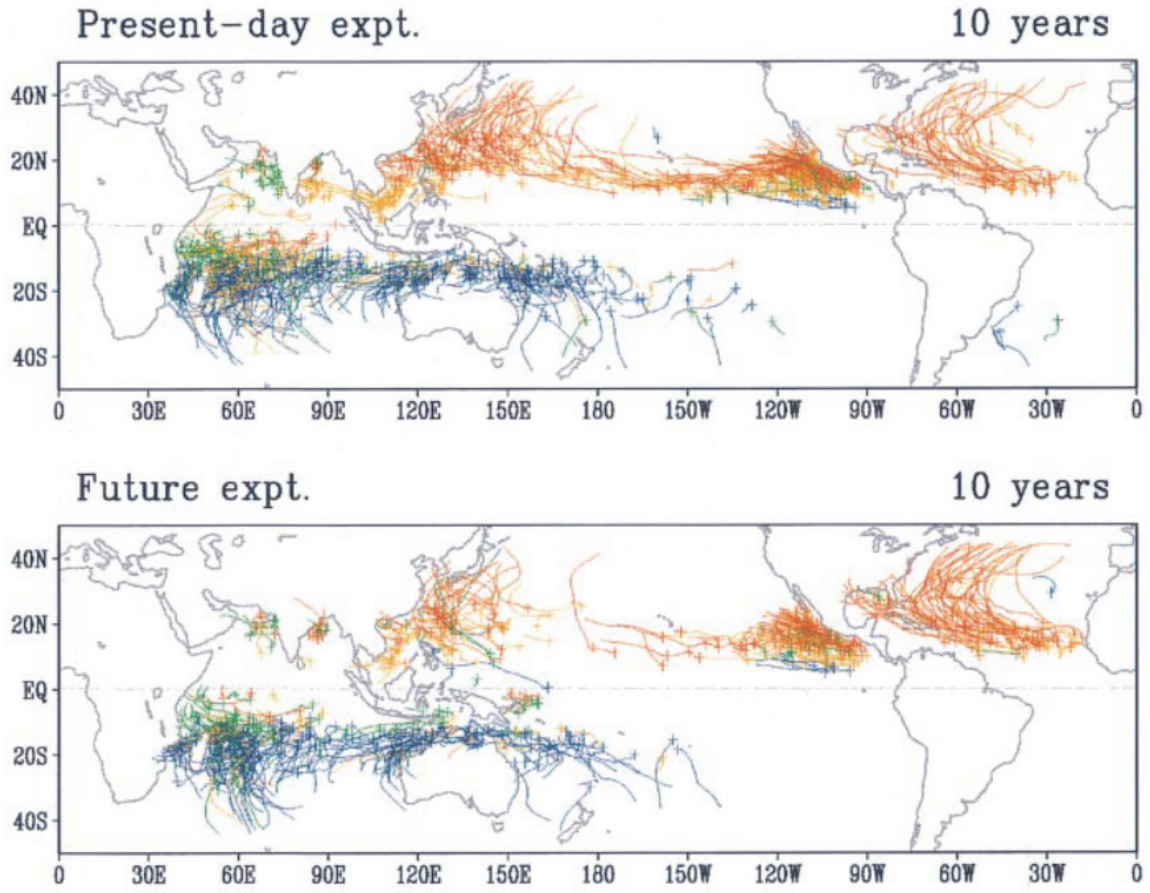

Figure 18. *Tracks of tropical cyclones simulated by the 20km resolution JMA climate model when it is driven by (top) present-day sea surface temperatures (SSTs) (1982-1993) and (bottom) SSTs from the MRI GCM for 2080-2099 under the A1B emissions scenario. Decreases in the number of tracks in the western Pacific and the South China Sea were observed, suggesting fewer tropical cyclones making landfall in East Asia. The figure is from Oouchi et al. (2006).*

Zhao et al. (2009) applied the 50km GFDL GCM with four future SST and sea ice distributions; 1) the ensemble mean from 18 GCMs, 2) the HadCM3 GCM, 3) the GFDL GCM, and 4) the ECHAM5 GCM. The SSTs distributions were for the A1B emissions scenario for the 2081-2100 time horizon. In all four experiments, the frequencies of cyclones in the West Pacific basin decreased, but the magnitude of this decrease varied considerably; the GFDL model simulated a decrease of 5%; HadCM3 simulated a decrease of 12%; the ensemble-mean projected a 29% decrease; and ECHAM5 simulated a 52% decrease.

Sugi et al. (2009) conducted a timeslice experiment with the JMA GCM, driven at 60km and 20km resolutions respectively, with SSTs and sea ice from three individual GCMs and the CMIP3 multi-model dataset ensemble mean for a total of eight predictions, all using the A1B emissions scenario. The West Pacific showed considerable variation in projected tropical-cyclone frequencies, with three experiments simulating increases (range of 13-64% across the eight simulations) and five simulating decreases (range of 14-36%). Three out of the four finer-resolution, 20km experiments simulated a decrease of at least 26%, including the experiment driven by the CMIP3 ensemble-mean SST data. Sugi et al. (2009) attributed the variations between the driving GCMs to the variations in regional SST changes simulated by those models. Those models that projected an SST warming in the West Pacific that was greater than the global-mean warming, tended to produce increases in cyclone frequency, while those models that simulated a relatively cooler West Pacific tended to reduce the number of cyclones relative to the present-day climate.

Emanuel et al. (2008) applied a hybrid statistical-dynamical downscaling method to seven GCMs under the A1B emissions scenario for 2180-2200 time horizon. The technique applied in the study “seeds” large numbers of tropical-cyclone vortices into each basin, then uses the models' large-scale climate fields (e.g., SSTs, wind shear, relative humidity) to determine whether the storms grow into cyclones or simply decay. The technique has shown considerable skill at simulating both frequency and intensity of storms over the past several decades. By comparing the A1B scenario results for 2180-2200 to downscaled reanalysis data for 1980-2000, the authors concluded that West Pacific tropical-cyclone frequency could increase by 6%. All seven models simulated an increase in frequencies. Importantly, Emanuel et al. (2008) observed increases in the number of tropical cyclones tracking close to the coast of China, due to a northward shift in the dominant region of cyclogenesis (formation of cyclones) in the West Pacific.

An assessment conducted for the West Pacific basin, applied a timeslice experiment with the International Pacific Research Centre (IPRC) RCM at 50km, driven by the SSTs and sea ice from the final 10 years of a $6xCO_2$ simulation from the NCAR GCM (Stowasser et al., 2007). This unrealistically large climate forcing was chosen to produce a strong climate change–related signal that may stand out among the unforced inter-annual variability in tropical cyclone statistics. The frequency of tropical cyclones remained relatively constant overall in the West Pacific, but there was approximately a doubling of the number of cyclones passing through the South China Sea (see Figure 19). The IPRC model simulated large increases in relative humidity and decreases in vertical wind shear in this region, both of which are conducive to tropical-cyclone genesis and maintenance. The scenario considered in this

study—a six-fold increase in CO_2 concentrations—is extreme, but the increases in South China storms agree with those from the broader study of Emanuel et al. (2008), which applied the A1B emissions scenario. An increase in tropical-cyclone activity in the South China Sea has also been observed over the last decade (Tu et al., 2009), although whether such a shift is due to natural variability or anthropogenic climate change is currently unclear.

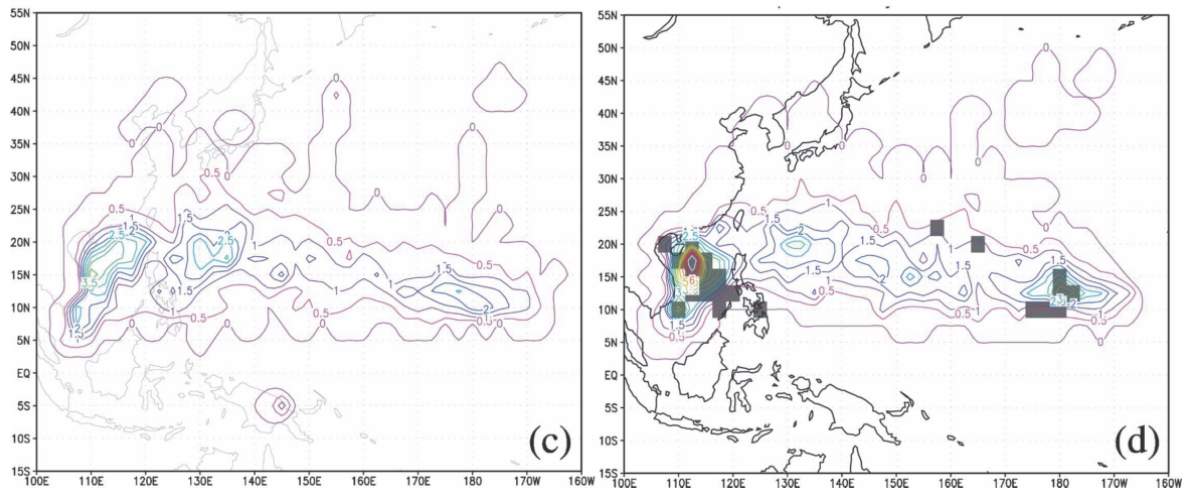

Figure 19. *The density of tropical-cyclone tracks in the Western Pacific simulated by the 50km resolution IPRC RCM when it is driven by the large-scale atmospheric conditions and SSTs from the NCAR GCM under (left) present-day conditions and (right) 6xCO_2 concentrations. The units are numbers per 5° grid cell per 4-month (July-October) period. Note the large increase in the number of tropical cyclones in the South China Sea near the coast of Southeast China. The shading indicates that the difference between the warmed and present-day simulations is statistically significant at the 5% level. The figure is from Stowasser et al. (2007).*

In contrast, Li et al. (2010b) found a substantial shift in cyclone activity away from the West Pacific and towards the central part of the basin. The authors conducted 20 year timeslice experiments with the 40km resolution ECHAM5 GCM, driven by the SSTs and sea-ice from the lower-resolution version of the model. Li et al. (2010b) explored two time horizons; one experiment used the period 1981-2000, representing the present-day climate; the other used the period 2081-2100 and applied an A1B emissions scenario here. The model simulated a 31% decrease in cyclone numbers in the West Pacific and a 65% increase in the Central Pacific, with a considerable decrease in the number of cyclones near China. Unlike Zhao et al. (2009), the authors found that the regional SST warming patterns simulated by ECHAM5 in the Pacific could not explain the shift of cyclone tracks toward the Central Pacific. Rather, the reduction in cyclone numbers in the West Pacific was due to a weakening of the Pacific trade winds and a more El Nino-like basic state in ECHAM5. This resulted in changes in the mean-state vertical wind shear that suppressed nascent tropical cyclones in the West Pacific and enhanced tropical cyclogenesis in the centre of the basin.

There is therefore considerable uncertainty in projections of tropical-cyclone *frequency* change in the West Pacific under climate change. There are some suggestions that the number of storms in the South China Sea could dramatically increase, but these come from either extreme scenarios (e.g., the 6xCO_2 conditions imposed by Stowasser et al. (2007)) or from projections of the late 22nd century (Emanuel et al., 2008). Furthermore, these are balanced by several studies showing basin-scale reductions in cyclone activity in the West Pacific (Bengtsson et al., 2007; Oouchi et al., 2006), e.g. see Figure 17 and Figure 18. It is therefore not possible to make a robust assessment of whether China could be impacted by more or fewer tropical cyclones in a warmer world.

Assessment of cyclone intensity

A number of studies suggest that tropical cyclones in the West Pacific could become *more intense* with climate change. Under their 6xCO_2 scenario, Stowasser et al. (2007) found a mean increase in the intensity of North Pacific storms, with a doubling in the frequency of storms exceeding 35 m s^{-1}. Further evidence for increases in tropical-cyclone intensity comes from the application of theoretical relationships between cyclone intensity and climate variables (e.g., SST, wind shear) to coarse-resolution climate models. Many such relationships are based on the Emanuel (1987) potential-intensity theory, or variations thereof. To this end, Vecchi and Soden (2007) applied this theory to 18 GCMs under the A1B emission scenario, finding that on average West Pacific cyclone intensities increased by 3.5% by 2100.

Knutson and Tuleya (2004) applied two versions of the Emanuel theory—one with reversible ascent and the other with pseudoadiabatic ascent—along with potential-intensity theory. When these were applied to GCMs from CMIP2 under a 1% per year CO_2 increase scenario run for 80 years, the authors found that the intensity of West Pacific cyclones increased by 4-9%, depending on the theory used. The authors also used a 9km version of the GFDL hurricane model, driven by the large-scale conditions simulated by the CMIP2 GCMs under the same 1% per year CO_2 increase scenario. Across all of the CMIP2 GCMs, the average wind speed of West Pacific cyclones increased by 5%, while central pressures fell by 13.6%. Also, in a global timeslice experiment with the JMA 20km resolution model, Oouchi et al. (2006) found that cyclone intensities increased by 4.2% in the West Pacific against the present-day climate, for 2080-2099 under the A1B emissions scenario. These intensity changes are expected to be strongest for the most extreme storms, as suggested by Stowasser et al. (2007) for the West Pacific and by many global-scale studies (McDonald et al., 2005; Oouchi et al., 2006).

Assessment of cyclone damages

Projections of climate-change-related tropical-cyclone damages in China by 2100 are also uncertain, due to the lack of robust projections of cyclone frequency changes. Mendelsohn et al. (2011) applied the cyclone "seeding" method described by Emanuel et al. (2008) to climate change projections from four GCMs under the A1B emissions scenario. They then constructed a damage model to estimate the damages from each landfalling storm. The method employed by Mendelsohn et al. (2011) separates the additional damages from the impact of climate change on tropical cyclones from the additional damages due to future economic development. This is accomplished through applying the damages from both present-day and future tropical cyclones to the projected economic conditions in 2100 (the "future baseline"). Against a future baseline of $7.16 billion in damages per year in China, three of the four GCMs considered by Mendelsohn et al. (2011) simulated an increase in cyclone damages; the CNRM GCM ($2.07 billion increase), the ECHAM5 GCM ($16.05 billion) and the MIROC GCM ($13.64 billion). The GFDL model simulated virtually no change in cyclone damages. Thus, two out of the four models simulated that damages in China could more than double, one model simulated a modest increase and the fourth model simulated no change. The largest estimated damage increases are due to the increased frequencies of the strongest tropical cyclones; the authors found that the most extreme 1% of storms accounted for 64% of the damages in 2100, as opposed to 58% of damages in the present-day climate. To this end, climate change may cause tropical-cyclone damage in China to increase even if the frequency of tropical cyclones decreases.

National-scale or sub-national scale assessments

Literature searches yielded no results for national-scale or sub-national scale studies for this impact sector.

Coastal regions

Headline

Recent global-scale assessments of the impact of sea level rise (SLR) on coasts, which include national estimates for China, suggest that China is one of the countries across the globe that could experience the most severe impacts (Dasgupta et al., 2009a; Dasgupta et al., 2009b; Hanson et al., 2011; Nicholls, 2000). One study showed that based upon an analysis of 136 port cities, China was the top country simulated to show an increased exposure from SLR relative to present in the 2070s. Another study showed that around 17% of China's coastal land area and coastal population could be affected by a 10% intensification of the current 1-in-100-year storm surge combined with a 1m SLR.

Supporting literature

Assessments that include a global or regional perspective

Climate change studies

The IPCC AR4 concluded that at the time, understanding was too limited to provide a best estimate or an upper bound for global SLR in the twenty-first century (IPCC, 2007b). However, a range of SLR, excluding accelerated ice loss effects was published, ranging from 0.19m to 0.59m by the 2090s (relative to 1980-2000), for a range of scenarios (SRES A1FI to B1). The IPCC AR4 also provided an illustrative estimate of an additional SLR term of up to 17cm from acceleration of ice sheet outlet glaciers and ice streams, but did not suggest this is the upper value that could occur. Although there are published projections of SLR in excess of IPCC AR4 values (Nicholls et al., 2011), many of these typically use semi-empirical methods that suffer from limited physical validity and further research is required to produce a more robust estimate. Linking sea level rise projections to temperature must also be done with caution because of the different response times of these two climate variables to a given radiative forcing change.

Nicholls and Lowe (2004) previously showed that mitigation alone would not avoid all of the impacts due to rising sea levels, adaptation would likely be needed too. Recent work by van Vuuren et al. (2011) estimated that, for a world where global mean near surface temperatures reach around 2°C by 2100, global mean SLR could be 0.49m above present

levels by the end of the century. Their sea level rise estimate for a world with global mean temperatures reaching 4°C by 2100 was 0.71m, suggesting around 40% of the future increase in sea level to the end of the 21st century could be avoided by mitigation. A qualitatively similar conclusion was reached in a study by Pardaens et al. (2011), which examined climate change projections from two GCMs. They found that around a third of global-mean SLR over the 21st century could potentially be avoided by a mitigation scenario under which global-mean surface air temperature is near-stabilised at around 2°C relative to pre-industrial times. Under their baseline business-as-usual scenario the projected increase in temperature over the 21st century is around 4°C, and the sea level rise range is 0.29-0.51m (by 2090-2099 relative to 1980-1999; 5% to 95% uncertainties arising from treatment of land-based ice melt and following the methodology used by the IPCC AR4). Under the mitigation scenario, global mean SLR in this study is projected to be 0.17-0.34m.

The IPCC 4th assessment (IPCCa) followed Nicholls and Lowe (2004) for estimates of the numbers of people affected by coastal flooding due to sea level rise. Nicholls and Lowe (2004) projected for the East Asia region that an additional 100 thousand people per year could be flooded due to sea level rise by the 2080s relative to the 1990s for the SRES A2 Scenario (note this region also includes other countries, such as Korea and Japan). China also has a coast within the South-East Asia region, which has a projected additional 400 thousand people per year who could be flooded by the 2080s. However, it is important to note that this calculation assumed that protection standards increased as GDP increased, although there is no additional adaptation for sea level rise. More recently, Nicholls et al. (2011) also examined the potential impacts of sea level rise in a scenario that gave around 4°C of warming by 2100. Readings from Figure 3 from Nicholls et al. (2011) for the East Asia coast (South East Asia) region an suggest an approximate 15 million (20 million) additional people could be flooded for a 0.5 m SLR (assuming no additional protection). Nicholls et al. (2011) also looked at the consequence of a 2m SLR by 2100, however as we consider this rate of SLR to have a low probability we don't report these figures here.

Dasgupta et al. (2009b) considered 84 developing countries and investigated the impact of a 10% intensification of the current 1-in-100-year storm surge combined with a 1m SLR. GIS inundation models were applied in the analysis and the method means that uncertainty associated with the climate system is inherently overlooked. Nevertheless, the projections give a useful indicator of the possible impact of SLR in China. Table 13 shows that around 17% of China's coastal land area and coastal population could be affected. Whilst other countries were projected to incur impacts on greater proportions of their coastal area, the absolute impacts for China are the largest across the 84 countries that Dasgupta et al.

(2009b) investigated; e.g. around 10.8 million people along China's coasts could be affected by a 1m SLR and around $31 billion of China's GDP.

Country	Incremental Impact: Land Area (sq. km)	Projected Impact as a % of Coastal Total	Incremental Impact: Population	Projected Impact as a % of Coastal Total	Incremental Impact: GDP (mil. USD)	Projected Impact as a % of Coastal Total	Incremental Impact: Agricultural Area (sq. km)	Projected Impact as a % of Coastal Total	Incremental Impact: Urban Extent (sq. km)	Projected Impact as a % of Coastal Total	Incremental Impact: Wetlands (sq. km)	Projected Impact as a % of Coastal Total
Africa												
South Africa	607	43.09	48,140	32.91	174	30.98	70	34.48	93	48.10	132	46.23
Egypt	2,290	13.61	2,600,000	14.68	4,600	16.67	692	5.23	627	15.30	640	28.36
Kenya	274	41.93	27,400	40.23	10	32.05	40	22.13	9	38.89	177	52.51
Americas												
Argentina	2,400	18.03	278,000	19.52	2,240	16.42	157	9.93	313	27.47	459	11.30
Brazil	6,280	15.08	1,100,000	30.37	4,880	28.48	275	16.47	960	33.67	2,590	11.48
Mexico	9,130	29.04	463,000	20.56	2,570	21.22	310	10.89	701	18.35	1,760	52.25
Peru	727	36.69	61,000	46.90	177	46.18	5	26.92	54	42.72	20	37.91
Asia												
China	11,800	17.52	10,800,000	16.67	31,200	17.15	6,640	11.66	2,900	15.70	4,360	39.77
Rep. of Korea	902	61.73	863,000	50.48	10,600	47.86	237	66.75	335	48.15	77	78.81
India	8,690	29.33	7,640,000	28.68	5,170	27.72	3,740	23.64	1,290	30.04	2,510	32.31
Indonesia	14,400	26.64	5,830,000	32.75	7,990	38.71	4,110	26.12	1,280	33.25	2,680	26.97
Saudi Arabia	1,360	41.58	243,000	42.92	2,420	40.60	0	0.00	390	45.85	715	51.04
Bangladesh	4,450	23.45	4,840,000	16.01	2,220	19.00	2,710	17.52	433	18.30	3,890	24.29

Table 13. *The impact of a 1m SLR combined with a 10% intensification of the current 1-in-100-year storm surge. Impacts are presented as incremental impacts, relative to the impacts of existing storm surges. Each impact is presented in absolute terms, then as a percentage of the coastal total; e.g. 9.93% of Argentina's coastal agricultural land is impacted. The table is adapted from a study presented by Dasgupta et al. (2009b), which considered impacts in 84 developing countries. Only those countries relevant to this review are presented here and all incremental impacts have been rounded down to three significant figures.*

Dasgupta et al. (2009a) investigated the consequences of prescribed SLR (1-5m in 1m increments) by GIS land inundation mapping on the same 84 developing countries as Dasgupta et al. (2009b) but they did not consider any effects of climate change (e.g. variability in storm surges). Indeed, the authors note that there impacts estimates are conservative because of this and they note that even a small SLR can significantly magnify the impact of storm surges, which occur regularly and with devastating consequences in some coastal areas. The analysis assumed that the level of coastal protection remained at present-day levels for all SLR scenarios. Out of the 84 countries that Dasgupta et al. (2009a) considered, China (with Taiwan) was ranked the 7th highest with respect to land area affected, and 10th highest for agricultural land affected, due to a 1m SLR (see Table 14).

Rank	Land area	Population	GDP	Urban areas	Agricultural land	Wetlands
1	The Bahamas (11.57)	Vietnam (10.79)	Vietnam (10.21)	Vietnam (10.74)	Egypt (13.09)	Vietnam (28.67)
2	Vietnam (5.17)	Egypt (9.28)	Mauritania (9.35)	Guyana (10.02)	Vietnam (7.14)	Jamaica (28.16)
3	Qatar (2.70)	Mauritania (7.95)	Egypt (6.44)	French Guiana (7.76)	Suriname (5.60)	Belize (27.76)
4	Belize (1.90)	Suriname (7.00)	Suriname (6.35)	Mauritania (7.50)	The Bahamas (4.49)	Qatar (21.75)
5	Puerto Rico (1.64)	Guyana (6.30)	Benin (5.64)	Egypt (5.52)	Argentina (3.19)	The Bahamas (17.75)
6	Cuba (1.59)	French Guiana (5.42)	The Bahamas (4.74)	Libya (5.39)	Jamaica (2.82)	Libya (15.83)
7	Taiwan & China (1.59)	Tunisia (4.898)	Guyana (4.64)	UAE (4.80)	Mexico (1.60)	Uruguay (15.14)
8	The Gambia (1.33)	UAE (4.59)	French Guiana (3.02)	Tunisia (4.50)	Myanmar (1.48)	Mexico (14.85)
9	Jamaica (1.27)	The Bahamas (4.56)	Tunisia (2.93)	Suriname (4.20)	Guyana (1.16)	Benin (13.78)
10	Bangladesh (1.12)	Benin (4.93)	Ecuador (2.66)	The Bahamas (3.99)	Taiwan & China (1.05)	Taiwan & China (11.70)

Table 14. *The top 10 most impacted countries with a 1m SLR according to a study across 84 developing countries. Figures in parenthesis are the percentage impact for each country; e.g. 13.09% of all agricultural land in Egypt was simulated to be affected by a 1m SLR. Countries considered in this review are highlighted. Adapted from Dasgupta et al. (2009a).*

The high vulnerability of China is confirmed by Hanson et al. (2010), a study which investigated port city population exposure to global SLR, natural and human subsidence/uplift, and more intense storms and higher storm surges, for 136 port cities across the globe. Future city populations were calculated using global population and economic projections, based on the SRES A1 scenario up to 2030. The study accounted for uncertainty on future urbanization rates, but estimates of population exposure were only presented for a rapid urbanisation scenario, which involved the direct extrapolation of population from 2030 to 2080. All scenarios assumed that new inhabitants of cities in the future will have the same relative exposure to flood risk as current inhabitants. The study is similar to a later study presented by Hanson et al. (2011) except here, different climate change scenarios were considered, and published estimates of port city exposure are available for more countries. Future water levels were generated from temperature and thermal expansion data related to greenhouse gas emissions with SRES A1B (un-mitigated climate change) and under a mitigation scenario where emissions peak in 2016 and decrease subsequently at 5% per year to a low emissions floor (2016-5-L). Table 15 shows the aspects of SLR that were considered for various scenarios and Table 16 displays regional port city population exposure for each scenario in the 2030s, 2050s and 2070s.

Scenario		**Water levels**				
		Climate			**Subsidence**	
Code	**Description**	**More intense storms**	**Sea-level change**	**Higher storm surges**	**Natural**	**Anthropogenic**
FNC	Future city	**V**	x	x	X	x
FRSLC	Future City Sea-Level Change	**V**	**V**	x	**V**	x
FCC	Future City Climate Change	**V**	**V**	**V**	**V**	x
FAC	Future City All Changes	**V**	**V**	**V**	**V**	**V**

Table 15. *Summary of the aspects of SLR considered by Hanson et al. (2010). 'V' denotes that the aspect was considered in the scenario and 'x' that it was not.*

Rapid urbanisation projection																
2030						2050						2070				
Country	Ports	Water level projection				Country	Ports	Water level projection				Country	Ports	Water level projection			
		FAC	FCC	FRSLC	FNC			FAC	FCC	FRSLC	FNC			FAC	FCC	FRSLC	FNC
CHINA	15	17,100	15,500	15,400	14,600	**CHINA**	15	23,000	19,700	18,700	17,400	**CHINA**	15	27,700	22,600	20,800	18,600
INDIA	6	11,600	10,800	10,300	9,970	**INDIA**	6	16,400	14,600	13,600	12,500	**INDIA**	6	20,600	17,900	15,600	13,900
US	17	8,990	8,960	8,830	8,460	**US**	17	11,300	11,200	10,800	9,970	**US**	17	12,800	12,700	12,100	10,700
JAPAN	6	5,260	4,610	4,430	4,390	**JAPAN**	6	6,440	5,280	5,000	4,760	**JAPAN**	6	7,800	5,970	5,580	5,070
INDONESIA	4	1,420	1,200	1,200	1,170	**INDONESIA**	4	2,110	1,610	1,610	1,500	**INDONESIA**	4	2,680	1,830	1,830	1,530
BRAZIL	10	833	833	833	802	**BRAZIL**	10	929	929	929	879	**BRAZIL**	10	940	940	940	864
UK	2	497	497	478	459	**UK**	2	609	609	564	521	**UK**	2	716	716	640	569
CANADA	2	459	433	422	405	**CANADA**	2	549	512	486	457	**CANADA**	2	614	585	545	489
REP OF KOREA	3	344	344	331	441	**REP OF KOREA**	3	361	361	341	318	**REP OF KOREA**	3	377	377	325	303
GERMANY	1	257	257	253	248	**GERMANY**	1	287	287	273	269	**GERMANY**	1	309	309	290	280
RUSSIA	1	177	177	177	177	**RUSSIA**	1	202	202	173	173	**RUSSIA**	1	226	226	197	169
AUSTRALIA	5	162	162	157	157	**AUSTRALIA**	5	197	197	191	181	**AUSTRALIA**	5	196	196	186	175
SAUDI ARABIA	1	24	24	24	22	**SAUDI ARABIA**	1	33	33	33	27	**SAUDI ARABIA**	1	38	38	38	29
SOUTH AFRICA	2	30	30	30	29	**SOUTH AFRICA**	2	28	28	28	27	**SOUTH AFRICA**	2	30	30	30	27
FRANCE	1	15	15	15	15	**FRANCE**	1	19	19	19	17	**FRANCE**	1	23	23	23	18
ITALY	1	2	2	2	2	**ITALY**	1	4	4	4	3	**ITALY**	1	6	6	6	4
MEXICO	0	0	0	0	0	**MEXICO**	0	0	0	0	0	**MEXICO**	0	0	0	0	0

Table 16. *National estimates of port city population exposure (1,000s) for each water level projection (ranked according to exposure with the FAC (Future City All Changes) scenario) under a rapid urbanisation projection for the 2030s, 2050s and 2070s. Estimates for present day exposure and in the absence of climate change (for 2070 only) for comparison are presented in Table 17. Data is from Hanson et al. (□ HYPERLINK \l "_ENREF_39" \o "Hanson, 2010 #177" □□2010□) and has been rounded down to three significant figures.*

The result show, similar to Dasgupta et al. (2009b), that China experiences the greatest impact from SLR (e.g. compare the projections in Table 16 with the estimates for exposure in the absence of climate change that are presented in Table 17). For instance, under the FAC (Future City All Changes) scenario and A1B emissions in 2070, around 9 million extra people are exposed to flooding, relative to no climate change in China. Hanson et al. (2010) also demonstrated that aggressive mitigation could avoid an exposure of around 1.1 million people in China, relative to un-mitigated climate change (see Table 17) in 2070.

Country	Ports	Population exposure				Exposure avoided
		Current	2070. Rapid urbanisation, FAC water level scenario			
			No climate change	A1B un-mitigated	Mitigated (2016-5-L)	
CHINA	15	8,740	18,600	27,700	26,500	1,140
UNITED STATES	17	6,680	10,700	12,800	12,300	505
RUSSIA	1	189	169	226	197	28
JAPAN	6	3,680	5,070	7,800	7,290	515
SOUTH AFRICA	2	24	27	30	29	0
INDIA	6	5,540	13,900	20,600	18,900	1,670
BRAZIL	10	555	864	940	926	14
MEXICO	0	0	0	0	0	0
CANADA	2	308	489	614	599	15
AUSTRALIA	5	99	175	196	190	6
INDONESIA	4	602	1,530	2,680	2,520	156
REP OF KOREA	3	294	303	377	343	34
UK	2	414	569	716	665	51
FRANCE	1	13	18	23	20	2
ITALY	1	2	4	6	6	0
GERMANY	1	261	280	309	295	15
SAUDI ARABIA	1	15	29	38	35	3

***Table 17**. Exposed port city population (1,000s) in present (current), and in the 2070s in the absence of climate change (no climate change), with unmitigated climate change (A1B un-mitigated), and mitigated climate change (mitigated 2016-5-L), under the rapid urbanisation and FAC (Future City All Changes) water level scenarios. The final column shows the potential avoided exposure, as a result of mitigation. Data is from Hanson et al. (2010) and has been rounded down to three significant figures.*

Hanson et al. (2011) also present estimates of the exposure of the world's large port cities (population exceeding one million inhabitants in 2005) to coastal flooding due to SLR and storm surge, now and in the 2070s, and the results support previous findings that point to China's high vulnerability to SLR impacts (Dasgupta et al., 2009b; Hanson et al., 2010). Population exposure was calculated as a function of elevation against water levels related to the 1 in 100 year storm surge. The analysis assumed a homogenous SLR of 0.5m by 2070. For tropical storms a 10% increase in extreme water levels was assumed, with no expansion in affected area; while for extratropical storms, a 10% increase in extreme water levels was assumed. A uniform 0.5 m decline in land levels was assumed from 2005 to the 2070s in those cities which are historically susceptible (usually port cities located in deltas). This approach provided a variable change in extreme water level from around 0.5m in cities only affected by global SLR, to as much as 1.5 m for cities affected by global SLR, increased storminess and human-induced subsidence. Population projections were based upon the UN medium variant, where global population stabilises at around 9 billion by 2050. Figure 20 shows that China was simulated to show the largest increase in exposure, compared to other countries, from SLR relative to present in the 2070s.

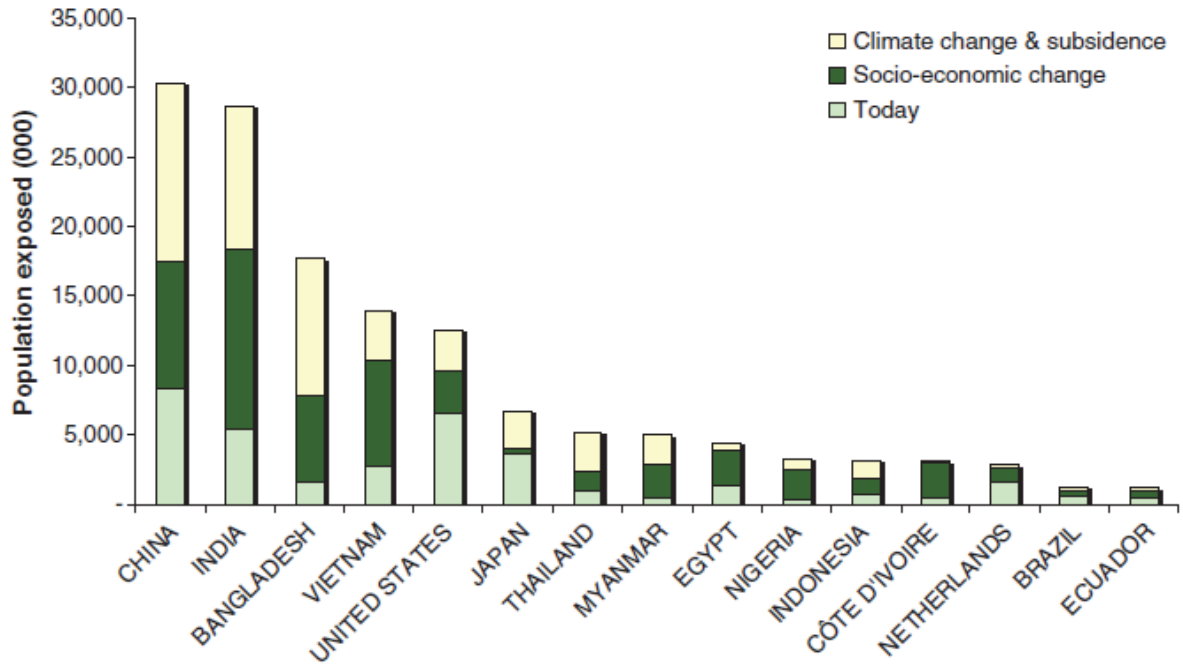

***Figure 20**. The top 15 countries in the 2070s for exposure to SLR, based upon a global analysis of 136 port cities (Hanson et al., 2011). The proportions associated with current exposure, climate change and subsidence, and socio-economic changes are displayed.*

To further quantify the impact of SLR and some of the inherent uncertainties, the DIVA model was used to calculate the number of people flooded per year for global mean sea

level increases (Brown et al., 2011). The DIVA model (DINAS-COAST, 2006) is an integrated model of coastal systems that combines scenarios of water level changes with socio-economic information, such as increases in population. The study uses two climate scenarios; 1) the SRES A1B scenario and 2) a mitigation scenario, RCP2.6. In both cases an SRES A1B population scenario was used. The results are shown in Table 18.

	A1B		**RCP**	
	Low	**High**	**Low**	**High**
Additional people flooded (1000s)	2463.55	19071.68	1651.40	12902.77
Loss of wetlands area (% of country's total wetland)	34.19%	44.37%	25.77%	42.24%

Table 18. *Number of additional people flooded (1000s), and percentage of total wetlands lost by the 2080s under the high and low SRES A1B and mitigation (RCP 2.6) scenarios (Brown et al., 2011).*

National-scale or sub-national scale assessments

Climate change studies

A national assessment of the impact of a prescribed 1m SLR on the coast of China suggests that large areas of land could be inundated. Jie et al. (2010) was able to identify areas that are most vulnerable to inundation. The results indicated a 1m SLR by 2100 could result in the inundation of 38,900 km^2 of land (0.4% of the total land area of China). This is close to the estimates of a previous national-scale study that estimated around 35,000 km^2 could be inundated due to a 1m SLR (Han et al., 1995). Whilst these large inundation estimates support the findings of Dasgupta et al. (2009b), in the sense that China is highly vulnerable, there is a difference of around 23,000km^2 in the estimates published by Dasgupta et al. (2009b) and the two national-scale studies (Han et al., 1995; Jie et al., 2010). This may be explained in part by the two national-scale studies applying higher resolution digital elevation models than are applied by Dasgupta et al. (2009b), thus affording them a more appropriate estimate of potential submergence.

References

AINSWORTH E.A. and McGRATH J.M. 2010 Direct Effects of Rising Atmospheric Carbon Dioxide and Ozone on Crop Yields. In: Lobell D and Burke M (eds) *Climate Change and Food Security.* Springer Netherlands, 109-130.

ALLISON E.H., PERRY A.L., BADJECK M-C, et al. 2009 Vulnerability of national economies to the impacts of climate change on fisheries. *Fish and Fisheries* 10: 173-196.

ARNELL N., OSBORNE T., HOOKER J., et al. 2010a. Simulation of AVOIDed impacts on crop productivity and food security. *Work stream 2, Report 17 of the AVOID programme (AV/WS2/D1/R17).* London: Department for Energy and Climate Change (DECC).

ARNELL N., WHEELER T., OSBORNE. T., et al. 2010b. The implications of climate policy for avoided impacts on water and food security. *Work stream 2, Report 6 of the AVOID programme (AV/WS2/D1/R06).* London: Department for Energy and Climate Change (DECC).

ARNELL N.W. 2004. Climate change and global water resources: SRES emissions and socio-economic scenarios. *Global Environmental Change* 14: 31-52.

ASIAN DEVELOPMENT BANK. 2011. ADB Celebrates World Environment Day and International Year of Forests. *Technical Report Asian Development Bank*.

ASSOCIATION OF BRITISH INSURERS. 2005. The financial risks of climate change. *ABI Reseatch Paper No. 19.* Association of British Insurers, 1-107.

AVNERY S., MAUZERALL D.L., LIU J.F., et al. 2011 Global crop yield reductions due to surface ozone exposure: 2. Year 2030 potential crop production losses and economic damage under two scenarios of O_3 pollution. *Atmospheric Environment* 45: 2297-2309.

BENGTSSON L., HODGES K.I., ESCH M., et al. 2007. How may tropical cyclones change in a warmer climate? *Tellus A* 59: 539-561.

BETTS, R. A., BOUCHER, O., COLLINS, M., COX, P. M., FALLOON, P. D., GEDNEY, N., HEMMING, D. L., HUNTINGFORD, C., JONES, C. D., SEXTON, D. M. H. & WEBB, M. J. 2007. Projected increase in continental runoff due to plant responses to increasing carbon dioxide. *Nature,* 448**,** 1037-1041.

BROWN, S., NICHOLLS, R., LOWE, J.A. and PARDAENS, A. 2011. Sea level rise impacts in 24 countries. Faculty of Engineering and the Environment and Tyndall Centre for Climate Change Research, University of Southampton.

CHAKRABORTY S. AND NEWTON A.C. 2011. Climate change, plant diseases and food security: an overview. *Plant Pathology* 60: 2-14.

CHEUNG W.W.L., LAM V.W.Y., SARMIENTO J.L., et al. 2010. Large-scale redistribution of maximum fisheries catch potential in the global ocean under climate change. *Global Change Biology* 16: 24-35.

CHOI G., COLLINS D., REN G., et al. 2009. Changes in means and extreme events of temperature and precipitation in the Asia-Pacific Network region, 1955–2007. *International Journal of Climatology* 29: 1906-1925.

CHRISTENSEN, J.H., HEWITSON, B., BUSUIOC, A., CHEN, A., GAO, X., HELD, I., JONES, R., KOLLI, R.K., KWON, W.-T., LAPRISE, R., MAGAÑA RUEDA, V., MEARNS, L., MENÉNDEZ, C.G., RÄISÄNEN, J., RINKE, A., SARR A., and WHETTON, P. 2007. Regional Climate Projections. In *Climate Change 2007: The Physical Science Basis. Contribution of Working Group I to the Fourth Assessment Report of the Intergovernmental Panel on Climate Change* [Solomon, S., D. Qin, M. Manning, Z. Chen, M. Marquis, K.B. Averyt, M. Tignor and H.L. Miller (eds.)]. Cambridge University Press, Cambridge, United Kingdom and New York, NY, USA.

CIA. 2011. World Factbook. US Central Intelligence Agency.

CUI X., HUANG.G., CHEN W., et al. 2009. Threatening of climate change on water resources and supply: Case study of North China. *Desalination* 248: 476-478.

DASGUPTA S., LAPLANTE B., MEISNER C., et al. 2009a. The impact of sea level rise on developing countries: a comparative analysis. *Climatic Change* 93: 379-388.

DASGUPTA S., LAPLANTE B., MURRAY S., et al. 2009b. Sea-level rise and storm surges: a comparative analysis of impacts in developing countries. Washington DC, USA: World Bank, 1-41.

DINAS-COAST Consortium. 2006 DIVA 1.5.5. Potsdam, Germany: Potsdam Institute for Climate Impact Research (on CD-ROM).

DOLL P. 2009. Vulnerability to the impact of climate change on renewable groundwater resources: a global-scale assessment. *Environmental Research Letters* 4.

DOLL, P. & SIEBERT, S. 2002. Global modeling of irrigation water requirements. *Water Resources Research*. Vol: 38 Issue: 4. Doi: 10.1029/2001WR000355.

EMANUEL K.A., SUNDARARAJAN R., and WILLIAMS J. 2008. Hurricanes and Global Warming: Results from Downscaling IPCC AR4 Simulations. *Bulletin of the American Meteorological Society* 89: 347-367.

EMANUEL K.A. 1987. The dependence of hurricane intensity on climate. *Nature* 326: 483-485.

FALKENMARK M., ROCKSTRÖM J., AND KARLBERG L. 2009. Present and future water requirements for feeding humanity. *Food Security* 1: 59-69.

FAO. 2008. *Food and Agricultural commodities production*. Available at: http://faostat.fao.org/site/339/default.aspx.

FSF. 2009. Financial Standards Report China: Insurance Core Principles. Financial Standards Foundation.

FUNG F., LOPEZ A., and NEW M. 2011. Water availability in +2°C and +4°C worlds. *Philosophical Transactions of the Royal Society A: Mathematical, Physical and Engineering Sciences* 369: 99-116.

GAO X.J., ZHAO Z.C., and GIORGI F. 2002. Changes of extreme events in regional climate simulations over East Asia. *Advances in Atmospheric Sciences* 19: 927-942.

GERTEN D., SCHAPHOFF S., HABERLANDT U., LUCHT W., SITCH S. 2004 . Terrestrial vegetation and water balance: hydrological evaluation of a dynamic global vegetation model *International Journal Water Resource Development* 286:249–270.

GORNALL, J., BETTS, R., BURKE, E., CLARK, R., CAMP, J., WILLETT, K., WILTSHIRE, A. 2010. Implications of climate change for agricultural productivity in the early twenty-first century. *Phil. Trans. R. Soc. B*, DOI: 10.1098/rstb.2010.0158.

GOSLING S., TAYLOR R., ARNELL N., et al. 2011. A comparative analysis of projected impacts of climate change on river runoff from global and catchment-scale hydrological models. *Hydrology and Earth System Sciences* 15: 279–294.

GOSLING S.N., and ARNELL N.W. 2011. Simulating current global river runoff with a global hydrological model: model revisions, validation, and sensitivity analysis. *Hydrological Processes* 25: 1129-1145.

GOSLING S.N., BRETHERTON D., HAINES K., et al. 2010. Global hydrology modelling and uncertainty: running multiple ensembles with a campus grid. *Philosophical Transactions of the Royal Society A: Mathematical, Physical and Engineering Sciences* 368: 4005-4021.

GUALDI S., SCOCCIMARRO E. and NAVARRA A. 2008. Changes in Tropical Cyclone Activity due to Global Warming: Results from a High-Resolution Coupled General Circulation Model. *Journal of Climate* 21: 5204-5228.

GUO H., HU Q., and JIANG T. 2008. Annual and seasonal streamflow responses to climate and land-cover changes in the Poyang Lake basin, China. *Journal of Hydrology* 355: 106-122.

HAN M., HOU J., and WU L. 1995. Potential impacts of sea level rise on China's coastal environment and cities: a national assessment. *Journal of Coastal Research* 14: 79–95.

HANSON S., NICHOLLS R., RANGER N., et al. 2011. A global ranking of port cities with high exposure to climate extremes. *Climatic Change* 104: 89-111.

HANSON S., NICHOLLS R., S H, et al. 2010. The effects of climate mitigation on the exposure of worlds large port cities to extreme coastal water levels. London, UK.

HARDING, R., BEST, M., BLYTH, E., HAGEMANN, D., KABAT, P., TALLAKSEN, L.M., WARNAARS, T., WIBERG, D., WEEDON, G.P., van LANEN, H., LUDWIG, F., HADDELAND, I. 2011. Preface to the "Water and Global Change (WATCH)" special collection: Current knowledge of the terrestrial global water cycle. *Journal of Hydrometeorology*, DOI: 10.1175/JHM-D-11-024.1.

HIRABAYASHI Y., KANAE S., EMORI S., et al. 2008. Global projections of changing risks of floods and droughts in a changing climate. *Hydrological Sciences Journal-Journal Des Sciences Hydrologiques* 53: 754-772.

HUGELIUS G. and KUHRY P. 2009. Landscape partitioning and environmental gradient analyses of soil organic carbon in a permafrost environment. *Global Biogeochemical Cycles* 23: -.

IFPRI. 2010. *International Food Policy Research Institute (IFPRI) Food Security CASE maps. Generated by IFPRI in collaboration with StatPlanet.* Available at: www.ifpri.org/climatechange/casemaps.html.

IGLESIAS A., GARROTE L., QUIROGA S., et al. 2009. Impacts of climate change in agriculture in Europe. PESETA-Agriculture study. *JRC Scientific and Technical Reports.* 51.

IGLESIAS A. and ROSENZWEIG C. 2009. Effects of Climate Change on Global Food Production under Special Report on Emissions Scenarios (SRES) Emissions and Socioeconomic Scenarios: Data from a Crop Modeling Study. . Palisades, NY: Socioeconomic Data and Applications Center (SEDAC), Columbia University.

IIASA. 1999. *Crop cultivation in China (8 maps)*. Available at: http://www.china-food-security.org/data/maps/crops/all_m.htm.

IPCC. 2007a *Climate Change 2007: Impacts, Adaptation and Vulnerability. Contribution of Working Group II to the Fourth Assessment Report of the Intergovernmental Panel on Climate Change.* In: Parry ML, Canziani OF, Palutikof JP, et al. (eds). Cambridge, UK, 976pp.

IPCC. 2007b. Climate Change 2007: *The Physical Science Basis. Contribution of Working Group I to the Fourth Assessment Report of the Intergovernmental Panel on Climate Change* In: Solomon S, Qin D, Manning M, et al. (eds). Cambridge, United Kingdom and New York, NY, USA, 996pp.

IPCC. 2007c. Summary for Policymakers. In: Parry ML, Canziani OF, Palutikof JP, et al. (eds) *Climate Change 2007: Impacts, Adaptation and Vulnerability. Contribution of Working Group II to the Fourth Assessment Report of the Intergovernmental Panel on Climate Change.* Cambridge: Cambridge University Press, 7-22.

JIANG T., KUNDZEWICZ Z.W., and SU B. 2008. Changes in monthly precipitation and flood hazard in the Yangtze River Basin, China. *International Journal of Climatology* 28: 1471-1481.

JIANG T., SU B., and HARTMANN H. 2007. Temporal and spatial trends of precipitation and river flow in the Yangtze River Basin, 1961-2000. *Geomorphology* 85: 143-154.

JIANG Z.H., SONG J., LI L., et al. 2011. Extreme climate events in China: IPCC-AR4 model evaluation and projection. *Climatic Change* Published Online May 2011.

JIE Y., SHIYUAN X., JUN W., et al. 2010. Vulnerability assessment of combined impacts of sea level rise and coastal flooding for China's coastal region using remote sensing and GIS. *Geoinformatics, 2010 18th International Conference on Geoinformatics.* Peking, China, 1-4.

JORGENSON M.T., SHUR Y.L. and PULLMAN E.R. 2006. Abrupt increase in permafrost degradation in Arctic Alaska. *Geophysical Research Letters* 33: -.

KNUTSON T.R. and TULEYA R.E. 2004. Impact of CO_2-Induced Warming on Simulated Hurricane Intensity and Precipitation : Sensitivity to the Choice of Climate Model and Convective Parameterization. *Journal of Climate*: 3477-3495.

KUNDZEWICZ Z.W., NOHARA D., TONG J., et al. 2009. Discharge of large Asian rivers - Observations and projections. *Quaternary International* 208: 4-10.

LAM J.C., WAN K.K.W., LAM T.N.T., et al. 2010. An analysis of future building energy use in subtropical Hong Kong. *Energy* 35: 1482-1490.

LAWRENCE D., SLATER A. and SWENSON S. 2011. Simulation of Present-day and Future Permafrost and Seasonally Frozen Ground Conditions in CCSM4. *Submiited to Journal of Climate*.

LAWRENCE D.M., SLATER A.G., TOMAS R.A., et al. 2008. Accelerated Arctic land warming and permafrost degradation during rapid sea ice loss. *Geophysical Research Letters* 35: -.

LI J.P., WU Z.W., JIANG Z.H., et al. 2010a. Can Global Warming Strengthen the East Asian Summer Monsoon? *Journal of Climate* 23: 6696-6705.

LI T., KWON M., ZHAO M., et al. 2010b. Global warming shifts Pacific tropical cyclone location. *Geophysical Research Letters* 37: 1-5.

LIU Z.F., XU Z.X., HUANG J.X., et al. 2010. Impacts of climate change on hydrological processes in the headwater catchment of the Tarim River basin, China. *Hydrological Processes* 24: 196-208.

LOBELL D.B., BANZIGER M., MAGOROKOSHO C., et al. 2011. Nonlinear heat effects on African maize as evidenced by historical yield trials. *Nature Climate Change* 1: 42-45.

LOBELL D.B., BURKE M.B., TEBALDI C., et al. 2008. Prioritizing climate change adaptation needs for food security in 2030. *Science* 319: 607-610.

LOBELL, D., SCHLENKER, W. and COSTA-ROBERTS, J. 2011. Climate Trends and Global Crop Production Since 1980. *Science,* 333, 616-620 [DOI:10.1126/science.1204531].

LUCK J., SPACKMAN M., FREEMAN A., et al. 2011. Climate change and diseases of food crops. *Plant Pathology* 60: 113-121.

MASUTOMI Y., TAKAHASHI K., HARASAWA H., et al. 2009. Impact assessment of climate change on rice production in Asia in comprehensive consideration of process/parameter uncertainty in general circulation models. *Agriculture, Ecosystems & Environment* 131: 281-291.

McDONALD R.E., BLEAKEN D.G., CRESSWELL D.R., et al. .2005. Tropical storms: representation and diagnosis in climate models and the impacts of climate change. *Climate Dynamics* 25: 19-36.

MENDELSOHN R., EMANUEL K. and CHONABAYASHI S. 2011. The Impact of Climate Change on Global Tropical Cyclone Damages. 1-36.

MU J. and KHAN S. 2009. The effect of climate change on the water and food nexus in China. *Food Security* 1: 413-430.

NELSON G.C., ROSEGRANT M.W., KOO J., et al. 2009. Climate change. Impact on Agriculture and Costs of Adaptation. Washington, D.C.: International Food Policy Research Institute, 19.

NELSON G.C., ROSEGRANT M.W., PALAZZO A., et al. 2010. Food Security, Farming and Climate Change to 2050. *Research Monograph, International Food Policy Research Institute.* Washington, DC, 115.

NICHOLLS R. 2000. Coastal zones. In: Parry M (ed) *Assessment of potential effects and adaptations for climate change in Europe: The Europe ACACIA Project.* Norwich, UK: University of East Anglia, 324.

NICHOLLS, R. J. and LOWE, J. A. 2004. "Benefits of mitigation of climate change for coastal areas." *Global Environmental Change* **14**(3): 229-244.

NICHOLLS, R. J., MARINOVA, N., LOWE, J. A., BROWN, S., VELLINGA, P., DE GUSMÃO, G., HINKEL, J. and TOL, R. S. J. 2011. "Sea-level rise and its possible impacts given a

‘beyond 4◦C world’ in the twenty-first century." *Philosophical Transactions of the Royal Society A* **369**: 1-21.

NOHARA D., KITOH A., HOSAKA M., et al. 2006. Impact of climate change on river discharge projected by multimodel ensemble. *Journal of Hydrometeorology* 7: 1076-1089.

O'CONNOR F.M., BOUCHER O., GEDNEY N., et al. 2010. Possible Role of Wetlands, Permafrost, and Methane Hydrates in the Methane Cycle under Future Climate Change: A Review. *Reviews of Geophysics* 48: -.

OOUCHI K., YOSHIMURA J., YOSHIMURA H., et al. 2006. Tropical Cyclone Climatology in a Global-Warming Climate as Simulated in a 20 km-Mesh Global Atmospheric Model: Frequency and Wind Intensity Analyses. *Journal of the Meteorological Society of Japan* 84: 259-276.

PARDAENS A.K., LOWE J. S B, et al. 2011. Sea-level rise and impacts projections under a future scenario with large greenhouse gas emission reductions. *Geophysical Research Letters* 38: L12604.

PARRY M.L., ROSENZWEIG C., IGLESIAS A., et al. 2004. Effects of climate change on global food production under SRES emissions and socio-economic scenarios. *Global Environmental Change-Human and Policy Dimensions* 14: 53-67.

PIAO S.L., CIAIS P., HUANG Y., et al. 2010. The impacts of climate change on water resources and agriculture in China. *Nature* 467: 43-51.

RAMANKUTTY N., EVAN A.T., MONFREDA C., et al. 2008. Farming the planet: 1. Geographic distribution of global agricultural lands in the year 2000. *Global Biogeochemical Cycles* 22: GB1003.

RAMANKUTTY N., FOLEY J.A., NORMAN J., et al. 2002 The global distribution of cultivable lands: current patterns and sensitivity to possible climate change. *Global Ecology and Biogeography* 11: 377-392.

RINGLER C., CAI X.M., WANG J.X., et al. 2010. Yellow River basin: living with scarcity. *Water International* 35: 681-701.

ROCKSTROM J., FALKENMARK M., KARLBERG L., et al. 2009. Future water availability for global food production: The potential of green water for increasing resilience to global change. *Water Resources Research* 45.

SCHUUR E.A.G., BOCKHEIM J., CANADELL J.G., et al. 2008. Vulnerability of permafrost carbon to climate change: Implications for the global carbon cycle. *Bioscience* 58: 701-714.

SHAKHOVA N., SEMILETOV I. and PANTELEEV G. 2005. The distribution of methane on the Siberian Arctic shelves: Implications for the marine methane cycle. *Geophysical Research Letters* 32: -.

SHEN C., WANG W.C., HAO Z., et al. 2007. Exceptional drought events over eastern China during the last five centuries. *Climatic Change* 85: 453-471.

SHEN Y.P., WANG S.D., WANG G.Y., et al. 2006. Response of glacier flash flood to global warming in Tarim River Basin [in Chinese]. *Adv. Clim. Change Res* 2: 32–35.

SHI Y.F., SHEN Y.P., KANG E., et al. 2007. Recent and future climate change in northwest china. *Climatic Change* 80: 379-393.

SILLMANN J. and ROECKNER E. 2008. Indices for extreme events in projections of anthropogenic climate change. *Climatic Change* 86: 83-104.

SMAKHTIN V., REVENGA C. and DOLL P. 2004. A pilot global assessment of environmental water requirements and scarcity. *Water International* 29: 307-317.

STOWASSER M., WANG Y. and HAMILTON K. 2007. Tropical Cyclone Changes in the Western North Pacific in a Global Warming Scenario. *Journal of Climate* 20: 2378-2396.

SU B., GEMMER M. and JIANG T. 2008. Spatial and temporal variation of extreme precipitation over the Yangtze River Basin. *Quaternary International* 186: 22-31.

SUGI M., MURAKAMI H. and YOSHIMURA J. 2009. A reduction in global tropical cyclone frequency due to global warming. *SOLA* 5: 164-167.

TAO F., YOKOZAWA M., LIU J., et al. 2009. Climate change, land use change, and China's food security in the twenty-first century: an integrated perspective. *Climatic Change* 93: 433-445.

TAO F.L., ZHANG Z. and YOKOZAWA M. 2011. Dangerous levels of climate change for agricultural production in China. *Regional Environmental Change* 11: S41-S48.

TATSUMI K,. YAMASHIKI Y., VALMIR DA SILVA R., et al. 2011. Estimation of potential changes in cereals production under climate change scenarios. *Hydrological Processes* Published online.

TU J-Y., CHOU C. and CHU P-S. 2009. The Abrupt Shift of Typhoon Activity in the Vicinity of Taiwan and Its Association with Western North Pacific–East Asian Climate Change. *Journal of Climate* 22: 3617-3628.

van VUUREN D., DEN ELZEN M., LUCAS P., et al. 2007. Stabilizing greenhouse gas concentrations at low levels: an assessment of reduction strategies and costs. *Climatic Change* 81: 119-159.

van VUUREN D.P., ISAAC M., KUNDZEWICZ Z.W., et al. 2011. The use of scenarios as the basis for combined assessment of climate change mitigation and adaptation. *Global Environmental Change* 21: 575-591.

VECCHI G.A. and SODEN B.J. 2007. Effect of remote sea surface temperature change on tropical cyclone potential intensity. *Nature* 450: 1066-1070.

VOROSMARTY C.J., McINTYRE P.B., GESSNER M.O., et al. 2010. Global threats to human water security and river biodiversity. *Nature* 467: 555-561.

WANG H.J., YANG Z.S., SAITO Y., et al. 2006. Interannual and seasonal variation of the Huanghe (Yellow River) water discharge over the past 50 years: Connections to impacts from ENSO events and dams. *Global and Planetary Change* 50: 212-225.

WARREN, R., ARNELL, N., BERRY, P., BROWN, S., DICKS, L., GOSLING, S., HANKIN, R., HOPE, C., LOWE, J., MATSUMOTO, K., MASUI, T., NICHOLLS, R., O'HANLEY, J., OSBORN, T., SCRIECRU, S. 2010. The Economics and Climate, Change Impacts of Various Greenhouse Gas Emissions Pathways: A comparison between baseline and policy emissions scenarios. *AVOID Report*, AV/WS1/D3/R01. http://www.metoffice.gov.uk/avoid/files/resources-researchers/AVOID_ WS1_D3_01_20100122.pdf.

WASHINGTON W.M., KNUTTI R., MEEHL G.A., et al. 2009. How much climate change can be avoided by mitigation? *Geophysical Research Letters* 36: -.

WELCH J.R., VINCENT J.R., AUFFHAMMER M., et al. 2010. Rice yields in tropical/subtropical Asia exhibit large but opposing sensitivities to minimum and maximum temperatures. *Proceedings of the National Academy of Sciences of the United States of America* 107: 14562-14567.

WOOD, E.F., ROUNDY, J.K., TROY, T.J., van BEEK, L.P.H., BIERKENS, M.F.P., BLYTH, E., de ROO, A., DOLL, P., EK, M., FAMIGLIETTI, J., GOCHIS, D., van de GIESEN, N., HOUSER, P., JAFFE, P.R., KOLLET, S., LEHNER, B., LETTENMAIER, D.P., PETERS-LIDARD, C., SIVAPALAN, M., SHEFFIELD, J., WADE, A. and WHITEHEAD, P. 2011. Hyperresolution global land surface modelling: Meeting a grand challenge for monitoring Earth's terrestrial water. *Water Resources Research,* 47, W05301.

WoS. 2011. *Web of Science*. Available at: http://thomsonreuters.com/products_services/science/science_products/a-z/web_of_science.

WU Q., CHENG G. and MA W. 2004. Impact of permafrost change on the Qinghai-Tibet Railroad engineering. *Science in China Series D: Earth Sciences* 47: 122-130.

WU W., TANG H., YANG P., et al. 2011. Scenario-based assessment of future food security. *Journal of Geographical Sciences* 21: 3-17.

XIONG W., HOLMAN I., LIN E.D., et al. 2010. Climate change, water availability and future cereal production in China. *Agriculture Ecosystems & Environment* 135: 58-69.

XIONG W., LIN E., JU H., et al. 2007. Climate change and critical thresholds in China's food security. *Climatic Change* 81: 205-221.

XU Y.L., ZHANG Y., LIN E.D., et al. 2006. Analyses on the climate change responses over China under SRES B2 scenario using PRECIS. *Chinese Science Bulletin* 51: 2260-2267.

ZHAI P.M., ZHANG X.B., WAN H., et al. 2005. Trends in total precipitation and frequency of daily precipitation extremes over China. *Journal of Climate* 18: 1096-1108.

ZHANG Q., LIU C.L., XU C.Y., et al. 2006. Observed trends of annual maximum water level and streamflow during past 130 years in the Yangtze River basin, China. *Journal of Hydrology* 324: 255-265.

ZHANG Z.X., ZHANG Q., XU C.Y., et al. 2009. Atmospheric moisture budget and floods in the Yangtze River basin, China. *Theoretical and Applied Climatology* 95: 331-340.

ZHAO M., HELD I.M., LIN S-J., et al. 2009. Simulations of Global Hurricane Climatology, Interannual Variability, and Response to Global Warming Using a 50-km Resolution GCM. *Journal of Climate* 22: 6653.

ZHUANG Q., MELACK J.M., ZIMOV S., et al. 2009. Global Methane Emissions From Wetlands, Rice Paddies, and Lakes. *Eos Trans. AGU* 90.

ZONG Y.Q. AND CHEN X.Q. 2000. The 1998 flood on the Yangtze, China. *Natural Hazards* 22: 165-184.

Acknowledgements

Funding for this work was provided by the UK Government Department of Energy and Climate Change, along with information on the policy relevance of the results.

The research was led by the UK Met Office in collaboration with experts from the University of Nottingham, Walker Institute at the University of Reading, Centre for Ecology and Hydrology, University of Leeds, Tyndall Centre — University of East Anglia, and Tyndall Centre — University of Southampton.

Some of the results described in this report are from work done in the AVOID programme by the UK Met Office, Walker Institute at the University of Reading, Tyndall Centre — University of East Anglia, and Tyndall Centre — University of Southampton.

The AVOID results are built on a wider body of research conducted by experts in climate and impact models at these institutions, and in supporting techniques such as statistical downscaling and pattern scaling.

The help provided by experts in each country is gratefully acknowledged — for the climate information they suggested and the reviews they provided, which enhanced the content and scientific integrity of the reports.

The work of the independent expert reviewers at the Centre for Ecology and Hydrology, University of Oxford, and Fiona's Red Kite Climate Consultancy is gratefully acknowledged.

Finally, thanks go to the designers, copy editors and project managers who worked on the reports.

Met Office
FitzRoy Road, Exeter
Devon, EX1 3PB
United Kingdom

Tel: 0870 900 0100
Fax: 0870 900 5050
enquiries@metoffice.gov.uk
www.metoffice.gov.uk

Produced by the Met Office.